


5-2014

Anti-GD2 Etoposide-Loaded Immunoliposomes for the Treatment of GD2 Positive Tumors

Brandon S. Brown

Follow this and additional works at: http://digitalcommons.library.tmc.edu/utgsbs_dissertations

 Part of the [Amino Acids, Peptides, and Proteins Commons](#), [Biological Factors Commons](#), [Lipids Commons](#), [Nanoscience and Nanotechnology Commons](#), and the [Therapeutics Commons](#)

Recommended Citation

Brown, Brandon S., "Anti-GD2 Etoposide-Loaded Immunoliposomes for the Treatment of GD2 Positive Tumors" (2014). *UT GSBS Dissertations and Theses (Open Access)*. Paper 437.

This Dissertation (PhD) is brought to you for free and open access by the Graduate School of Biomedical Sciences at DigitalCommons@The Texas Medical Center. It has been accepted for inclusion in UT GSBS Dissertations and Theses (Open Access) by an authorized administrator of DigitalCommons@The Texas Medical Center. For more information, please contact laurel.sanders@library.tmc.edu.

ANTI-GD2 ETOPOSIDE-LOADED IMMUNOLIPOSOMES FOR THE
TREATMENT OF GD2 POSITIVE TUMORS

by

Brandon Scott Brown, B.S.

APPROVED:

Andrew Bean, Ph.D., Supervisory Professor

Ennio Tasciotti, Ph.D., Supervisory Professor

Diane Bick, Ph.D.

Russell Broaddus, M.D., Ph.D.

Neal Waxham, Ph.D.

Jack Waymire, Ph.D.

APPROVED:

Dean, The University of Texas
Graduate School of Biomedical Sciences at
Houston

ANTI-GD2 ETOPOSIDE-LOADED IMMUNOLIPOSOMES FOR THE TREATMENT OF GD2
POSITIVE TUMORS

A

DISSERTATION

Presented to the Faculty of

The University of Texas

Health Science Center at Houston

and

The University of Texas

MD Anderson Cancer Center

Graduate School of Biomedical Sciences

in Partial Fulfillment

of the Requirements

for the Degree of

DOCTOR OF PHILOSOPHY

by

Brandon Scott Brown, B.S.

Houston, Texas

Date of Graduation May, 2014

I dedicate this work to my parents because they've always supported me
and helped me become what I am today.

ACKNOWLEDGEMENTS

I wish to express my deep gratitude to my two primary advisors, Dr. Ennio Tasciotti and Dr. Andrew Bean, for their guidance and support throughout my PhD experience. Both advisors have seen considerable growth in their careers and duties during my time with them and still always made sure to share knowledge, ideas, and advice on a regular basis. Dr. Tasciotti taught me many lessons, not only in scientific exploration of innovative ideas, but also in the approach to life's challenges. I've learned that no task is unachievable, and I will enter the next phase of my life with the confidence, tenacity, and determination necessary to materialize what I once viewed as impossible. Dr. Bean has also been instrumental in my personal development as a scientist and theorist, always encouraging critical thought and clarity of explanation. He always took time to contribute to my research focus but also entertained the theoretical exploration of science outside of our respective fields.

I would like to thank Dr. Pramod Dash, Dr. Neal Waxham, Dr. Diane Bick, Dr. Russell Broaddus, Dr. Victoria Knutson, and Dr. Waymire as my committee members.

I'd also like to thank Dr. Parodi who was always available to help discuss and plan anything from grants and experimental endeavors to philosophies on human nature. Dr. Parodi helped me view the world with more optimism, which will have a lasting effect on my career. Dr. Bean's other PhD students, Natalie Sirisaengtaksin and Monica Gireud, were invaluable in both technical and moral support throughout my endeavors, and I've greatly benefitted from their friendship and collaboration.

Funding for liposome-related experiments came from an NIH (CA166749), Innovator Extension Grant (W81XWH-12-1-0414) and R21 (R21CA173579).

Finally, and most of all, I could not have done any of this without the love and support of my family.

ANTI-GD2 ETOPOSIDE-LOADED IMMUNOLIPOSOMES FOR THE
TREATMENT OF GD2 POSITIVE TUMORS

Brandon Scott Brown, B.S.

Advisory Professors: Andrew Bean, Ph.D. and Ennio Tasciotti, Ph.D.

Systemic chemotherapeutics remain the standard of care for most malignancies even though they frequently suffer from narrow therapeutic index, poor serum solubility, and off-target effects. Monoclonal antibodies that specifically bind antigens overexpressed on many tumors such as the ganglioside, GD2, can be conjugated to drug-loaded liposomes to create a targeted drug delivery system. In this study, we have encapsulated etoposide, a topoisomerase inhibitor effective against a wide range of cancers, in surface modified liposomes decorated with anti-GD2 antibodies. We characterized the properties of the liposomes using a variety of methods including dynamic light scattering, electron microscopy, and Fourier transformed infrared spectroscopy. We examined whether these immunoliposomes were able to target cell lines expressing varying levels of surface GD2 and affect cellular proliferation. Anti-GD2 liposomes were generally targeted in a manner that correlated with GD2 expression and inhibited proliferation in cell lines to which they were efficiently targeted. The mechanism by which the immunoliposomes entered targeted cells appeared to be via clathrin-dependent uptake as demonstrated using flow cytometry and confocal microscopy. We initiated pilot studies in animals to examine the biodistribution and antitumor effects of immunoliposome mediated etoposide therapy. Fluorescent liposomes were observed at the tumor site with *in vivo* imaging, warranting further animals studies for antitumor efficacy. These studies suggest that anti-GD2-targeted, etoposide-loaded liposomes represent a potential strategy for more effective delivery of anti-cancer drugs that could be used for GD2 positive tumors.

Table of Contents

<u>DEDICATION</u>	<u>III</u>
<u>ACKNOWLEDGEMENTS</u>	<u>IV</u>
<u>ABSTRACT.....</u>	<u>V</u>
<u>TABLE OF CONTENTS.....</u>	<u>VI</u>
<u>TABLE OF FIGURES</u>	<u>X</u>
<u>ABBREVIATIONS.....</u>	<u>XIII</u>
CHAPTER 1: INTRODUCTION – CANCER AND TARGETED THERAPY.....	1
1.1 CANCER IN THE US.	1
1.2 NEUROBLASTOMA.	2
1.3 ETOPOSIDE CHEMOTHERAPY FOR NEUROBLASTOMA.....	4
1.4 OFF-TARGET EFFECTS OF ETOPOSIDE.....	4
1.5 CANCER BIOMARKERS AND GD2 EXPRESSION.....	6
1.6 CANCER IMMUNOTHERAPY.	7
1.7 MONOCLONAL ANTIBODIES AND ANTI-GD2 IMMUNOTHERAPY.....	8
1.8 NANOTECHNOLOGY IN MEDICINE.	11
1.9 TARGETED LIPOSOMES.	12
1.10 OVERALL HYPOTHESIS.....	13
<u>SECTION I: FORMATION OF THE TARGETED ETOPOSIDE NANOCARRIER</u>	<u>14</u>

CHAPTER 2: LIPOSOME ASSEMBLY AND ETOPOSIDE LOADING	15
2.1 LIPOSOMAL BACKGROUND.	15
2.2 LIPOSOME PHYSICS.	17
2.3 SUMMARY OF LIPOSOME CHARACTERIZATION METHODS.	20
2.4 FORMATION STRATEGIES FOR LIPOSOMES.	23
2.5 ETOPOSIDE LOADING INTO LIPOSOMES.	27
2.6 RELEASE OF ETOPOSIDE FROM LIPOSOMES.	32
2.7 SYNTHESIS CONCLUSIONS.....	34
CHAPTER 3: TARGETING MOIETY ATTACHMENT AND VERIFICATION.....	35
3.1 PASSIVE LIPOSOMAL TARGETING.	35
3.3 STRATEGIES FOR TARGETING MOIETY ATTACHMENT.....	37
3.4 POST-INSERTION OF CROSSLINKERS INTO LIPOSOMES.....	40
3.5 EVALUATING MALEIMIDE-ENABLED ANTIBODY DECORATION.	42
3.6 IMMUNOLIPOSOME SYNTHESIS AND CHARACTERIZATION CONCLUSIONS.....	51
<u>SECTION II: GANGLIOSIDE EXPRESSION AND NANOPARTICLE TARGETING.....</u>	<u>53</u>
CHAPTER 4: GD2 SURFACE EXPRESSION ACROSS CANCER LINES	55
4.1 GANGLIOSIDE SURFACE EXPRESSION.	55
4.2 VARIABILITY IN GD2 EXPRESSION.	55
4.3 CONCLUSIONS CONCERNING GD2 SURFACE EXPRESSION.	57
CHAPTER 5: ANTI-GD2 LIPOSOMAL TARGETING AND UPTAKE.....	59
5.1 ASSESSMENT OF ANTI-GD2 IMMUNOLIPOSOME TARGETING.....	59
5.2 ANTI-GD2 IMMUNOLIPOSOMES BIND GD2 POSITIVE CELLS.....	59
5.3 ANTI-GD2 IMMUNOLIPOSOME FLOW CHAMBER CELLULAR UPTAKE.	75

5.4 INHIBITION OF IMMUNOLIPOSOME ENDOCYTOSIS.	77
5.4 CONCLUSIONS FOR ANTI-GD2 IMMUNOLIPOSOME TARGETING AND UPTAKE.	80
<u>SECTION III: <i>IN VITRO</i> EFFICACY AND <i>IN VIVO</i> PILOT STUDY.....</u>	82
CHAPTER 6: <i>IN VITRO</i> INHIBITION OF CANCER CELL PROLIFERATION.....	84
6.1 INHIBITION OF PROLIFERATION OVER TIME.	84
6.2 ANTI-GD2 ETOPOSIDE LIPOSOME DOSE ESCALATION STUDY.....	86
6.3 ANTI-GD2 IMMUNOLIPOSOME EFFICACY CONCLUSIONS.	91
CHAPTER 7: PILOT <i>IN VIVO</i> STUDY.....	93
7.1 <i>IN VIVO</i> PILOT INJECTIONS.	93
7.2 <i>IN VIVO</i> ANTITUMOR ACTIVITY OF ANTI-GD2 IMMUNOLIPOSOMES.....	95
7.3 <i>IN VIVO</i> PILOT STUDY CONCLUSIONS.....	98
<u>SECTION IV: DISCUSSION AND FUTURE DIRECTIONS.....</u>	100
CHAPTER 8: DISCUSSION.....	100
CHAPTER 9: FUTURE DIRECTIONS.....	107
9.1 EXPANSION OF <i>IN VIVO</i> EVALUATION.....	107
9.2 FUTURE APPLICATIONS OF ANTI-GD2 IMMUNOLIPOSOMES.	108
9.3 THE FUTURE OF MULTIFUNCTIONAL NANOPARTICLES.	109
9.4 THE FUTURE OF TARGETED NANOMEDICINE DEVELOPMENT.	110
CHAPTER 10: MATERIALS AND METHODS.....	112
10.1 CHEMICALS AND LIPIDS.....	112
10.2 LIPOSOME PREPARATION AND PHYSICOCHEMICAL CHARACTERIZATION.	112
10.3 PREPARATION OF 3F8 ANTI-GD2 IMMUNOLIPOSOMES.	113

10.4 TRANSMISSION ELECTRON MICROSCOPY (TEM).	114
10.5 FOURIER TRANSFORMED INFRARED SPECTROSCOPY (FTIR).	114
10.6 CELL CULTURE.	115
10.7 FLOW CYTOMETRY ANALYSIS OF GD2 EXPRESSION AND LIPOSOME TARGETING.	115
10.8 LIPOSOME TARGETING TO CANCER CELLS.	115
10.9 CONFOCAL IMAGING OF LIPOSOME UPTAKE.	116
10.10 HIGH PRESSURE LIQUID CHROMATOGRAPHY QUANTIFICATION OF DRUG LOADING.	116
10.11 ETOPOSIDE-INDUCED PROLIFERATION INHIBITION.	116
10.12 ENDOCYTOSIS INHIBITION STUDY.....	117
10.13 ETOPOSIDE RELEASE STUDY.	118
10.14 MOUSE ORTHOTOPIC XENOGRAPTS	118

Table of Figures

Figure 1. Three types of nanoparticles for medical applications.	12
Figure 2. Depiction of basic liposome components.....	16
Figure 3. Packing parameters determine lipid assembly geometry.....	18
Figure 4. Characterization of liposome size and polydispersity by light scattering and transmission electron microscopy.....	19
Figure 5. Representation of particle morphology, size, and size distribution via transmission electron microscopy.	22
Figure 6. Schematic of liposome synthesis by the thin film rehydration method.....	24
Figure 7. Schematic of etoposide loading into liposomes via the ethanol injection method.....	26
Figure 8. Effects of thin film rehydration or ethanol injection liposome synthesis methods on size and polydispersity.	28
Figure 9. Characterization of size and polydispersity in liposomes with 0-3 mg/mL encapsulated etoposide.	29
Figure 10. Quantification of etoposide drug loading and entrapment efficiency within liposomes.	31
Figure 11. Cumulative etoposide release from immunoliposomes.....	33
Figure 12. Schematic showing DSPE-PEG2000-Maleimide crosslinker location and reaction.	39
Figure 13. Immunoliposome formation by micellar post-insertion schematic.	41
Figure 14. Verification of crosslinker-antibody coupling via nuclear magnetic resonance spectroscopy.....	43
Figure 15. Verification of crosslinker-antibody coupling via fourier transformed infrared spectroscopy.....	44
Figure 16. Native gel separation of immunoliposomes from unconjugated antibody.....	46
Figure 17. Immunofluorescence of untargeted and anti-GD2 liposomes.....	48

Figure 18. Transmission electron microscopic analysis of immunogold labeled control and GD2 targeted liposomes.....	50
Figure 19. Surface expression of GD2 in neuroblastoma cell lines and across cancer types...	56
Figure 20. Anti-GD2 targeted immunoliposome targeting to LA-155N cells at different concentrations.....	60
Figure 21. Anti-GD2 targeted immunoliposome targeting to LA-155N cells at different time points.	61
Figure 22. GD2 expression and anti-GD2 liposome targeting in cervical, breast, and neuroblastoma cells.	63
Figure 23. Comparison of targeted vs untargeted liposomal binding in cells with high GD2 expression.....	65
Figure 24. Comparison of targeted vs untargeted liposomal binding in cells with low GD2 expression.....	67
Figure 25. Characterization of targeted and mis-targeted immunoliposomes in cell lines with high GD2 expression.....	69
Figure 26. Characterization of targeted and mis-targeted immunoliposomes in cell lines with low GD2 expression.	71
Figure 27. Average targeting activity of anti-GD2 and control immunoliposomes on cells with high GD2 expression.....	73
Figure 28. Average targeting activity of anti-GD2 and control immunoliposomes on cells with low GD2 expression.	74
Figure 29. In vitro liposomal and immunoliposomal cellular uptake in flow conditions.....	76
Figure 30. Characterization of immunoliposome uptake with pharmacologic inhibition of endocytosis pathways in neuroblastoma cells.	78

Figure 31. Cell proliferation effects on cells treated with empty liposomes and drug emulsifiers.
..... 85

Figure 32. Cell proliferation effects on neuroblastoma cells exposed to liposomal and free
etoposide. 86

Figure 33. Dose response study on LA-155N cells exposed to liposomal and free etoposide.. 88

Figure 34. Dose response study on 143B cells exposed to liposomal and free etoposide. 89

Figure 35. Dose response study on SY5Y cells exposed to liposomal and free etoposide. 90

Figure 36. Preliminary in vivo imaging of mice injected with different formulations of fluorescent
liposomes..... 94

Figure 37. In vivo imaging of mice bearing luciferase-expressing SKNAS orthotopic xenografts
after injection of GD2 targeted and untargeted immunoliposomes. 96

Figure 38. Explanted tumor weights from orthotopically implanted neuroblastoma xenografts in
mice treated with etoposide..... 97

ABBREVIATIONS

ADCC – Antibody-Dependent Cellular Cytotoxicity

Asp – Aspartic Acid

CAR – Chimeric Antigen Receptor

CNS – Central Nervous System

Cys – Cysteine

DiR – Dioctadecyl-3,3,3',3'-Tetramethylindotricarbocyanine Iodide

DL – Drug Loading

DLS – Dynamic Light Scattering

DNA – Deoxyribonucleic Acid

DPPC – Dipalmitoylphosphatidylcholine

DSPE – Distearoyl-sn-glycero-3-phosphoethanolamine

EDC – Carbodiimide

EE – Entrapment Efficiency

EGFR – Epidermal Growth Factor Receptor

EPR – Enhanced Permeation and Retention

Fab – Fragment Antigen Binding

Fc – Fragment Crystallizable

FDA – United States Food and Drug Association

FTIR – Fourier Transformed Infrared Spectroscopy

Glu – Glutamic Acid

GM-CSF – Granulocyte Macrophage Colony-Stimulating Factor

HER-2 – Human Epidermal Growth Factor Receptor 2

HPLC – High Pressure Liquid Chromatography

IC₅₀ – Inhibitory Concentration 50%

IgG – Immunoglobulin Gamma

IL-2 – Interleukin 2

K_D – Dissociation Constant

Lys – Lysine

MAb – Monoclonal Antibody

mM – Millimolar

MPS – Mononuclear Phagocyte System

MTT – 3-(4,5-Dimethylthiazol-2-yl)-2,5-diphenyltetrazolium Bromide

NB – Neuroblastoma

NHS – N-hydroxysuccinimide

nm – Nanometer

nM – Nanomolar

PDI – Polydispersity Index

PEG – Polyethylene Glycol

PNS – Peripheral Nervous System

RPM – Rotations Per Minute

TEM – Transmission Electron Microscopy

WST-1 – Water Soluble Tetrazolium Salt

ZP – Zeta-potential

Chapter 1: Introduction – Cancer and Targeted Therapy

Cancer is a term describing diseases characterized by uncontrolled division of abnormal cells in one part of the body that can spread to other tissues. There are a multitude of molecular mechanisms thought to underlie this uncontrolled cell proliferation resulting in the hypothesis that cancer is not a single disease, but many related disorders. Cancer leads to approximately 1,600 deaths per day and causes an estimated \$207 billion in medical costs in the United States¹. Despite the advances in understanding its underlying molecular mechanisms and development of new treatment strategies, surgery and traditional cytotoxic therapies remain mainstays of cancer therapy².

1.1 Cancer in the US. Over 200 different types of cancer are recognized and stratified according to the originating organ system and cell type. Malignant transformation of healthy cells is believed to occur in a multistep process due to a combination of environmental and genetic insults resulting in an accumulation of genetic damage³. Cancers generally occur more frequently with advanced age due to the accumulation of cellular damage over years of cell replication and environmental exposure. Genetic causes have been implicated in 5-10% of cancers, suggesting that environmental exposures may underlie up to 95% of cancer cases⁴. Tobacco is the suspected cause of 30% of cancer deaths with diet linked to cancer in 30-35%, and about 15% of cancer deaths are attributed to infections⁴. The remainder of environmentally-associated cancers are likely due to other factors such as stress and exposure to radiation⁴.

Pediatric cancer, while less common than cancer in adults, has increased by 0.6% annually from 1975 to 2002 in the US and 1.1% annually in Europe⁵. Rising incidence may be due to a combination of increased environmental exposures and advances in diagnostic technologies⁴. While adult cancers are typically solid tumors, pediatric tumors are more likely to occur in the blood in the form of leukemias and lymphomas that make up 46% of new pediatric

cancer cases in the US^{5,6}. These liquid tumors arise from white blood cells that fail to mature correctly and often replicate in the bone marrow where they suppress healthy blood cell production, or hematopoiesis. Solid tumors such as neuroblastoma and osteosarcoma also occur in pediatric patients, although less frequently.

Osteosarcomas make up 2-3% of pediatric tumors, and close to 20% of all primary bone cancers⁷. Osteosarcomas form from primitive mesenchymal cells that develop incorrectly for unknown reasons, resulting in tumors that typically arise at the ends of long bones⁸. Healthy mesenchymal cells usually differentiate into lymphatic, circulatory, connective tissues as well as bone. Osteosarcoma cells retain some function of their mesenchymal origin, producing osteoid, a precursor to bone formation⁷. Other pediatric malignancies such as neuroblastoma form tumors that also retain some properties of their originating cells.

To treat cancers aggressively, anti-cancer therapies have become toxic, invasive, and often cause significant morbidity of their own. Nonetheless, therapies have remained largely the same over the past several decades without appreciable increases in high-grade cancer cures. This trend is especially apparent in the pediatric cancer neuroblastoma, where tumors are found at advanced levels in as many as 2/3 of patients with the disease.

1.2 Neuroblastoma. Neuroblastomas are solid tumors of neuroectodermal origin that occur heterogeneously in pediatric patients with regard to histopathologic appearance, biological characteristics, and location of primary tumors. These tumors originate from primitive sympathetic ganglion cells. Neuroectodermal cells that comprise the tumor arise from the neural crest during neurodevelopment in utero and are predestined for the sympathetic nervous system and adrenal medulla⁹. Neuroblastoma tumors occur most often in the adrenal glands (40%), but they can also originate in the abdomen (25%), thorax (15%) or within pelvic sympathetic ganglia (10%), and in a minority of cases, the location of the primary tumor cannot be identified. Approximately 600 new cases occur per year in the US making neuroblastoma

the most common extracranial solid tumor of childhood responsible for 7% of childhood cancers and resulting in 12% of deaths in pediatric cancer patients^{5, 10}. Despite multiple treatments being developed to address this malignancy, almost two-thirds of neuroblastoma patients diagnosed are found to have metastatic disease coupled with high occurrences of residual disease and low long-term survival^{11, 12}. Ultimately, long term survival is only about 40% in patients with high-risk neuroblastoma, defined by age above 18 months and disease dissemination or unfavorable histologic markers.

To treat neuroblastoma, a multimodal approach is typically implemented, involving a combination of surgical resection, radiation, chemotherapy, and endocrine or biological therapy¹³. Surgical resection is an excellent option for primary tumors that have clear localization and well-defined borders, but is of little use in neuroblastoma that is widely disseminated. Surgical intervention is not used for rapidly spreading tumors, particularly within soft tissues are primarily addressed with systemic treatments involving cytotoxic chemicals and radiation. Radiation therapy in neuroblastoma is utilized when tumors are unresectable or unresponsive to chemotherapy. Radiotherapy involves exposure to the body with ionizing radiation (such as gamma rays) resulting in nonspecific genetic damage within cells of the exposed tissue. The side effects of radiotherapy are wide ranging and can be long lasting. Irradiated healthy tissue often develops diffuse scar tissue, resulting in fibrosis, dryness, lymphedema, and potential secondary malignancies¹⁴. Radiotherapy for neuroblastoma is generally avoided in neuroblastoma patients unless the tumors are resistant to chemotherapy due to the long-term complications frequently encountered after radiotherapy.

The most common therapeutic tool for reducing neuroblastoma tumor mass before and after bulk surgical resection is chemotherapy. Unfortunately, the majority of disseminated neuroblastoma cases do not survive despite aggressive multimodal therapy including chemotherapy¹⁵.

1.3 Etoposide chemotherapy for neuroblastoma. A first line treatment for neuroblastoma is the chemotherapeutic drug etoposide. Chemotherapeutics are chemicals that induce toxicity in rapidly dividing cells by interfering with cellular mechanisms of genetic replication. Etoposide, a topoisomerase II inhibitor, causes the irreversible binding of DNA with topoisomerase II, preventing further function of the enzyme and resulting in high levels of torsional stress to the DNA strand. The effect of etoposide at a nuclear level is the accumulation of single and double-stranded DNA breaks that lead to eventual cell death by a combination of cell death mechanisms (e.g. apoptosis, autophagy, and necrosis)¹⁶.

Very poor prognosis has been observed in high-risk neuroblastomas characterized by disseminated disease at the time of diagnosis and *MYCN* amplification (a protein marker correlated with a poor prognosis), and the chemotherapeutic etoposide remains a first line treatment. Often, doses are increased to maximally tolerated levels, with the dose-limiting toxicity being myelosuppression¹³. Intensive multiagent chemotherapy including etoposide is applied despite increased off-target effects observed with high concentrations of chemotherapeutics. The accumulation of dose-limiting toxicities in these drugs manifests the need for a more effective delivery platform to decrease off-target effects while maintaining the effects of intensive therapy.

1.4 Off-target effects of etoposide. Cytotoxic off target effects can be observed upon systematic administration of chemotherapeutics because their therapeutic activity is often derived by targeting molecular pathways that are shared between rapidly proliferating cancer cells and healthy cells. Although, these drugs are somewhat more effective at killing tumor cells by virtue of their rapid cell division or defects in signaling pathways.

Clinically, etoposide is one of the most common and effective chemotherapeutic drugs administered for cancers like neuroblastoma despite being poorly soluble in aqueous solutions. Administration of hydrophobic etoposide necessitates slow infusion over 30-60 minutes and the

use of solubilizing agents such as surfactants and alcohols to prevent precipitation of etoposide during systemic treatment¹⁷. In addition to difficulty in administration, major side effects of etoposide include myelosuppression and acute hypotension due to activity of the drug on the bone marrow and cardiovascular system. Observed low levels of white blood cells, called leukopenia, is part of a larger condition called myelosuppression in which the bone marrow produces fewer vital circulating cells due to etoposide toxicity. Many other organ systems are subject to off-site effects, including the cardiovascular, nervous, gastrointestinal, and genitourinary systems³. Unfortunately, many effects, such as neurologic deficits and fibrosis fail to resolve following cessation of chemotherapy.

Etoposide is cleared from the body primarily via the renal system, and blood levels of the drug can fluctuate significantly in patients suffering renal dysfunction due to other nephrotoxic drugs or underlying disease^{18, 19}. Maintaining therapeutic etoposide levels in the body while avoiding toxicity becomes challenging, especially in pediatric patients with a much smaller volume of distribution. Thus, a more effective delivery platform is necessary to shuttle etoposide to its target site of a given tumor or disseminated cancer growth. Nanoparticle delivery systems have been formulated to carry various drugs during systemic administration.

The prevalence of off-target effects has been the driving force behind the investigation into alternative therapeutic approaches that specifically target cancer cells. Changes to traditional cancer therapy include the implementation of new types of treatment, such as hormone therapy, usually in conjunction with older strategies such as surgery and radiation therapy²⁰. These courses of combinational therapies result in enhanced remission in patients, but approximately one third of cancer patients will fail to defeat their disease^{21, 22}. Dose escalation over the last 20-30 years has pushed traditional chemotherapeutics to the limits of patient tolerance, in many cases without appreciable benefits in survival, hence the need for better biologically-based therapies with higher specificity and fewer unintended effects.

Therapeutics that target biological processes perhaps using antibodies or peptides that precisely target specific signaling pathways, aberrant protein interactions, or tumor-specific markers are on the horizon of cancer therapy.

1.5 Cancer biomarkers and GD2 expression. Biomarker research is a way to understand disease and potentially provide a framework for approaches, other than traditional chemotherapy, that target either aberrant cellular processes or signaling. A feature of cancer cells is that particular proteins are sometimes over or under expressed relative to healthy cells. This could be due to disruptions in metabolic factors and pathways, malfunctioning signaling mechanisms, or other unknown cellular perturbations. Cancer-specific protein overexpression has been the focus of a large proportion of drug development research in recent years. While both intracellular and extracellular proteins can serve as biomarkers and potential drug targets, surface-expressed proteins are being utilized for new targeted therapies using antibodies and modern drug delivery systems. For example, vascular endothelial growth factor (VEGF) is a protein overexpressed in the cells of multiple cancer types²³. Bevacizumab is an antibody that specifically binds VEGF and is being utilized for cancer therapy in patients with colorectal cancer, lung cancer, renal cell carcinoma, and some aggressive brain tumors^{24, 25}.

Targeting by specific antibodies is expanding from tumor-specific protein expression to characteristic lipids and macromolecules found in tumor cells. One such example is the cancer biomarker GD2, a specialized lipid expressed by tumors of neuroendocrine origin (e.g., melanoma, ganglioneuroma and neuroblastoma)^{26, 27}. GD2 is a ganglioside composed of a glycosphingolipid (a lipid containing a combination of a carbohydrate and sphingosine group) specifically modified with two sialic acid groups²⁸. Gangliosides naturally exist within the cell membrane where they modulate cell recognition and signal transduction, converge in lipid rafts, and are expressed on all vertebrate tissues^{29 30}. Gangliosides are present abundantly in the central nervous system where they function by interacting with ganglioside-binding lectins such

as myelin-associated glycoprotein and assist with the myelination of axons³¹. Gangliosides GD2 and GD3 have been identified in surface adhesion domains of melanoma cells and are postulated to mediate adhesion of melanoma as well as neuroblastoma tumor cells by interacting with and modulating receptors for the extracellular matrix^{32 33}. GD2 expression in healthy tissue is largely restricted to the central and peripheral nervous system, and the highest levels of expression are seen during early stages of neurodevelopment³⁴. Alterations in ganglioside synthesis pathways in cancer can result in high levels of gangliosides such as GD2, GD1, and GT1 in particular cancer types³⁵. For example, greater than 90% of soft tissue sarcomas analyzed in one study were found to overexpress the ganglioside GD2³⁵. Levels of overexpression and heterogeneity between and within neuroblastoma cell lines are not well described in the literature^{9, 36}.

The vast majority of neuroblastoma tumors are expected to express elevated levels of GD2. One study found that only 3 cases lacked GD2 positive staining among 191 patients and 288 bone marrow samples³⁷. Of those 3 cases, two of the three were found to express GD2 at the time of diagnosis and not at relapse. It was suggested that anti-GD2 therapy might select for GD2 negative blastoma. However, Kramer et al. communicated that 98% of neuroblastoma express homogenous GD2 expression both before and after anti-GD2 monoclonal antibody therapy, suggesting that loss of GD2 expression is uncommon and cannot account for failure of treatment³⁸. GD2 expression in human samples in studies appears to be limited to positive or negative GD2 reactivity as assessed by bone marrow immunofluorescence or tumor immunohistochemistry.

1.6 Cancer immunotherapy. One alternative to traditional chemotherapy that makes use of biomarker technology is immunotherapy, where biological agents engage a patient's immune system in the cancer-fighting process. The concept of using biological agents to stimulate the immune system to fight cancer growth was proposed in 1890, when William Coley

demonstrated remission of an inoperable tumor by repeated injections of bacterial extracts, establishing the new field of immunotherapy³⁹. Successive research led to the use of Bacillus Calmette-Guerin (BCG) and other immune system-activating substances as treatment for certain solid tumors (e.g., bladder cancer⁴⁰). Widespread use of immunomodulators for cancer therapy was not adopted until later in the 19th century due to concurrent advances in molecular biology^{41 42}.

Current immunotherapeutics can be separated into three major categories: monoclonal antibodies (MAbs), non-specific therapies, and vaccines⁴³. Non-specific therapies include biological and chemical agents such as interferons and interleukins found to enhance the immune system's ability to attack cancer cells⁴⁴. Interleukin-2 and granulocyte macrophage colony-stimulating factor (GM-CSF) are currently given alone or in combination with immunotherapeutics such as vaccines to enhance the patient's immune reaction against cancer and other diseases⁴³. Cancer vaccines engineered to focus immune reactions against tumor antigens are currently being investigated, and one drug, sipuleucil-T, has achieved FDA approval in the US for the treatment of prostate cancer, with a reported increase in survival of 4.1 months compared to traditional treatment in patients with high grade metastatic disease⁴⁵⁴⁶. Both nonspecific immunomodulators and vaccines have many merits, but MAbs designed to specifically target particular antigens on tumor cells are of particular interest for the development of new drug delivery systems.

1.7 Monoclonal antibodies and anti-GD2 immunotherapy. In the 1970's and 1980's, tumor-binding antibodies were developed by cancer immunologists that enabled white blood cells to target tumor cells after activation with cytokines (e.g interleukin-2)^{47, 48}. Since then, immunotherapy via antitumor MAbs has been investigated aggressively thanks to concurrent discovery of numerous tumor-associated biomarkers⁴⁹. The production of MAbs was invented

by Georges J. F. Köhler and César Milstein in 1975 ultimately earning them the Nobel Prize in 1984 for Medicine and Physiology.

Targeted monoclonal antibodies are typically produced by first exposing an animal to a given antigen. Next, antibody-producing cells are collected from the exposed mouse and fused with immortal myeloma cells capable of indefinite growth in cell culture⁵⁰. Finally, the fused cells are separated and grown individually, producing cell lines generated from a single myeloma-immune cell hybrid, also called a hybridoma⁵¹. The resulting antibodies are then analyzed for target antigen binding by traditional molecular biology techniques such as immunoprecipitation⁵². Hybridomas producing desired antibodies are then expanded to produce clonal populations which produce one single monoclonal antibody or MAb^{51 52}. The hybridoma cells can facilitate production of MAbs *in vitro*, or they can be injected into the peritoneal cavity of mice where they produce large amounts of the MAb in abdominal fluid which can be purified for pharmaceutical use⁵².

MAb production methods were applied using cellular material from neuroblastoma cells as antigens, ultimately leading to the discovery of anti-GD2 MAbs⁵³. The monoclonal antibody, 3F8, was isolated after immunizing mice with neuroblastoma lysates and found to specifically bind GD2 without cross reactivity to similar other gangliosides such as GT1b, GM1a, or GD1a^{53, 54}. Pre-clinical studies suggested that 3F8 induces an immune response where monocytes, lymphocytes, and granulocytes attack neuroblastoma cells that have bound the 3F8 antibody via antibody-directed cellular cytotoxicity (ADCC), and dose-dependent toxicity was observed by complement-mediated cytotoxicity (CMC)⁵⁵.

The first anti-GD2 MAb tested in humans was the 3F8 (IgG3) antibody, developed as a treatment for neuroblastoma⁵⁶. A single-arm study evaluating the use of 3F8 in addition to immunomodulators interleukin-2 (IL-2) and cytokine granulocyte macrophage colony-stimulating factor (GM-CSF) in patients with high-risk stage 4 neuroblastoma found a 5-year

progression-free survival of 62% compared to the current treatments that result in less than 40% survival^{9, 57}. Immunomodulators have been included in most studies with 3F8 and other anti-GD2 antibodies due to the increased 3F8-induced ADCC observed compared to 3F8 without immunomodulator therapy⁵⁸. Additionally, a phase II clinical study combining 3F8 with GM-CSF observed complete remission of bone marrow disease in 80% of 19 patients resistant to neuroblastoma chemotherapy⁵⁹.

Despite encouraging clinical results, the majority of success with 3F8 immunotherapy has been observed as a tertiary therapy in patients with minimal residual disease as opposed to bulky tumor masses³⁶. Additionally, patients with repeated 3F8 treatment in short time periods develop human anti-mouse antibodies (HAMA) to 3F8 antibodies causing decreased anti-tumor efficacy and limiting the frequency of 3F8 doses possible⁵⁷. Genetic techniques have been employed to humanize 3F8 and other anti-GD2 antibodies such as ch14.18 by replacing mouse-specific residues with those of human antibodies⁶⁰. Humanized antibodies (prefixed “hu”) such as hu14.18 and hu3F8 were found to decrease the occurrence of HAMA, although human anti-human antibodies (HAHA) still interfere with repeated dosing⁶¹.

Dose-limiting features of 3F8 include off-target effects and inactivation by the patient’s immune system. 3F8 immunotherapy is associated with significant pain and pain-associated hypertension, likely due to the off-target effects because of GD2 present on peripheral nerves⁶². Although the pain usually resolves, it may result in persistent arthralgia. The vascular system can also react badly to high levels of the 3F8 antibody in “capillary leak syndrome”, where the patient’s vascular system temporarily loses the ability to maintain volume, resulting in a loss of effective gas exchange, or hypoxia⁶³.

The combination of side effect profiles, necessity for additional immunomodulators, and dose-limiting immune responses results in an increased need to make anti-GD2 immunotherapies more effective at lower doses.

1.8 Nanotechnology in medicine. Medical nanotechnology is the use of synthetic materials, or nanomedicines, that have nanoscale properties for medical applications. “Nano” from the greek νᾶνος for "dwarf", is a prefix meaning one billionth and typically refers to particles and materials with features less than 1,000 nanometers in diameter. Nanotherapeutics are nanoscale particles being developed from numerous materials such as gold, silicon, and lipids, figure 1. Nanomaterials have unique physical properties that manifest when materials are synthesized with nanoscale features. For example, hollow gold nanoshells have been engineered to absorb near infrared light by altering the gold shell thickness⁶⁴, figure 1, B. Hollow gold nanoshells can be engineered to release drug or heat up locally upon exposure of the particles to infrared light which passes harmlessly through living tissue⁶⁵.

Silicon-based porous nanoparticles have been used to carry drugs and genetic payloads for medicinal applications like anti-cancer therapy and gene therapy⁶⁶, Figure 1 C. Inorganic nanomaterials (e.g. silica nanoparticles) can be produced in many shapes such as rods or disks and undergo surface modification such as cationic coatings to modulate interactions with cells^{66 67}. Problems with inorganic nanoparticles arise with cellular toxicity due to difficulty metabolizing silicon nanomaterials and toxic remnant chemicals present from synthetic processes⁶⁷.

Early clinical successes in nanomedicine included the production of lipid vesicles to carry chemotherapeutics⁶⁸, Figure 1 A. Doxil, the first FDA-approved lipid vesicle carrier, consists of the DNA intercalating agent, doxorubicin, encapsulated inside lipid vesicles about 100 nanometers in diameter⁶⁹. These lipid vesicle carriers, called liposomes, altered the biodistribution of doxorubicin when injected systemically and decreased cardiotoxicity and other cytotoxic effects often observed with chemotherapeutics administered alone^{70 71}. Liposomes have emerged as the dominant nanoparticle with respect to translation from the lab into the

clinic due to their nontoxic profiles, ease of manufacture and potential for modification and targeting^{72 73}.

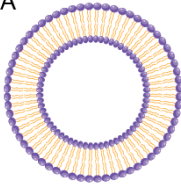


	Nanoparticle Type	Raw Materials	Size (nm)	Applications	
A		Liposome	Phospholipids, cholesterol	30-800	Model cell membrane Drug delivery Gene therapy
B		Hollow Gold Nanoshell	Gold, Au	20-300	Thermal ablation Drug delivery Electron microscopy
C		Porous Silica Nanosphere	Silica, SiO ₂	80-500	Drug delivery Catalysis Imaging

Figure 1. Three types of nanoparticles for medical applications.

Liposomes, hollow gold nanoshells, and silica microspheres are illustrated alongside respective synthetic materials, typical sizes in nanomedical applications, and common applications in the scientific field.

1.9 Targeted liposomes. The combination of biomarker research with nanomedicine yields the possibility to target therapeutic nanoparticles to specific cells of interest. Indeed, multiple targeted drug delivery platforms have been developed and studied^{74, 75}. With respect to GD2 expression, anti-GD2 antibodies have shown promise as targeting agents for nanoparticle systems carrying biological and cytotoxic payloads^{76, 77}. For instance, Allen et al. produced liposomes carrying genetic payloads that were delivered specifically to GD2-expressing cells resulting in the depletion of the anaplastic lymphoma kinase gene *in vitro* and *in vivo*⁷⁸.

Alternatively, the synthetic retinoid, fenretinide has been delivered with competitive and specific binding to melanoma and neuroblastoma cells via anti-GD2 liposomes²⁶. Despite these advances, no targeted liposomal formulations have been fully approved by the FDA for clinical use suggesting that manufacturing complications or insufficient efficacy has delayed approval for clinical applications⁷⁹. These barriers to FDA approval can be negotiated by adapting more simple and precise manufacturing techniques along with more effective drug encapsulation and targeting tactics. To our knowledge, no attempts have been made to deliver one of the first line agents (e.g. etoposide), a topoisomerase inhibitor, to GD2-positive malignancies, even though systemic etoposide treatment remains a first-line therapeutic option for high-grade neuroblastomas.

This work describes the combination of modern, specific anti-GD2 antibodies with the traditional chemotherapeutic agent, etoposide via synthetic nanocarriers to produce a more precise and effective drug delivery system for GD2-positive malignancies. While all of the components within the final nanocarriers have been studied independently, their synergistic combination imparts new properties to an existing front-line therapy for neuroblastoma that may allow increased dosing to specific tumor cells and decreased off-target effects that may produce a more robust and better tolerated treatment approach.

1.10 Overall Hypothesis. I hypothesize that immunoliposomes can be decorated with anti-GD2 antibodies and loaded with etoposide for targeted drug delivery to tumor cells with GD2 surface expression. Moreover, I hypothesize that the targeted immunoliposomes will inhibit proliferation of GD2-positive cells more than untargeted therapies due to receptor-mediated increased tumor cell uptake of drug-loaded liposomes.

Section I: Formation of the Targeted Etoposide Nanocarrier

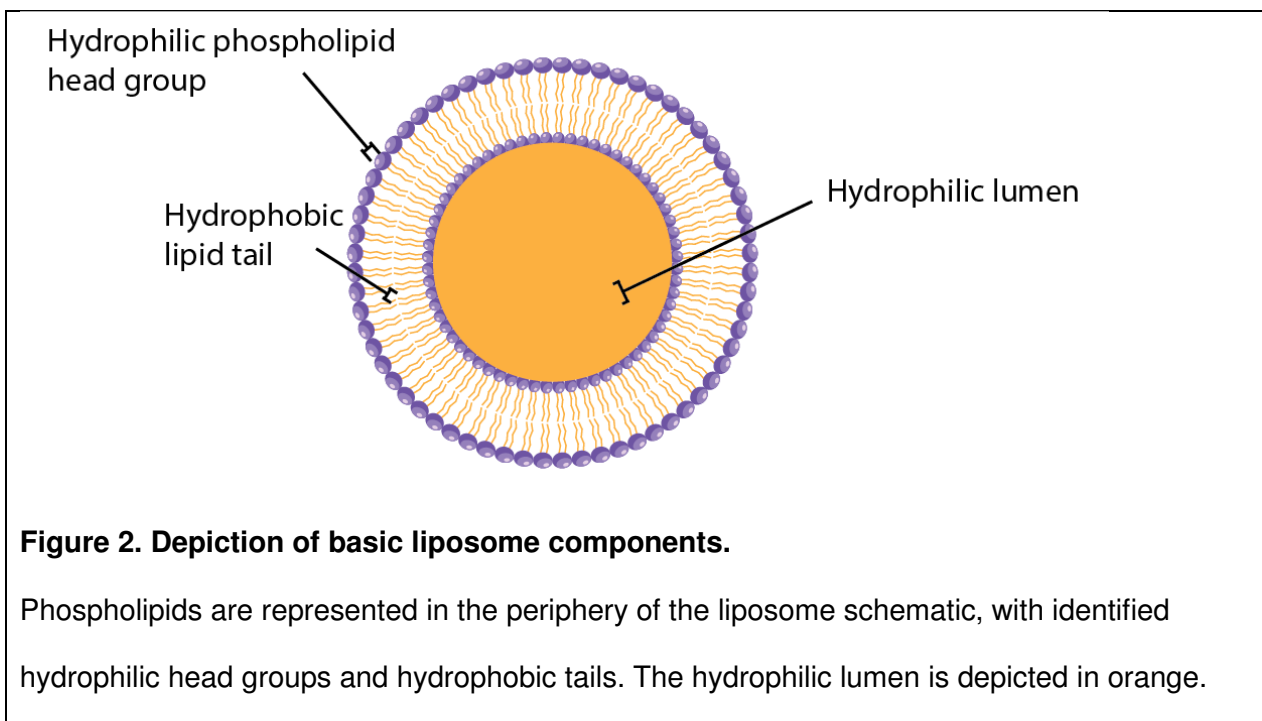
Rationale: Etoposide has been incorporated into untargeted liposomes previously. Attempts at the encapsulation of etoposide into untargeted liposomes yielded promising results, with Sistla et al. suggesting liposomal etoposide maintained more stable blood levels over time and resists clearance compared to the drug alone⁸⁰. Other liposomal etoposide studies examined alternative routes of administration, including oral⁸¹ and inhaled liposomes⁸². Previously produced etoposide liposomes either sought enhanced drug effects through combination therapy with other drugs or via passive features of the liposomes that enhanced tumor uptake.

Liposomal etoposide alleviates some problems with drug solubility but fails to manage off-site effects. Targeting of liposomes potentially drives down dosing requirements and off-site effects while increasing the efficacy of treatments. Combination of powerful liposomal etoposide with a proven targeting antibody such as 3F8 provides a viable strategy to treat GD2 positive malignancies. To our knowledge, there are no other targeted etoposide immunoliposomes. Prior to biological testing drug platform, this targeted drug delivery system must be fully characterized physiochemically, and efforts must be made to ensure a reproducible and reliable product.

Chapter 2: Liposome Assembly and Etoposide Loading

2.1 Liposomal background. Liposomes were first described in 1961 by Alec D Bangham, a British hematologist who was experimenting with phospholipids and observed circular bilayer structures on a newly acquired electron microscope⁸³. The cell-like vesicles observed mimicked a cell membrane and represented pioneering evidence that the cell membrane consisted of a lipid bilayer. Phospholipids are amphiphilic lipids with a hydrophilic phosphate head group and a hydrophobic tail made up of glyceride bearing two hydrocarbon chains. Lipids vary in their head groups as well as hydrophobic tails, resulting in different melting temperatures and tendencies to form membranes⁸⁴.

The circular bilayer structures observed by Dr. Bangham are now known as liposomes. Liposomes are hollow phospholipid-based spheres with an outer lipid bilayer shell. Lipid bilayers are composed of two polar lipid sheets with hydrophobic tails of each sheet oriented toward each other and polar hydrophilic heads facing outward from the bilayer as seen in Figure 2.



This configuration of lipids is driven mainly by hydrophobic effects which act to orient amphiphilic macromolecules (phospholipids) in such a way as to minimize interactions of the hydrophobic fatty acid tails with the surrounding water-based environment⁸⁵. This organization of amphiphilic material into a bilayer results in a barrier capable of separating aqueous compartments, Figure 2. Compartmentalization is vitally important in cells allowing the separation of subcellular organelles and nuclei, and liposomes utilize this feature by carrying cargo (such as drugs or imaging agents) intact through dynamic environments.

Artificially formed lipid membranes are used to study model membrane function, and when formed into hollow spheres, single or multi-lamellar vesicles (also called liposomes) have been utilized in diverse applications such as carriers for dyes, pesticides, enzymes, nutritional supplements, cosmetics, and with respect to this work, targeted drug delivery⁷². Basic properties of these membranes originate from the lipids that make them up, while functional

properties are often determined by surface characteristics in combination with a cargo, or payload.

2.2 Liposome physics. Physical features of liposomes are largely dependent on the nature of the lipids that make them up. Certain lipids self-assemble into vesicles when introduced into an aqueous solution. In order for lipids to form lipid bilayers and liposomes, lipids must be able to move freely near each other, and they must have the capacity to pack together to form a sphere. Lipid movement and membrane flexibility involve a critical temperature called the “transition temperature,” defined as the minimum temperature for lipids required to induce a fluid-like state where liposomes can self-assemble. This state is called the disordered liquid crystalline state, contrasting with the ordered gel phase where lipids are closely packed and movement of lipids is restricted⁸⁶. This is important for both liposome formation and drug loading because the liquid crystalline state is required for liposome formation, but drug release is slower and more controlled in the ordered gel phase. At temperatures exceeding the critical temperature, liposomes reenter the liquid crystalline state where more loaded cargo leaks out due to increased permeability of the membrane. For this reason, dipalmitoylphosphatidylcholine (DPPC) is commonly used when forming liposomes because DPPC is a lipid with a transition temperature (41 °C) above that of the body’s temperature (37 °C) and thus DPPC liposomes would retain their loaded drugs during administration in humans or animals. In addition to temperature requirements, lipids must be chosen with volumetric properties that allow formation into small vesicles, as indicated by their packing parameter.

Different sized particles, both single and bilayer, can spontaneously form when formulating vesicles. The ability for the lipids to pack together can be described mathematically by a packing parameter (Figure 3), which describes the shape of a lipid with respect to its

ability to pack together into an aggregate when exposed to an aqueous medium and provides an estimate of the type of particles that will self-assemble for a given lipid⁸⁷.

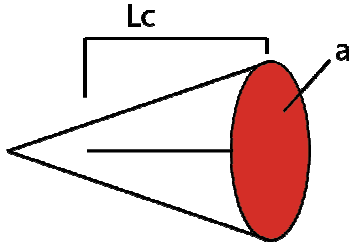
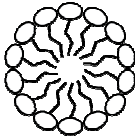
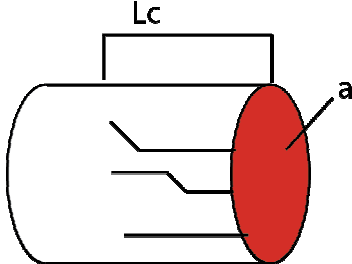
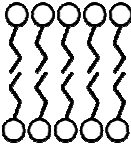
Packing Parameter (N_s)	Volumetric Shape	Aggregate Shape
$<1/3$		 Micelle
$1/3-1/2$		 Lipid bilayer

Figure 3. Packing parameters determine lipid assembly geometry.

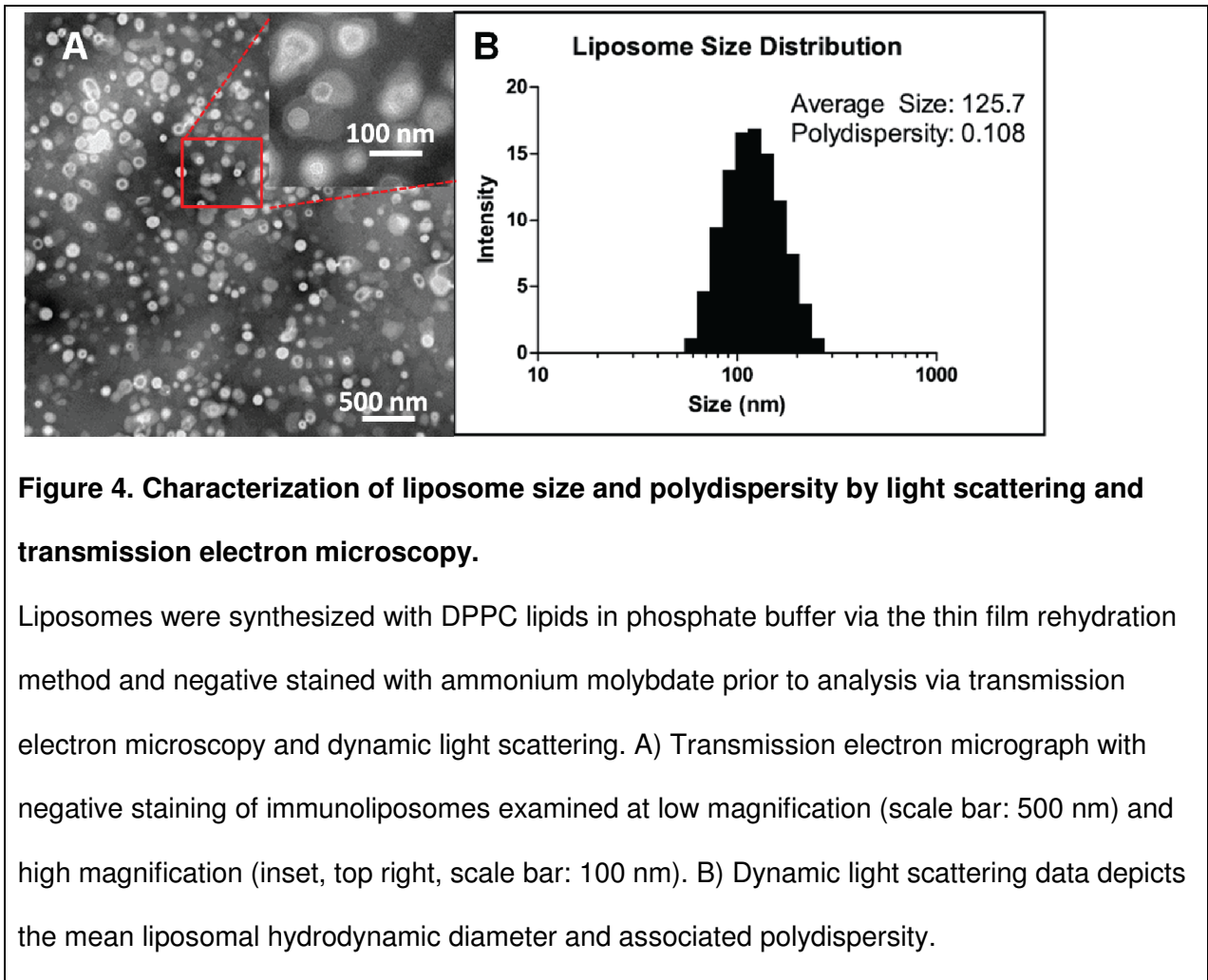
Depicted here are two lipids with packing parameters less than 0.33 (top) and 0.33-0.5 (bottom). The volumetric shape (middle) is determined by the fatty acid tail length, L_c , area of hydrophobic core, a , and volume of the hydrophobic chain V_c . Resulting structures when the lipids are aggregated together in an aqueous environment are depicted in the right column.

The formula for the packing parameter is:

$$N_s = V_c / (a * L_c)$$

where (V_c) represents the volume of the hydrophobic fatty acid chains, (a) denotes the cross sectional area of the liposome or aggregate and (L_c) signifies the fatty acid length. Lipids with an $N_s \leq 1/2$ tend to form micelles, described later in this work, and lipid formulations with an $N_s > 1/2$ tend to form lipid bilayers when in an aqueous environment. DPPC within a bilayer has a

packing parameter of 0.7, indicating the ability to form lamellar structures such as liposomes⁸⁸. Figure 4 represents a standard liposomal formulation using DPPC lipids and cholesterol, analyzed by electron microscopy and light scattering, methods described in the next section of this chapter.



Lipids can be dissolved completely in organic solutions, and lipid bilayers spontaneously form when the organic solution is evaporated while the solution is heated above the transition temperature. The bilayers formed are typically in thin layers, called thin films. When thin films of phospholipids such as DPPC encounter an aqueous solution at a temperature above the transition temperature, vesicles spontaneously form, or self-assemble.

The vesicles are typically multilamellar and among a varied size distribution, but dimensions can be tailored by managing the lipids and environment where they self-assemble.

In addition to temperature and material selection, liposome preparation protocols have been generated utilizing an array of synthetic methods including sonication, microinjection, extrusion, and freeze-thaw cycles. With respect to drug delivery, two major liposome preparation protocols, thin film rehydration and ethanol injection, are discussed here for the encapsulation of the hydrophobic drug, etoposide.

2.3 Summary of liposome characterization methods. Liposomes are characterized by an array of techniques in a multimodal approach, as no one single technique adequately describes all liposomal features. These methods are introduced here and are discussed throughout the section.

Liposome size, size distribution, and surface charge are all experimentally determined using the dynamic light scattering (DLS) technique. During DLS analysis, a colloidal suspension of the particle of interest is illuminated with a laser at a known angle within an aqueous medium of known viscosity. The pattern of light scattering yields variations in intensity that correlate with particle diameter. The distribution of particle diameters within a solution is described by the polydispersity index (PDI). The PDI ranges from 0 to 1, with 0 being completely monodispersed, and 1 being a completely heterogeneous mixture of sizes. Experimentally, all liposomal formulations have some degree of polydispersity, and formulations with a controlled size for medical applications should have a PDI of less than 0.3⁸⁹.

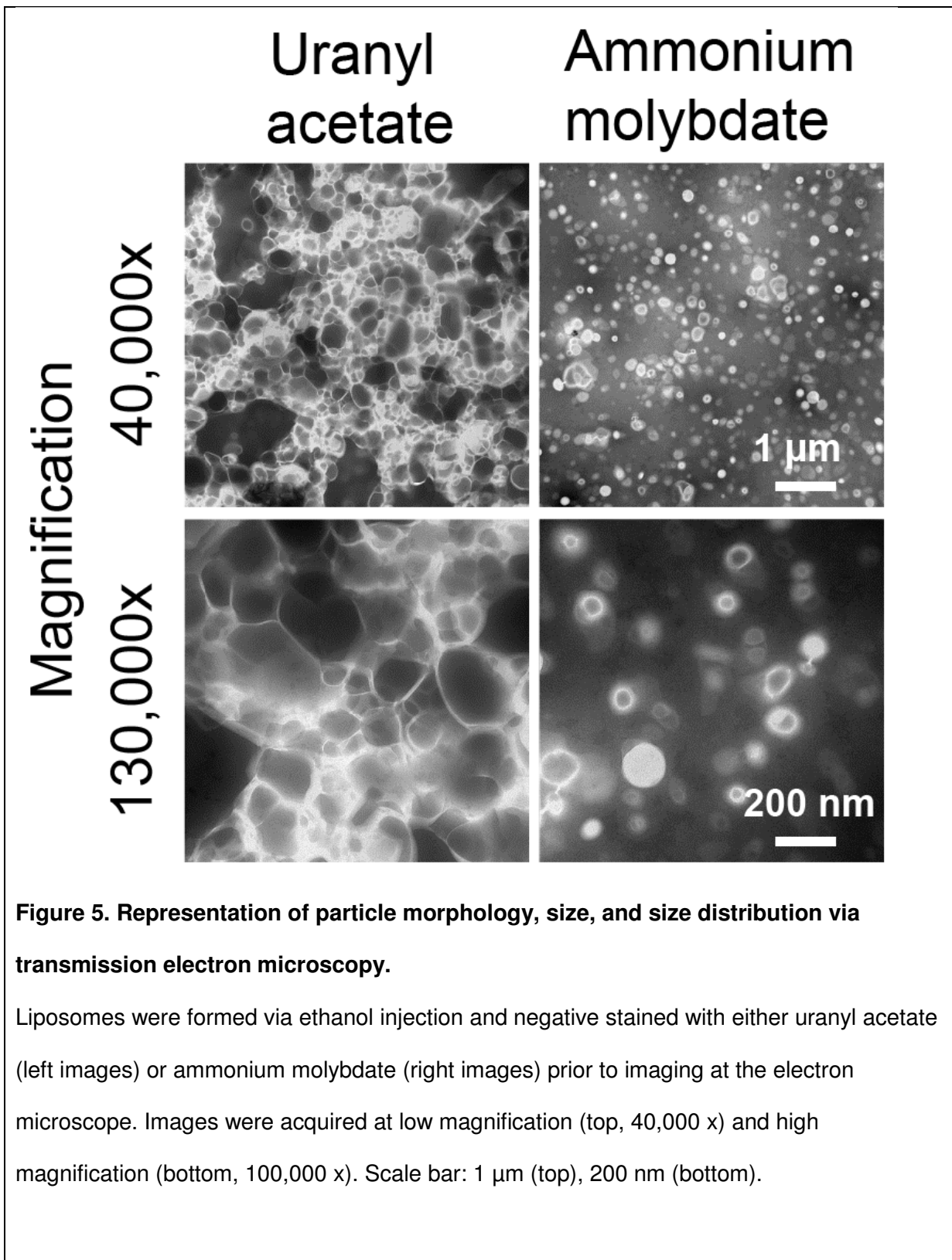
When a charge is applied across the sample in DLS, scattering intensity fluctuations produce data that can be translated to particle surface charge or zeta potential (ZP). Surface charge is important for nanomedicines because positively charged or cationic nanoparticles can be more readily taken up by negatively charged cellular membranes, and neutrally charged

nanoparticles lack sufficient repulsion from each other and may aggregate. Most commercially available liposomes for medicinal use have a negative ZP.

Drug loading with etoposide is determined after liposome synthesis by separation of drug-loaded liposomes from free drug via ultracentrifugation or ultrafiltration. Free drug is then quantified via high pressure liquid chromatography (HPLC). The process of HPLC involves passing the drug through a column where it is isolated and analyzed by absorbance of a given wavelength of light (228 nm for etoposide).

The presence or absence of specific molecular bonds can be determined by both Fourier transform infrared spectroscopy (FTIR) and nuclear magnetic resonance (NMR). Both techniques identify a spectrum of a given sample that produces peaks correlating with specific bonds and arrangements of atoms. For FTIR, the spectrum is obtained by analyzing an infrared spectrum of absorbance within a sample. Conversely, NMR uses a large magnet and specialized detectors to analyze the resonance frequency of particular bond conformations. In essence, NMR analysis is used to confirm the identity of a substance.

Transmission electron microscopy (TEM) is often used for nanoparticles including liposomes and generates an image based on the transmission of electrons through a sample onto a detector. The detector then produces a visible image from the transmission data. TEM has tremendously high magnification abilities, approaching 500,000 x. Light microscopy approaches 2,000 x. Lipid bilayer structure, particle size, and immunolabeling with gold-conjugated IgG allow visualization of specific structures. Liposomes are typically negative-stained with electron-dense materials such as uranyl acetate or ammonium molybdate to opacify areas around liposomes, thus highlighting their shapes and membrane features. We examined liposomes with the electron microscope using uranyl acetate or ammonium molybdate, Figure 5.



We found that ammonium molybdate resulted in better images with respect to expected size, shape, and polydispersity based on prior dynamic light scattering,

2.4 Formation strategies for liposomes. Preparing liposomes for self-assembly typically involves dissolving lipids in an organic solution followed by removal of the organic solvent and addition of an aqueous solution in order to optimize organization of lipids into lipid bilayers. One of the most widely utilized methods for this type of liposome formulation is known as thin film rehydration and involves producing a thin film of lipids on glass prior to addition of the aqueous solution. Thin film rehydration is depicted graphically in Figure 6.

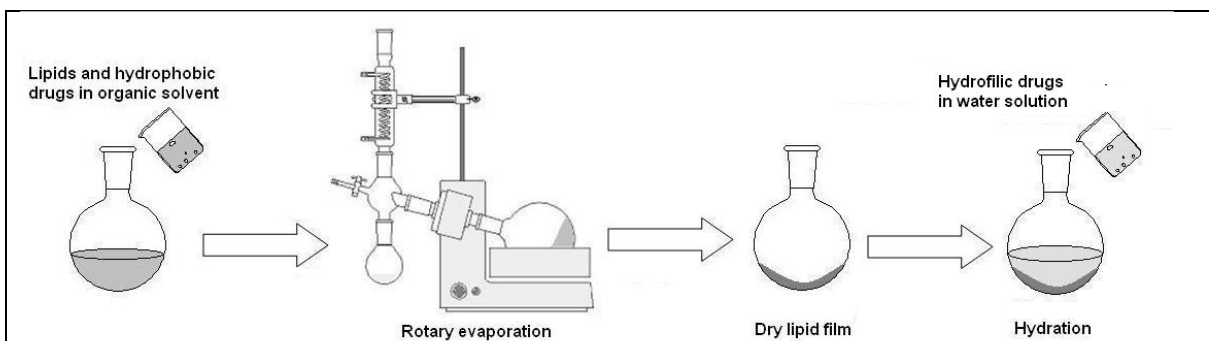


Figure 6. Schematic of liposome synthesis by the thin film rehydration method.

Thin films are produced by dissolving lipids and hydrophobic drugs into an organic solvent such as chloroform. The organic solvent is then removed with heating via rotary evaporation under negative pressure to produce a thin film on the round bottom flask. The dry lipid film is then rehydrated with an aqueous solution to induce the self-assembly of lipid vesicles.

Reference:

Sávia Caldeira de Araújo Lopes, Cristiane dos Santos Giuberti, Talita Guieiro, Ribeiro Rocha, Diêgo dos Santos Ferreira, Elaine Amaral, Leite and Mônica Cristina Oliveira (2013). Liposomes as Carriers of Anticancer Drugs, Cancer Treatment - Conventional and Innovative Approaches, Prof. Letícia Rangel (Ed.), ISBN: 978-953-51-1098-9, InTech, DOI: 10.5772/55290. Open access, permission freely available from: <http://www.intechopen.com/books/cancer-treatment-conventional-and-innovative-approaches/liposomes-as-carriers-of-anticancer-drugs>

To form thin films, dissolved lipids are deposited onto a round bottom flask forming a dried film of lipids consisting of lipid bilayers stacked upon each other. The thin film is then rehydrated with an aqueous medium such as water or buffer followed by high speed agitation

to break up the large sheets of bilayers into smaller vesicles. The dispersion of vesicles produced through thin film rehydration is then be extruded through polycarbonate membranes containing micro-and nanometer pores⁹⁰. Extruding the lipid mixture through membranes of sequentially decreasing size results in unilamellar liposomes of a controlled size⁹¹. Particle diameter could be controlled by using membranes with different pore sizes, while particle charge could be manipulated by altering the types of lipids used as starting material⁹². Advantages of thin film rehydration are its relative simplicity and ability to produce a concentrated solution of liposomes quickly. Blank liposomes (without drug or other loaded substance) produced via thin film rehydration maintain colloidal stability in solution for more than two months at 4 °C. Commercially available extrusion membranes from companies like Wattman[®] and Millipore[®] enable the extrusion of many different sized liposomes from 30-800 nanometers.

Disadvantages of thin film rehydration are apparent when loading hydrophobic drugs into liposomes and quantifying payload or fluorescent lipids. Liposome-encapsulated drugs as well as specialized fluorescent lipids can be lost during extrusion by precipitation onto the extrusion membranes, and exact amounts of remaining lipid and payload must be determined following synthesis via analytical methods such as high-pressure liquid chromatography (HPLC)⁹³. We found that thin films produced with DPPC lipids and the drug etoposide were irregular and resulted in drug precipitants during extrusion.

An alternative to thin film rehydration is the ethanol injection method. Ethanol injection is accomplished by first dissolving a lipid mixture in a pure ethanolic solution followed by injection of this solution into an aqueous medium of much larger volume, Figure 7.

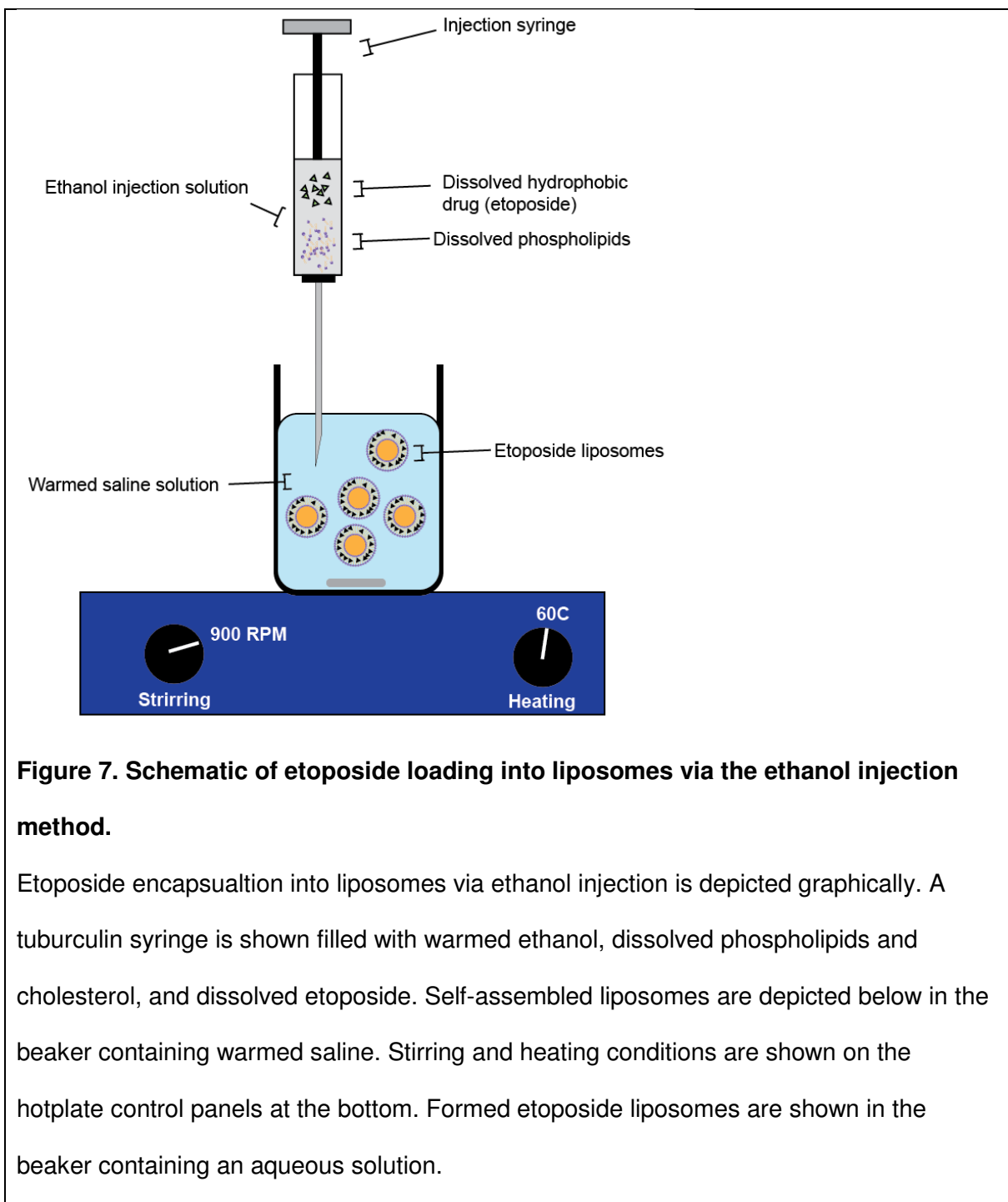


Figure 7. Schematic of etoposide loading into liposomes via the ethanol injection method.

Etoposide encapsulation into liposomes via ethanol injection is depicted graphically. A tuberculin syringe is shown filled with warmed ethanol, dissolved phospholipids and cholesterol, and dissolved etoposide. Self-assembled liposomes are depicted below in the beaker containing warmed saline. Stirring and heating conditions are shown on the hotplate control panels at the bottom. Formed etoposide liposomes are shown in the beaker containing an aqueous solution.

As ethanol-dissolved lipids contact the excess volume of aqueous media (such as water or salt buffer), the lipids spontaneously arrange into vesicles⁹⁴. Nanoscale liposomes can be produced by controlling several factors during injection. The size of injection needle, type of

phospholipids, ratio of ethanol to aqueous media, rate of injection and temperature of fluids involved are all factors that contribute to the final diameter of ethanol injected self-assembled liposomes.

Advantages to the ethanol injection are enhanced simplicity (in comparison with thin film rehydration) and the ability to produce liposomes of a controlled size without extrusion. While ethanol injected liposomes can be extruded for further modification of size and lamellarity, it is not necessary if the parameters of injection are well controlled. Monodispersed liposomes with a PDI <0.1 can be produced in sizes between 100-200 nanometers without extrusion⁹⁵. This advantage is of paramount importance for the production of etoposide liposomes, where difficulties can arise during extrusion.

Disadvantages of the ethanol injection method involve the lack of control over the number of liposomal layers or lamella when extrusion is not performed. Additionally, there have been reported difficulties in performing ethanol injection to produce highly concentrated liposomes as limits of dissolved lipids within the ethanolic solution are reached⁹⁶.

2.5 Etoposide loading into liposomes. Initial attempts to encapsulate etoposide into liposomes were performed via the thin film rehydration method followed by serial extrusion through polycarbonate membranes. The thin film method proved ineffective for etoposide encapsulation due to drug precipitation during extrusion at concentrations above 0.25 mg/mL. Etoposide concentrations of at least 2 mg/mL were required for therapeutic doses in future animal studies. Empty, unloaded liposomes or etoposide-loaded liposomes were produced by either thin film rehydration or ethanol injection techniques and analyzed for size and polydispersity, Figure 8.

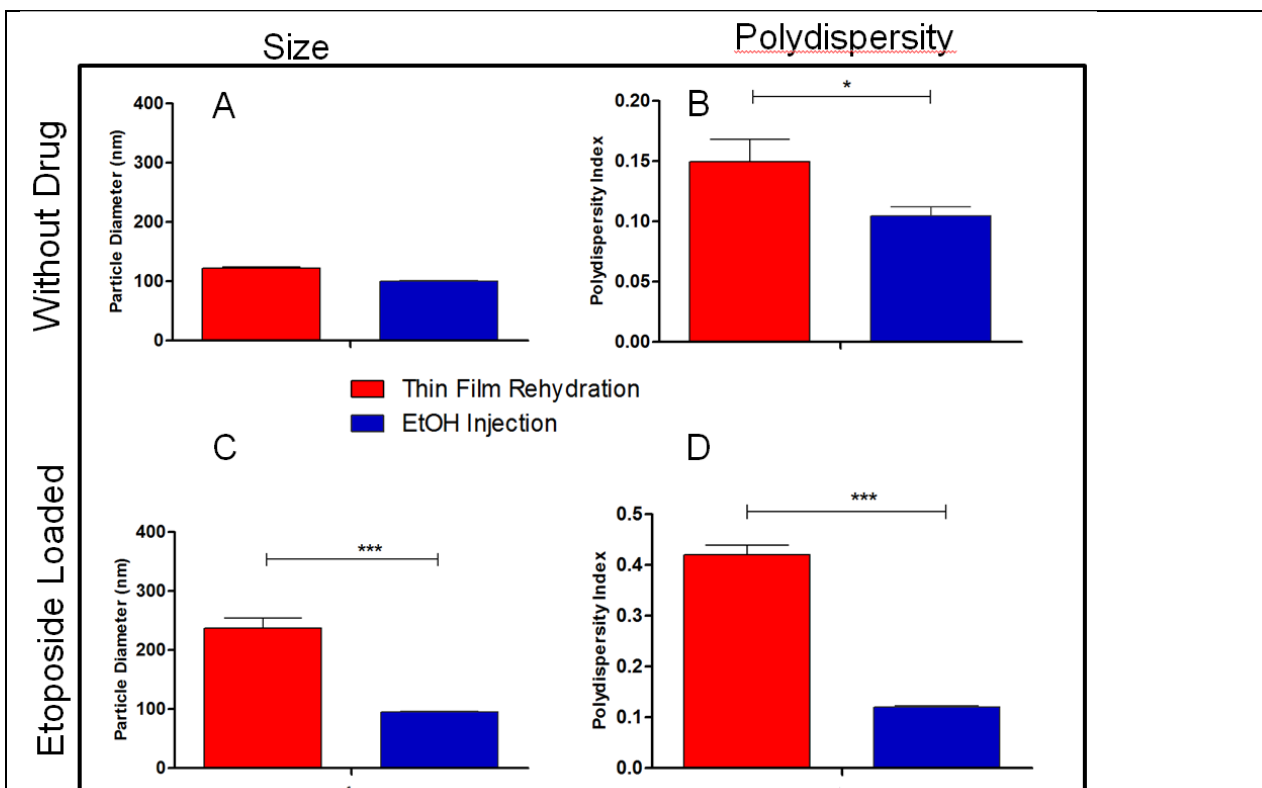
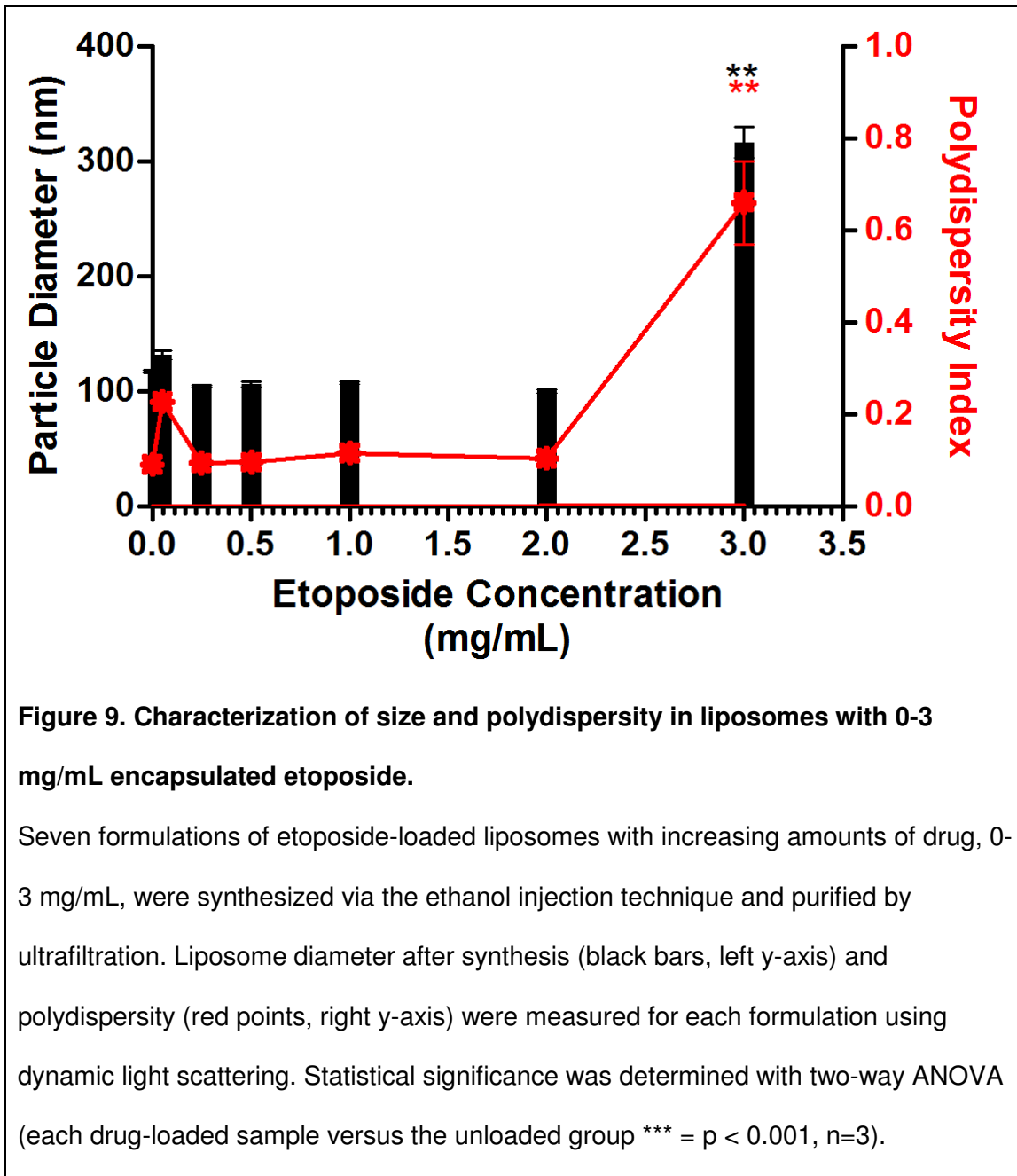


Figure 8. Effects of thin film rehydration or ethanol injection liposome synthesis methods on size and polydispersity.

Liposomes with or without 1 mg/mL etoposide were synthesized by ethanol injection (blue) or thin film rehydration followed by extrusion (red). A, C) Particle diameters from all four formulations were analyzed by dynamic light scattering with a goal size of 100-200 nm for optimal circulation time. B, D) Polydispersity measures of size distribution were also determined by dynamic light scattering. Polydispersities below 0.3 were considered adequately monodispersed formulations. * = $p < 0.05$; *** = $p < 0.001$

Etoposide loading into liposomes via the thin film rehydration technique was found to cause a significant increase in both size and polydispersity of liposomes representing a relatively unstable and non-uniform formulation. The ethanol injection method was adopted, and drug encapsulation was dramatically improved up to 3 mg/mL etoposide without

precipitation encountered with thin film rehydration. We then analyzed the effects on liposome size and polydispersity in liposomes of increasing etoposide concentration, Figure 9.



We found that etoposide loading via the ethanol injection method did not significantly affect size or polydispersity of liposomes up to 2 mg/mL. Above 2 mg/mL, liposome size was

found to increase above 300 nm with a high polydispersity, representing a heterogeneous population of liposomes. Above 3 mg/mL, significant drug precipitants were observed which interfered with obtaining sizes and polydispersity readings via DLS.

Next, the quantity of drug physically encapsulated into liposomes was quantified. Etoposide-loaded liposomes were separated from free, unencapsulated etoposide by ultrafiltration, and free etoposide was quantified by HPLC to determine the entrapment efficiency (EE) and drug loading (DL).

$$EE (\%) = (\text{Quantity of drug encapsulated}) / (\text{Total quantity of drug added}) \times 100$$

$$DL (\%) = (\text{Quantity of drug encapsulated}) / (\text{Total quantity of lipids added}) \times 100$$

EE is a measure of how much drug must be used to load a given amount of drug, while DL concedes information about the amount of liposomal material required to carry a given amount of drug. The EE and DL were determined to be 88.2% (SD 0.5) and 30.4% (SD 4.34), Figure 10.

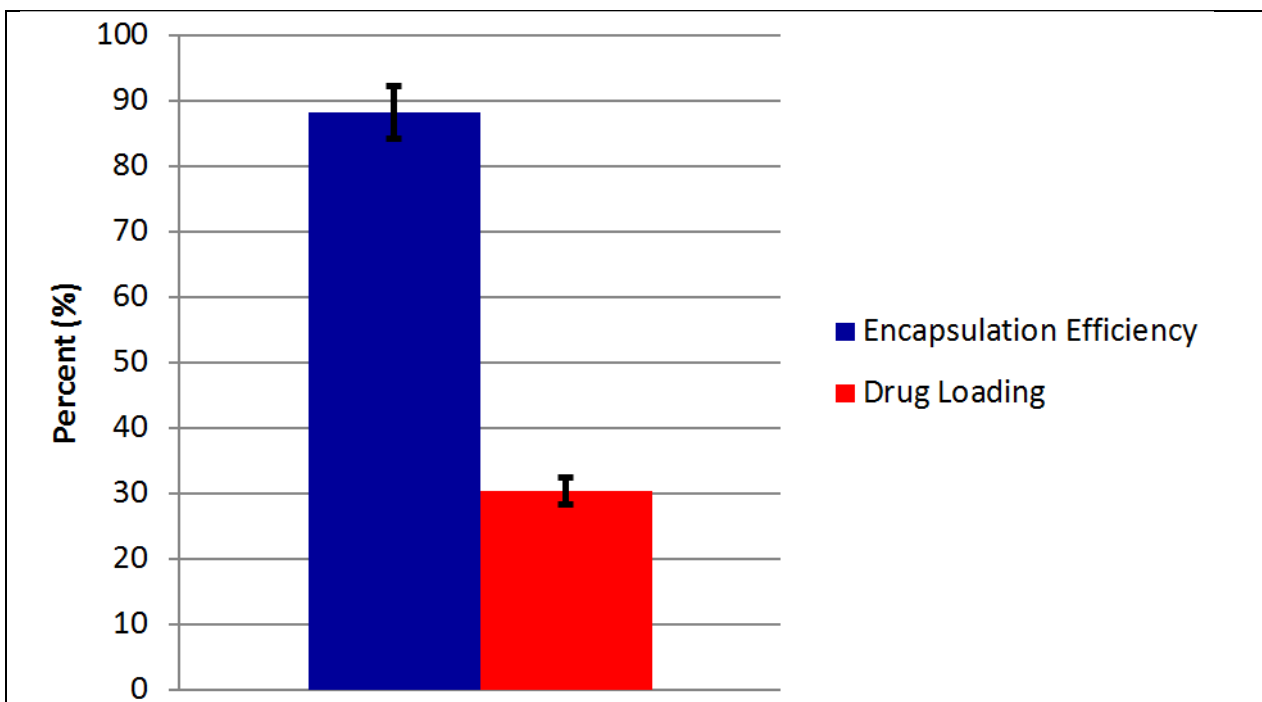


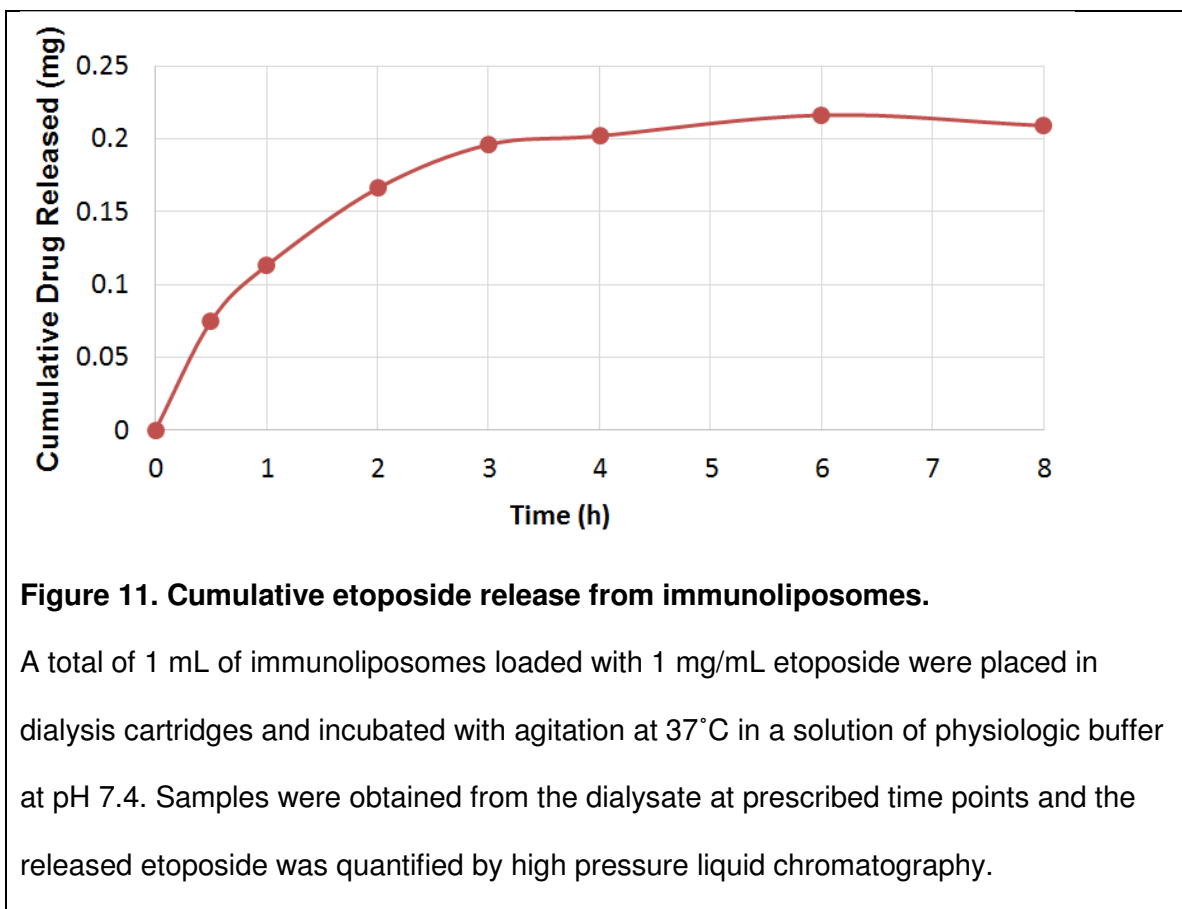
Figure 10. Quantification of etoposide drug loading and entrapment efficiency within liposomes.

Liposomes were formulated with 2 mg/mL etoposide using the ethanol injection technique, and unencapsulated etoposide was separated from liposomal etoposide by repeated ultrafiltration via centrifuge filters. Purified etoposide-loaded liposomes were then lysed and etoposide was quantified by high pressure liquid chromatography. The percent entrapment efficiency (mg drug encapsulated / mg of drug starting material) and drug loading (mg of drug encapsulated / mg of lipid starting material) were calculated from measured unencapsulated drug.

Effectively, the DL is a measure of how effective the carrier material is for containing a given drug, while EE provides information about how much drug is lost during synthesis due to inefficient loading. These values were comparable to those produced in untargeted etoposide liposomes produced by other groups^{81, 82}.

2.6 Release of etoposide from liposomes. Liposomes begin releasing etoposide immediately following synthesis at a variable rate depending on multiple environmental factors. The concentration, temperature, pH, and level of agitation all contribute to the rate that etoposide is released from the liposome carriers. For antitumor efficacy, etoposide must be released from liposomes at a rate slow enough to allow accumulation at the tumor site. While untargeted liposomes require longer circulation times due to a lack of specific binding process, targeted liposomes are expected to interact with target tissue in the first 3 hours in a well vascularized tumor⁷².

Drug release from liposomes was performed using dialysis tubes, but initial attempts at determining the rate of etoposide release failed due to undetectable drug levels from all samples. We presumed this to be due to the poor solubility and precipitation of etoposide prior to sample collection or aggregation of etoposide at the dialysis membrane itself, preventing representative sample collection. This was corrected by adding a small amount of surfactant to the receptor phase of the dialysis experiment similar to the release study conducted by Jinturkar et al.⁸². We investigated the rate of etoposide release from immunoliposomes from 1-8 hours at physiologic temperature and pH, Figure 11.



The final results of the release study indicated that etoposide liposomes exhibited a sustained release of etoposide over the course of 6 hours. Notably, only 0.25 mg of the 1 mg/mL was detected in the dialysate, suggesting that a portion of released material either became entrapped in the dialysis membrane or failed to be released from the liposomes over the duration of the experiment.

Difficulties encountered with etoposide encapsulation underline the need to fully characterize each new synthesis strategy for drug encapsulation. Successful verification of drug loading into the liposomal delivery system laid the foundation for a targeted drug delivery platform. The next stage of liposome functionalization involves surface modification of liposomes with targeting moieties to enhance the efficacy and antitumor activity of liposomes.

2.7 Synthesis conclusions. The notion that we have reached dose-limited toxicity, often with a non-proportional decrease in disease, has driven the search for new therapeutics and new approaches for targeted drug delivery. One approach to treat disease with higher efficacy is the use of liposomal drug carriers that can control the release of cytotoxic chemotherapeutics like the first line agent, etoposide. We hypothesized that etoposide could be stably encapsulated into nanoscale liposomes and subsequently decorated with anti-GD2 antibodies for active targeting.

Indeed, DPPC liposomes were self-assembled via a modified ethanol injection technique that allowed for the simultaneous formation of liposomes and passive drug loading without direct extrusion. This was advantageous and could make manufacturing and scaling production up easier and more efficient. This process resulted in stable 125.7 nm (+/- 1.4) particles with a polydispersity of 0.108. These parameters were previously described as ideal for liposome systemic treatment in the avoidance of nonspecific removal from circulation by the liver and spleen. Entrapment efficiency and drug loading were maximized at 88.2% and 30.4%, respectively, as determined by HPLC analysis. This procedure simultaneously encapsulated up to 4 mg/mL etoposide into 10 mM liposomal formulations, comparing favorably to other etoposide formulations^{81, 97}.

Chapter 3: Targeting Moiety Attachment and Verification

3.1 Passive liposomal targeting. Nanoparticle applications in medicine potentially alter and enhance control over particle and drug biodistribution during treatment. Liposomes have the advantage of a cell-like lipid membrane that is capable of alterations and modifications to control surface interactions between the liposome and the dynamic circulatory environment during medicinal administration. Targeting with liposomes is generally divided into two main genres: passive targeting and active targeting.

Passive targeting involves the size and general surface properties of liposomes capable of altering their biodistribution. Liposomes and other nanoparticles below a certain size threshold (approximately 200nm for normal human circulation) are known to accumulate into cancerous tissue preferentially due to the enhanced permeation and retention (EPR) effect⁹⁸. The EPR effect is the result of nanoparticles circulating through altered vasculature within the tumor microenvironment. Cancer causes rapid development of blood vessels through the release of several angiogenic growth factors such as vascular endothelial growth factor. Cancer-induced angiogenesis results in blood vessels composed of poorly aligned endothelial cells with larger-than-normal fenestrations (producing what is often called “leaky vasculature”) capable of the passage of liposomes and other large macromolecular drugs⁹⁹. Enhanced tumor accumulation of liposomes via the EPR effect is often cited as one of the primary mechanisms for current successes in passively targeted nanomedicines¹⁰⁰.

To maximize the time in circulation for the EPR effect to occur, liposomes can be coated with polyethylene glycol (PEG), a hydrophilic polymer chain. Surface modification with PEG, or “PEGylation”, results in a hydration shell around the liposome or nanoparticle protecting it from removal by the mononuclear phagocyte system (MPS) from circulation. The MPS is composed largely of monocytes and macrophages within the spleen in combination with Kupffer cells within the liver. These cells work together to recognize and remove foreign

substances and senescent blood cells via phagocytosis. MPS recognition of foreign particles is hindered by PEG chains. Hence, PEGylated liposomes remain in circulation for longer periods of time, enabling more particles to accumulate at the tumor site via the EPR effect¹⁰¹.

Other mechanisms for the passive targeting of liposome payloads to tumor cells involve nanoparticle surface modifications. Cationic liposomes have been found to more readily fuse with negatively charged cell membranes, resulting in a particular use for the delivery of genetic contents to the cytoplasm¹⁰². Thermal or pH responsive liposomes have been shown in studies to release payloads at tumor microenvironments that are at slightly higher temperatures or relatively more acidic, respectively¹⁰³.

While innovative, most nanomedicines utilizing passive mechanisms other than the EPR effect have failed to reach federal approval for clinical use due to lack of efficacy or unanticipated side effects due to specialized materials on healthy tissue¹⁰⁴. Additionally, these mechanisms lack true specificity for the tumor cells themselves, underlining the need for a more precise form of targeting. Active targeting addresses this demand by utilizing molecular mechanisms and binding kinetics to directly target tumor cells.

3.2 Active liposomal targeting. Controlling the biodistribution of liposomes via specific targeting mechanisms is termed “active targeting” and is one of the leading edge fields of medical nanotechnology. Active targeting refers to ligand-directed targeting of liposomes to specific sites via monoclonal antibodies, peptides, or other small molecule targeting moieties attached to the liposome surface⁷⁹. Advances in molecular biological techniques revealing multitudes of cancer-specific biomarkers produced countless potential targets for liposomes. For example, folate receptors have been found to be significantly overexpressed in numerous cancerous lines, likely related to the high metabolic requirements of malignant cells. Hence, folate decorated liposomes were produced and shown to be taken up preferentially by the folate-receptor positive cancer cells via receptor mediated endocytosis⁷⁴. Small molecules and

vitamins have been used intermittently as targeting agents for liposomes and other particles, but they have not demonstrated the specificity of more precise targeting moieties such as peptides and antibodies. Of the more stringent targeting moieties, MAbs and antibody fragments are the principal method of targeting liposomes.

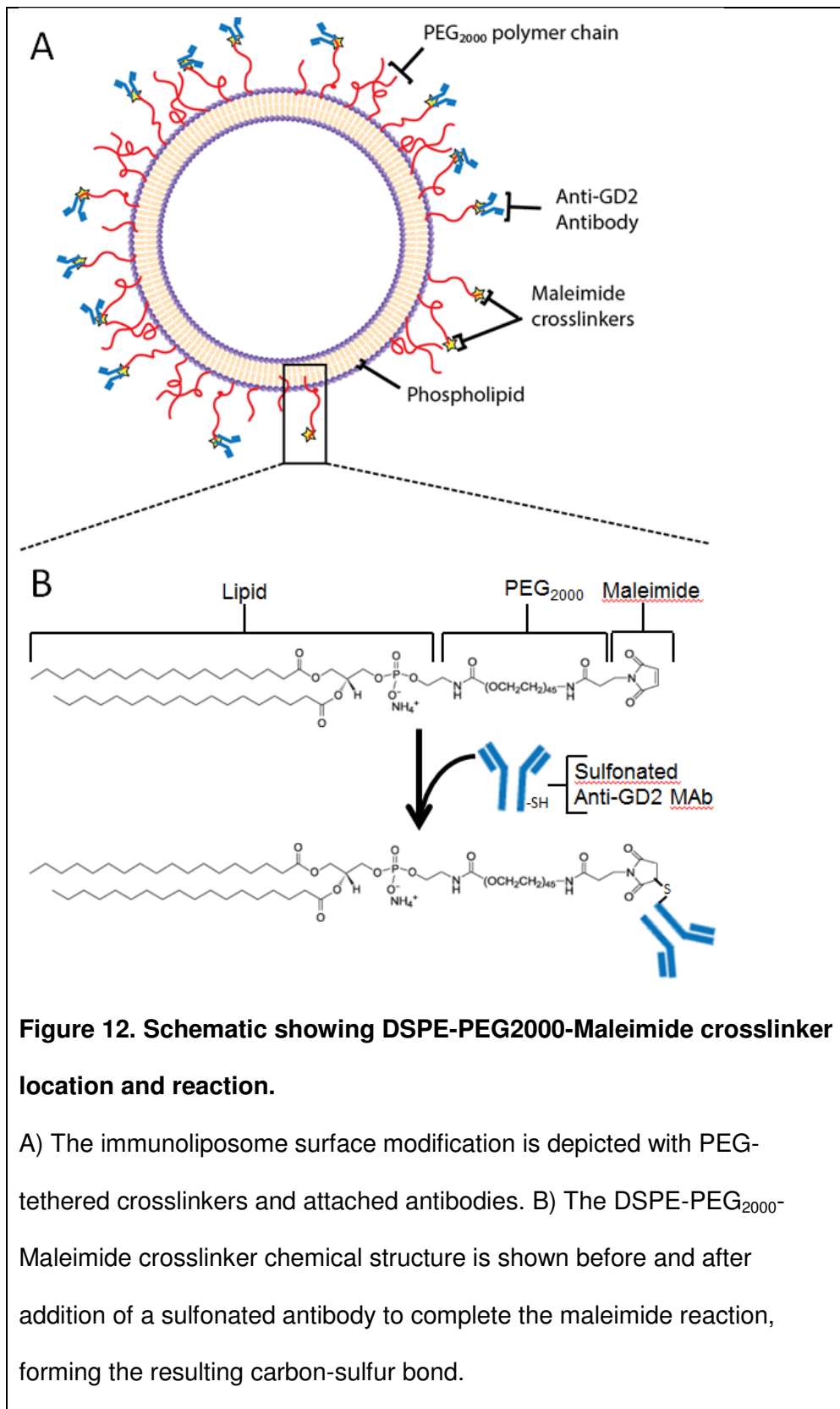
Monoclonal antibodies (MAbs) are rapidly being developed to address the growing number of identified cancer biomarkers. MAbs under development are being used both as standalone immunotherapeutics and targeting moieties for drug delivery systems simultaneously. Anti-GD2 antibodies have been attached to liposomes with some success in targeting delivery of drugs. One example is the GD2-targeted delivery of fenretinide, a synthetic vitamin-like drug, to melanoma cells *in vitro*²⁶ using the 3F8 anti-GD2 antibody. Targeted delivery of fenretinide using anti-GD2 immunoliposomes reduced melanoma cell growth and had no evident cytotoxicity on cells without GD2 expression.

In our study, anti-GD2 antibodies were attached to immunoliposomes via specialized crosslinkers containing a covalent conjugation group called maleimide. MAb attachment to liposomes can be accomplished by different biomolecular mechanisms, and covalent attachment is generally accepted as the most stable and reliable method for attachment¹⁰⁵. Several commercially available covalent crosslinkers are available to standardize connective reactions.

3.3 Strategies for targeting moiety attachment. Effective attachment of a targeting moiety to the surface of a liposome depends both on the nature of the moiety and intended function of the targeted liposome. Liposomes are formulated with crosslinkers at the lipid membrane surface or at the end of PEG chains extending from the surface of liposomes. PEG chains between liposomes and targeting antibodies function as flexible tethers, decreasing steric hindrances between the antibody and liposome during ligand binding¹⁰⁶.

An array of crosslinkers exist for protein immobilization; two of the most commonly used modalities are *N*-Hydroxysuccinimide (NHS)/ ethyl(dimethylaminopropyl) carbodiimide (EDC) and maleimide crosslinkers. Both NHS/EDC and maleimide chemical reagents can be utilized in physiologic conditions to prevent disturbing tertiary and quaternary structure of antibodies in order to preserve targeting abilities. Deciding which conjugation strategy is ideal for a particular application depends largely on the conjugation material and intended function post-conjugation. NHS/EDC reactions activate carboxylates (-COOH) for conjugation to primary amines (-NH₂). Primary amines are found in lysine (Lys, K) side chains, and carboxyls can be found at the C-terminus as well as within aspartic acid (Asp, D) and glutamic acid (Glu, E) residues. While biologically compatible, NHS/EDC reactions are difficult to control in MAbs due to the omnibus presence of primary amines in antibodies. This lack of specificity is alleviated by using a more specific crosslinker such as maleimide.

Maleimide reaction chemistry involves the specific reaction of maleimide with sulfhydryl groups (-SH). Sulfhydryl groups are located in the side chain of cysteine (Cys, C) amino acids which are often unavailable for crosslinking due to their activity in disulfide bonds (-S-S-) where they support secondary and tertiary protein structure. Hence, the majority of crosslinking reactions occur secondary to a controlled thiolation reaction at primary amine sites via thiolating agents such as 2-iminothiolane. Traut's reagent (2-Iminothiolane) is used to add sulfhydryl groups to the side chain of primary amines found at the side chain of lysine amino acids. Thiolation at lower levels (molar excess of 2-iminothiolane to antibody of less than 20:1) has been shown to have little effect on the binding ability of targeting antibodies. Thus, maleimide crosslinking is the approach we utilized for attaching anti-GD2 antibodies to liposomes in this system due to the increased control over the number of active reaction sites at each MAb, Figure 12.



The specific GD2 binding area of 3F8 is the antigen binding fragment (Fab), and the constant region (Fc) contains conserved antigens not essential for the targeted ligand binding. The Fab region typically contains fewer free lysine groups than the Fc region, supporting the claim that sulfonation and subsequent crosslinking to liposomes at these sites will not usually affect specific binding of MAbs. Indeed, sulfonation at lower levels was not found to significantly affect antibody binding to its target¹⁰⁷.

Incorporation of the conjugation product into a function liposome is the final stage of immnoliposome formation. Lipid-PEG-maleimide crosslinkers can be included with other liposomal materials during initial ethanol injection. However, this results in some crosslinkers being trapped in the liposome interior. A solution to this problem, called “post-insertion” involves inserting the crosslinker-modified lipids into the liposomes after they have been formed.

3.4 Post-insertion of crosslinkers into liposomes. Post-insertion is the process of mixing micelles with liposomes to combine the two particle types into a new modified liposome. Micelles are single-lipid-layer spheres with hydrophilic surfaces and hydrophobic interiors, typically much smaller in diameter than liposomes (10-30 nm)¹⁰⁸. During post-insertion, heat and agitation enables lipid micelles to fuse with the outermost leaflet, or “limiting membrane” of the lipid bilayer on a liposome in solution, Figure 13.

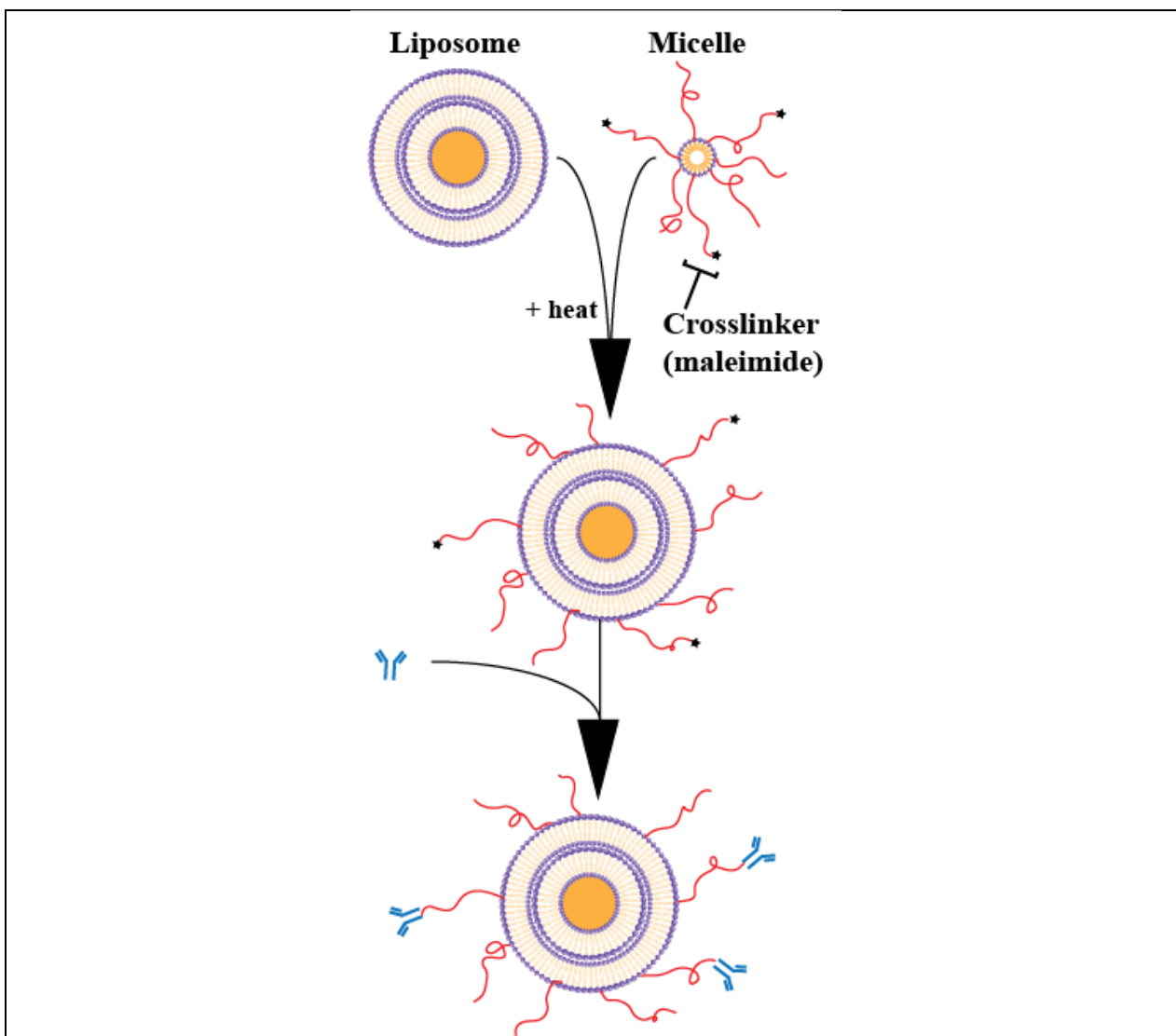


Figure 13. Immunoliposome formation by micellar post-insertion schematic.

Immunoliposomes are formed with post-insertion in a two-step process for the anti-GD2 immunoliposome drug delivery system. First, unmodified liposomes functionalized by co-incubated with maleimide-bearing micelles at 60°C for 1 hour or 65°C for 10 minutes (top) inducing fusion of micelles with the limiting membrane of the liposomes. Next, sulfonated targeting antibodies are incubated with the liposomes after post-insertion facilitating the spontaneous formation of stable thioether bonds between the maleimide linker and antibody.

The process for producing etoposide-loaded immunoliposomes via post-insertion is as follows: First, liposomes containing etoposide are produced via ethanol injection as described earlier. Remaining ethanol is removed via rotary evaporation. Next, micelles are formed by dissolving DSPE-PEG-maleimide first in ethanol followed by addition of an equal volume of aqueous solution. Third, the two solutions are warmed to 65°C and combined under agitation at 300 RPM for 10 minutes. During this phase, the micelles fuse with the liposomes to produce PEG-maleimide decorated liposomes. Lastly, thiolated MAbs are added to the liposomal solution where active maleimide spontaneously reacts with the antibody sulfhydryl groups producing a stable carbon-sulfur bond.

Post-insertion can be accomplished in a relatively short time interval (10 minutes at 65°C to 1 hour at 60°C), allowing for standardization of the amount of time maleimide is exposed to hydrolyzing aqueous reagents. Maleimide crosslinkers can be preserved in anhydrous refrigerated conditions until use just before post-insertion. This results in decreases in variable hydrolysis of the maleimide reactive group prior to conjugation.

3.5 Evaluating maleimide-enabled antibody decoration. Successful post-insertion and subsequent antibody attachment proved difficult to assay using traditional proteomic methods. Minimal amounts of 3F8 were used in each synthesis due to the high cost and relative scarcity of the antibody in the lab. Sensitive protein analysis assays used in western blotting applications such as micro-BCA were attempted multiple times but were not sensitive enough to detect the sub-microgram amounts of MAb conjugated to the surface of immunoliposomes. FTIR and NMR were employed to detect the presence of successful conjugation reactions between the PEG-maleimide linker and the 3F8 MAb Figure 14,15.

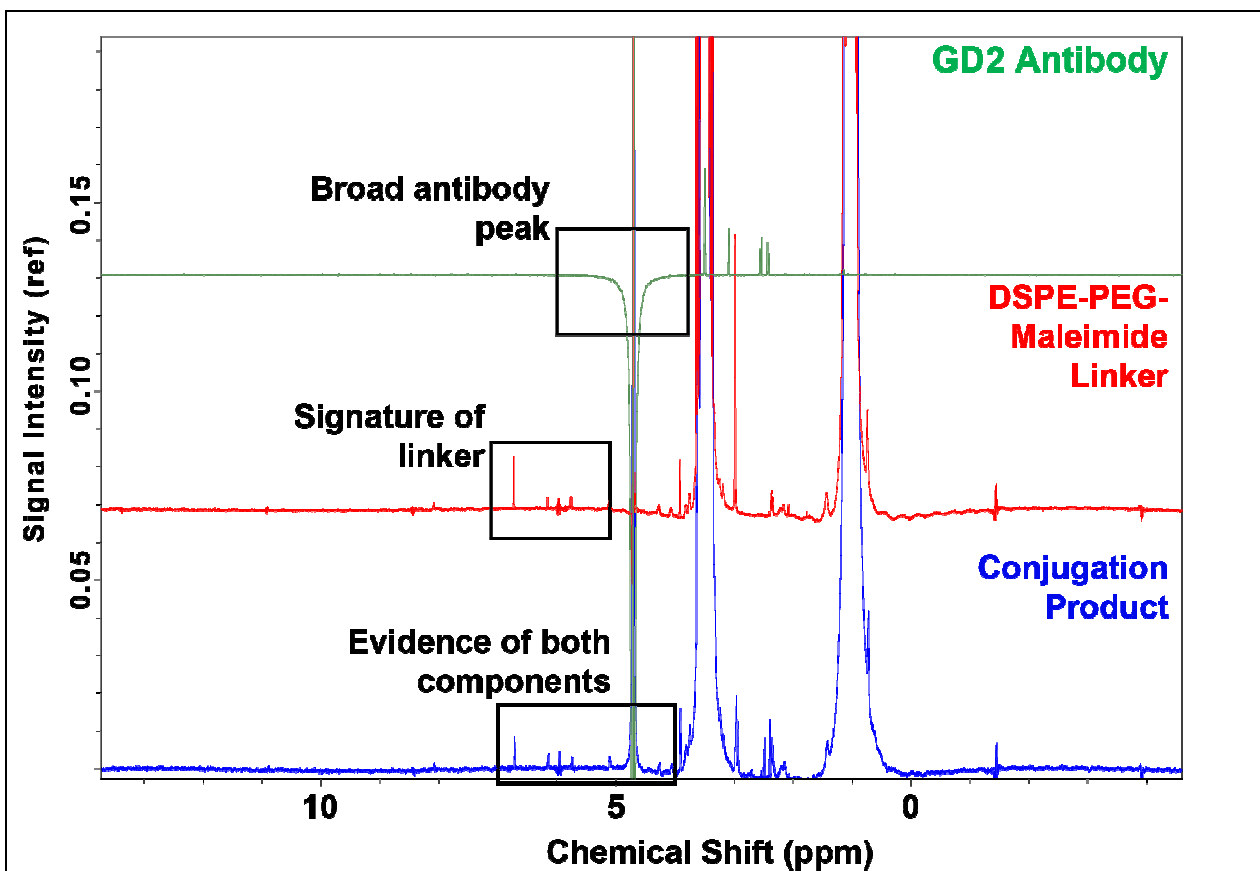


Figure 14. Verification of crosslinker-antibody coupling via nuclear magnetic resonance spectroscopy.

DSPE-PEG₂₀₀₀-maleimide was conjugated to thiolated anti-GD2 antibodies in similar conditions to those used during immunoliposome formulation. Then the conjugation product as well as individual components were analyzed via nuclear magnetic resonance spectroscopy. Antibody alone (top), DSPE-maleimide linker (middle), and the conjugation product of the two (bottom) were analyzed by nuclear magnetic resonance on a Bruker 700 MHz spectrometer. Boxed areas represent intensity shift peaks representing the chemical signature for each component of the immunoliposome targeting moiety. The bottom spectrum revealed characteristic intensity peaks for both components.

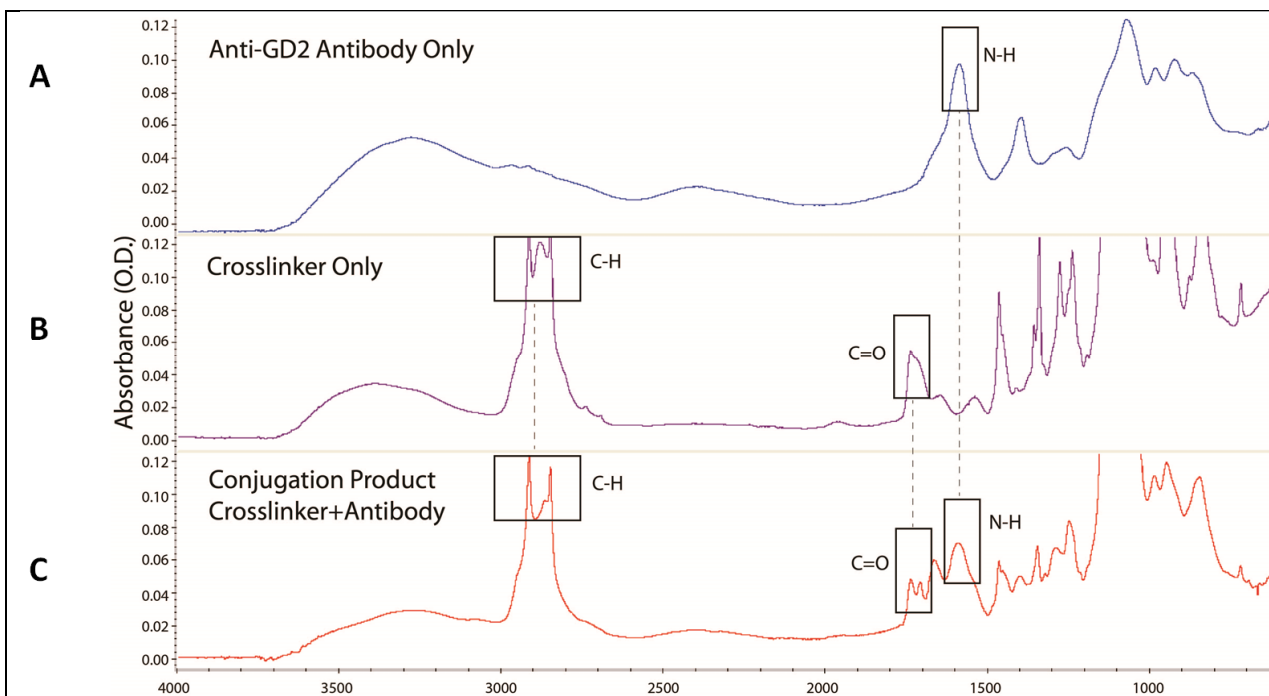


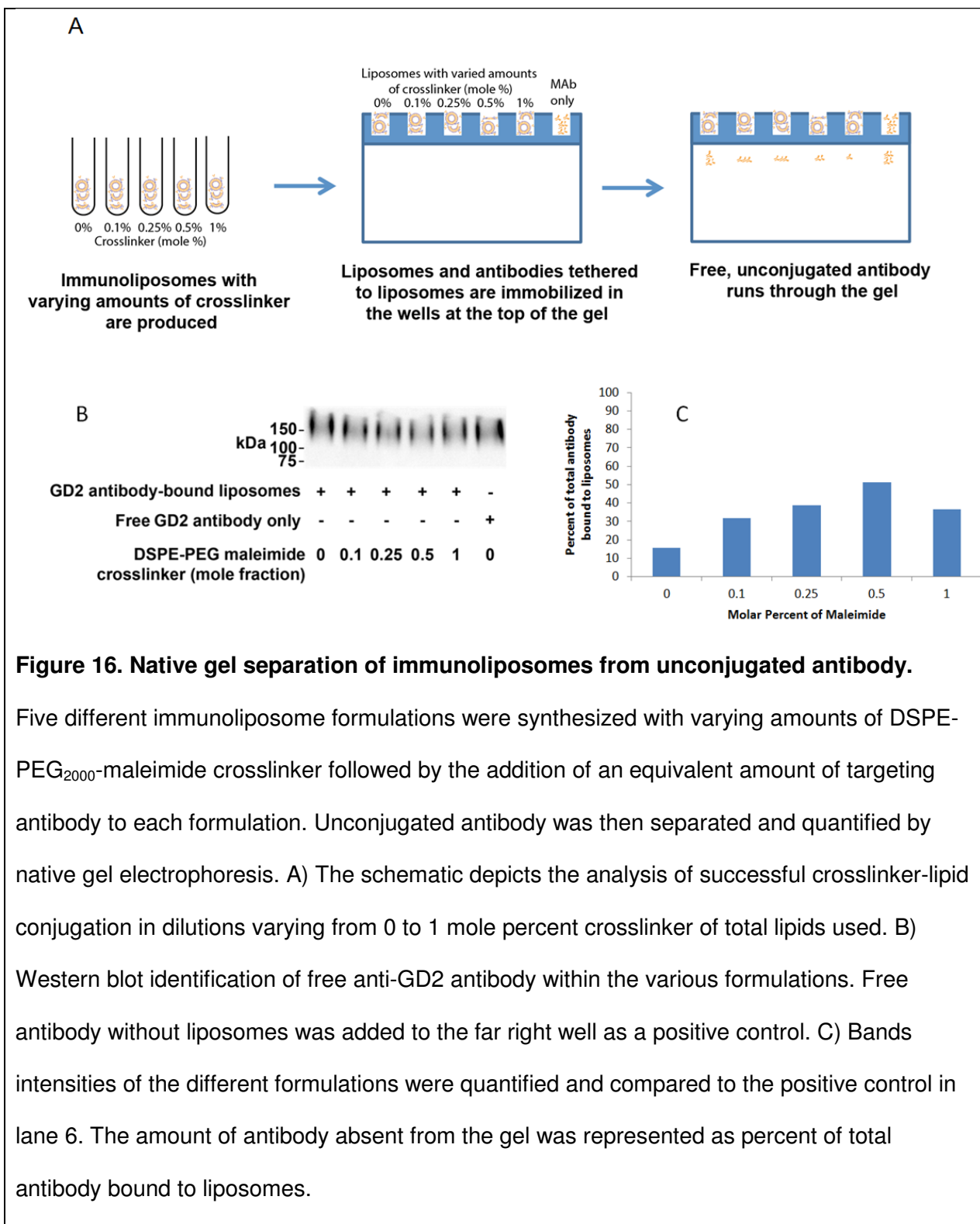
Figure 15. Verification of crosslinker-antibody coupling via fourier transformed infrared spectroscopy.

Anti-GD2 antibody (A), DSPE-PEG₂₀₀₀-maleimide crosslinker (B), and the conjugation product of the antibody with the DSPE-PEG₂₀₀₀-maleimide crosslinker (C) were examined via Fourier transformed infrared spectroscopy. Boxed areas represent characteristic bond peaks of the represented components. Primary amines (N-H) were recognized within the antibody while carbonyl (C=O) and methyl (C-H) groups were detected in the DSPE-PEG₂₀₀₀-maleimide crosslinker. Peaks representing all three bond types were detected in the conjugation product.

For sample preparation, the antibody was sulfonated, purified, and combined with the active PEG-maleimide linker in the same chemical conditions as was previously described for immunoliposome formation. Excess linker was removed and the conjugated DSPE-PEG-maleimide-3F8 product was washed multiple times by ultracentrifugation. We found that both NMR chemical shifts containing spectral signatures of both the linker and 3F8 antibody present

in the conjugation product. Moreover, FTIR revealed peaks representative of the amine bonds found in the antibody (NH 1602 cm^{-1}), as well as the DSPE-mPEG2000 linker (CH 2920-2852 cm^{-1} , and CO 1700 cm^{-1}); both peaks were present in the conjugation product after ultrafiltration to remove unconjugated linker. These data support the existence of a successfully conjugated lipid-linker-antibody product.

The effect of different amounts of DSPE-PEG-maleimide crosslinkers inserted into liposomes was investigated by native gel electrophoresis. Native gels lack detergents which unfold proteins and destroy liposomal membranes. Liposomes are immobilized due to their large size while free proteins are able to migrate through the gel. Hence, the detection of migrating proteins such as 3F8 in a native gel is indicative of unconjugated antibodies, Figure 16, A. We created liposomes with final concentrations of 0-1 mole % DSPE-PEG-maleimide relative to total lipids. Next we added equal amounts of antibody to each formulation and analyzed the amount of unconjugated antibody by western blotting followed by quantitation of band intensities, Figure 16, B-C.



We found that the least amount of antibody was found migrating in the gel in the 0.5 mole % formulation. This data suggests that the 0.5 mole % formulation contained the highest amount of conjugated antibody, resulting in the least amount of free antibodies running in the gel. This is important because efficient conjugation of the antibody to the surface of liposomes decreases the amount of antibody needed, and MAbs such as 3F8 are the most delicate and expensive component of the targeted liposome system.

Next analyzed the presence of intact 3F8 immunoliposomes by microscopy. Traditional light microscopy was inadequate for viewing individual liposomes due to their nanoscale size. The resolving power of an optical microscope is ultimately limited by the wavelength of visible light, and the immunoliposomes produced were on the order of 100-200 nm in diameter. However, aggregates of anti-GD2 immunoliposomes were visualized via fluorescence microscopy by treatment with fluorescent anti-mouse secondary antibodies, Figure 17.

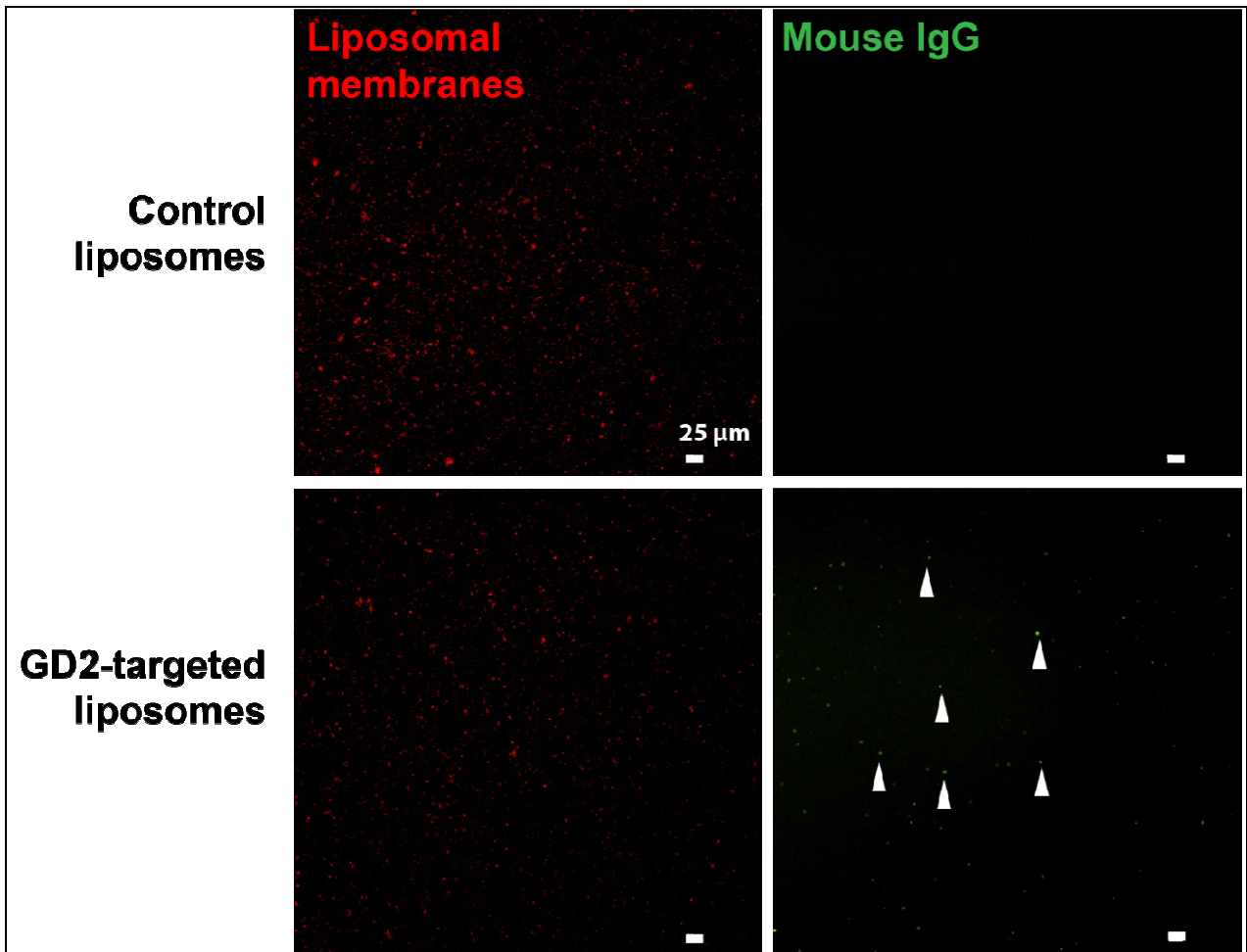
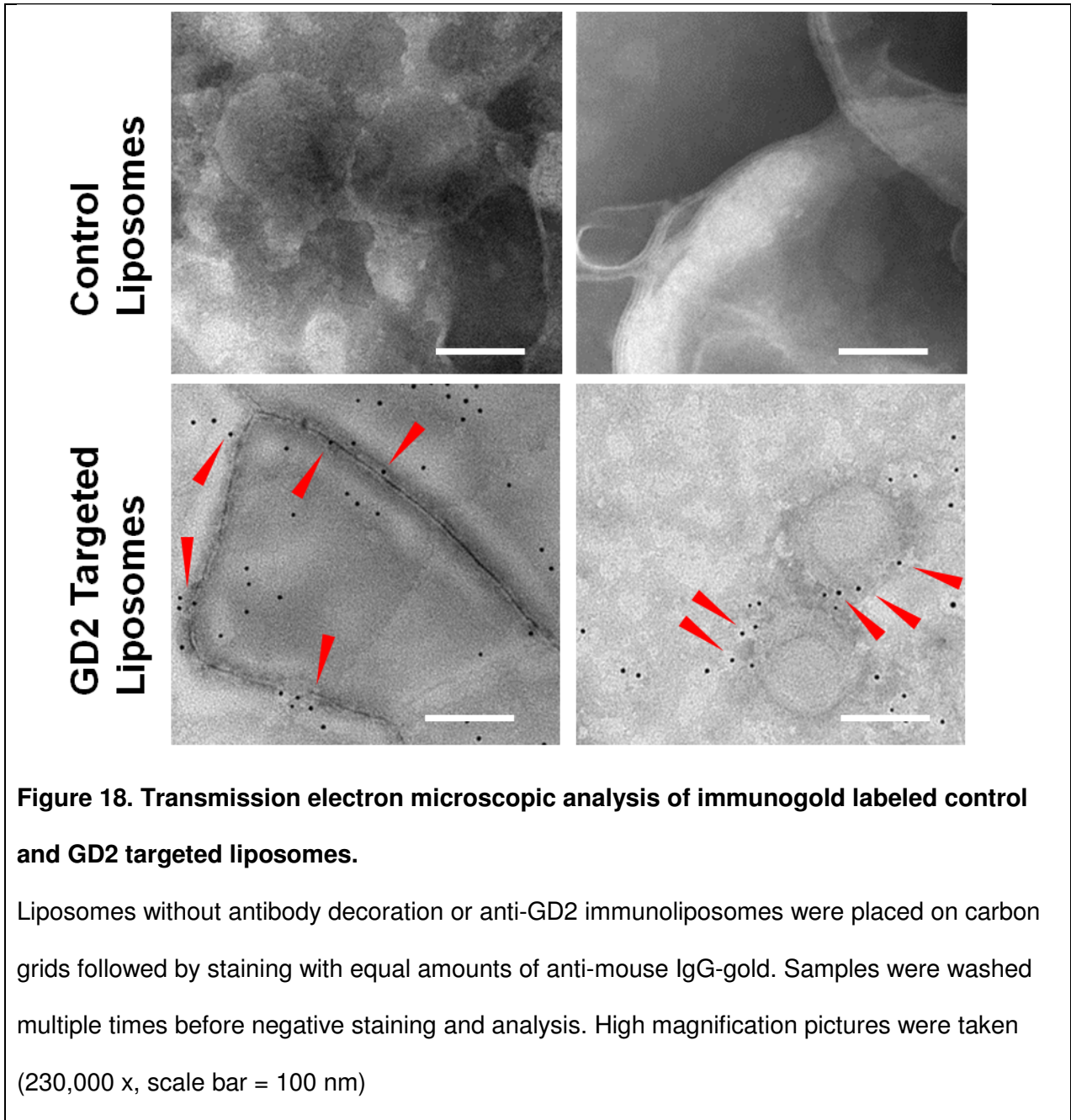


Figure 17. Immunofluorescence of untargeted and anti-GD2 liposomes.

Control untargeted liposomes (A) and anti-GD2 targeted immunoliposomes (B) were incubated with fluorescent anti-mouse antibodies followed by centrifugation to remove free secondary antibody. Liposomes were analyzed by fluorescence microscopy with a 20x objective. Liposomal membranes contained lissamine rhodamine (red) while the anti-mouse IgG secondary antibody contained alexafluor 488 (green). IgG secondary antibody aggregates are represented by white arrows. Scale bar: 25 μm .

Secondary antibody fluorescence was only visible in anti-GD2 immunoliposomes and not untargeted control liposomes. This data suggests that anti-GD2 antibodies were present in

the liposomal formulation. However, colocalization with liposome fluorescence was not clear. For the visualization of individual immunoliposomes, TEM analysis was invaluable. Anti-mouse IgG-gold particles (with reactivity against the murine anti-GD2 MAbs) were incubated with anti-GD2 immunoliposomes on TEM-grade carbon grids followed by washing steps and negative-staining with an electron-dense ammonium molybdate solution, Figures 18.



TEM analysis revealed gold particles located along the liposome membranes suggesting that liposomes were in fact surface labeled with anti-GD2 antibodies. Gold particles were not visualized in similarly treated samples containing control liposomes without anti-GD2 antibodies.

Immunoliposomes decorated with antibodies to a tumor associated antigen are expected to bind tumor cells expressing the antigen with significantly enhanced efficacy compared to controls without antigen binding abilities. We next sought to demonstrate active targeting of anti-GD2 immunoliposomes to tumors of interest. GD2 expression in tumor cells was expected in most neuroblastoma cell lines, but it was unclear from the literature to what extent the ganglioside was produced in individual cell lines. Prior to targeting analysis, we first verified expression of the GD2 ganglioside on an array of cancer cell lines.

3.6 Immunoliposome synthesis and characterization conclusions. We created actively-targeted immunoliposomes by inserting crosslinker-bound lipid micelles into preformed liposomes followed by the addition of sulfonated targeting MAb. We hypothesized that successful conjugation could be demonstrated by chemical analysis via NMR and FTIR as well as fluorescence and electron microscopy techniques. We discovered characteristic chemical shift peaks of the conjugation products themselves via NMR. Moreover, FTIR revealed absorption peaks of characteristic bonds in the individual components of the conjugation product. These data collectively suggest that the maleimide reaction occurred joining DSPE-mPEG₂₀₀₀-Maleimide together with the 3F8 MAb.

The final immunoliposomes product was characterized by DLS analysis for size and polydispersity as well as immunogold TEM. Complete immunoliposomes were found to have an average size of 128.1 nm (+/- 1.6) with a polydispersity of 0.116. While the size and polydispersity values of the final immunoliposome product displayed an upward trend compared to the size and polydispersity of blank liposomes, the values were not significantly different between the complete formulation and the blank liposomes. This suggests that the liposomes are not significantly altered during the post-insertion process with respect to liposome diameter and monodispersity.

Immunoreactive aggregates were visible in final anti-GD2 etoposide immunoliposomes but not control liposomes when viewed via fluorescence microscopy, and TEM images depicted similar immunoreactivity with anti-GD2 immunoliposomes and anti-mouse IgG gold antibodies. These imaging studies were important because they provide visual evidence of the assembled drug delivery system and enable qualitative assessment of liposomal structural properties. We concluded that the drug loaded liposomes displayed the attached antibodies at the liposome surface, as demonstrated with immunogold labeling and TEM analysis. Further characterization of the complete immunoliposome system was conducted with regard to targeting and drug delivery efficacy.

Section II: Ganglioside Expression and Nanoparticle Targeting

Rationale: Gangliosides found in healthy tissue serve the purpose of cell-cell recognition as well as modulation of cell signal transduction events¹⁰⁹. The number and position of sialic acid groups linked to the sugar chain are the differentiating features of the more than 60 known gangliosides³⁴. Gangliosides are believed to coalesce in lipid rafts which are microdomains on the plasma membrane rich in glycosphingolipids and protein receptors, and this association can stabilize specific signaling molecules necessary for cell differentiation during development⁶¹. Gangliosides are predominantly found in the membranes of nervous system cells in both the central nervous system (CNS) and peripheral nervous system (PNS), where they make up approximately 6% of all phospholipids⁸⁹. Interestingly, tumors of neural crest origin are also found to have high ganglioside expression, particularly the ganglioside GD2. Further investigation of GD2 expression revealed that multiple cancer types, including melanoma, osteosarcoma, as well as some adenocarcinomas express GD2 gangliosides; although, the consistency and degree of GD2 expression remains unclear^{61, 110}. Our studies examined the levels of GD2 expression across multiple cancer cell types to elucidate differences among GD2 expressing tumors.

GD2 expression in multiple tumor types and lack of restricted expression in most healthy tissues enables anti-GD2 antibodies such as the MAb 3F8 to specifically target tumor tissue. The 3F8 antibody is utilized for characterization of GD2 expression in cells experimentally as well as intravenously administered as an immunotherapeutic for children with high grade neuroblastoma⁹. Specificity of the 3F8 MAb for GD2 binding has been established *in vitro* and *in vivo*. Cheung et al. found that 3F8 antibodies bound GD2 exclusively without cross-reactivity for other gangliosides such as GD1a, GT1b and GM1⁵³. High precision enabled 3F8

to be used independently for both quantification of GD2 on cancer cells as well as targeting for immunoliposomes.

Chapter 4: GD2 Surface Expression across Cancer Lines

4.1 Ganglioside surface expression. Surface expression of proteins and specialized lipids enable cells to identify themselves for differentiation, modulate adhesion, maintain polarity, and manage numerous other cellular properties. Cancer cells containing copious mutations often overexpress specific surface proteins and lipids that may have been particular to the healthy cell-type from which the cancer originated. For instance, cancer types originating from neural crest cells, in particular neuroblastoma, typically overexpress GD2. For this reason, patients with high-risk neuroblastoma are often candidates for immunotherapy with anti-GD2 antibodies. The neural crest also progenerates smooth muscle, peripheral and enteric neurons, craniofacial cartilage and bone, as well as melanocytes. Consequently, multiple other cancer types, such as melanoma, some osteosarcomas, and other soft-tissue sarcomas have been found to overexpress GD2⁶¹.

4.2 Variability in GD2 expression. Despite some mention of uniform expression in tumors³⁵, we challenged the idea that GD2 is uniformly overexpressed in neuroblastomas, and when overexpressed, we hypothesized that its expression may be variable between cell lines within the same cancer type^{111, 112}. Many other cancers such as melanoma are known to express high levels of GD2, likely due to the neural crest origin of melanocytes. Neural crest cells also differentiate into diverse cell types including craniofacial bone and cartilage, peripheral and enteric neurons and smooth muscle¹⁰⁹. Tumors involving these tissues have also been found to overexpress GD2¹¹³. We included an osteosarcoma as well as melanoma cell line in our GD2 expression and targeting characterization in addition to the four different neuroblastoma lines examined. Neuroblastoma cells previously shown to express GD2, SKNAS and IMR-32 were included along with SY5Y cells that have been characterized to have low GD2 expression. HeLa cervical carcinoma cells were studied in parallel as a negative control for GD2 quantification and targeting.

To determine GD2 surface expression, we used flow cytometry and 3F8 anti-GD2 antibodies to analyze the relative expression of GD2 between cell lines. Cells treated with fluorescent secondary antibodies alone served as a baseline, and GD2 expression was quantified as fold-increases in fluorescence intensity by flow cytometry after treatment with GD2-specific 3F8 MAbs followed by fluorescent secondary antibodies, Figure 19.

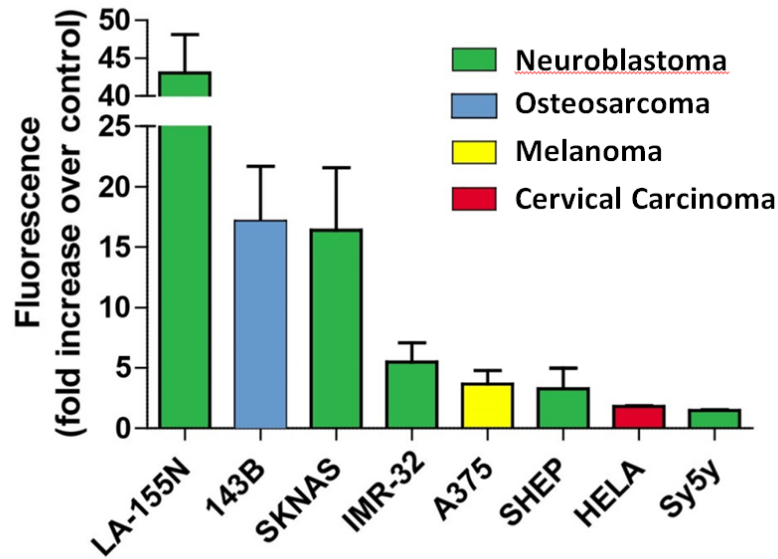


Figure 19. Surface expression of GD2 in neuroblastoma cell lines and across cancer types.

Eight cell lines from neuroblastoma, osteosarcoma, melanoma and adenocarcinoma were treated with anti-GD2 antibodies followed by fluorescent anti-mouse secondary antibodies or fluorescent secondary antibodies alone as a control and analyzed by flow cytometry. GD2 expression is represented as fold increases in geometric means of fluorescence intensity in anti-GD2 antibody + secondary antibody treated cells compared to cells incubated with secondary antibodies alone. Values represent averages of at least three independent experiments with at least 10,000 counts per experiment.

We found that neuroblastomas exhibited dramatically different surface expression of GD2 gangliosides based on 3F8 immunoreactivity, and other tumor types showed anti-GD2 immunoreactivity at high and intermediate levels. The neuroblastoma cell lines LA-155N and SKNAS as well as osteosarcoma 143B showed more than a 10 fold increase in GD2-associated fluorescence compared to control. Moderate GD2 expression was detected in IMR-32, SH-EP (both neuroblastoma) and A375 (melanoma) cell lines. GD2-negative HeLa adenocarcinoma cells and SY5Y neuroblastoma cell lines each expressed little 3F8 reactivity suggesting low GD2 expression. These data suggest that GD2 expression varies widely across tumor types and between different neuroblastoma cell lines.

The consequence of variable levels of GD2 overexpression has an unclear impact on targeted therapies. We hypothesized that variability in GD2 expression across cell lines would result in correlated variable targeting by anti-GD2 liposomes. Variable targeting ability, poorly addressed in the literature, could have obvious and important implications for anti-GD2 therapy because cell lines with variable or low GD2 expression might have a poorer response to anti-GD2 immunotherapy or anti-GD2 immunoliposomes than other cell lines. Therefore, liposomal binding and uptake of anti-GD2 liposomes to these cell lines was further investigated.

4.3 Conclusions concerning GD2 surface expression. Gangliosides are expressed variably during neurodevelopment to guide differentiation of the central and peripheral nervous system. We hypothesized that different cancer types would heterogeneously express GD2 because tumors likely form from cells in variable developmental stages at different baseline GD2 expression levels^{30, 114}. Moreover, we hypothesized that active targeting of anti-GD2 liposomes to the same cell lines would result in varied active targeting correlated with levels of GD2 expression due to the fluctuant amount of ligands available for immunoliposome binding. Osteosarcoma, melanoma and an array of neuroblastoma cancer cell lines were evaluated by

flow cytometry for GD2 expression using the GD2-specific 3F8 monoclonal antibody in conjunction with fluorescent secondary antibodies.

The neuroblastoma cell lines LA-155N and SKNAS as well as osteosarcoma 143B showed more than a 10 fold increase in GD2-associated fluorescence compared to control. This indicates that high levels of GD2 are expected to be available for anti-GD2 binding and targeting. Moderate GD2 expression was detected in IMR-32, SH-EP (both neuroblastoma) and A375 (melanoma) cell lines. GD2-negative HeLa adenocarcinoma cells and SY5Y neuroblastoma cell lines each expressed little 3F8 reactivity suggesting low GD2 expression. These data suggest that GD2 expression varies widely across tumor types and between different GD2 expressing neuroblastoma cell lines, in support of our hypothesis that GD2 expression is heterogeneous across cell lines. While the molecular mechanisms behind the GD2 overexpression are not clear at this time, these findings may have significant importance for GD2-targeted therapies.

Chapter 5: Anti-GD2 Liposomal Targeting and Uptake

5.1 Assessment of anti-GD2 immunoliposome targeting. Modern tracking of liposomes during *in vitro* and *in vivo* work is accomplished by most nanomedicine labs by the use of fluorescently tagged lipids⁷². In appropriately formulated liposomes, nonspecific diffusion of fluorescent lipids is reportedly low, and immediate visualization via confocal and other fluorescence-based analytic techniques renders traditional radiolabeling methods obsolete. For our *in vitro* studies, phospholipids conjugated to the red fluorescent molecule lissamine rhodamine were added in small quantities (0.2 mole %) to liposome formulations for tracking during cellular experiments.

Cells treated with liposomes were observed using confocal microscopy and flow cytometry. Confocal microscopy was used to analyze particle uptake by individual cancer cells while flow cytometry analyzed surface binding of liposomes to cancer cells populations.

5.2 Anti-GD2 immunoliposomes bind GD2 positive cells. The anti-GD2 MAb, 3F8 has an established binding profile for tumor cells bearing the ganglioside GD2¹¹⁵. It was our hypothesis that GD2 positive cancer cells incubated with fluorescent anti-GD2 immunoliposomes would have an increased fluorescent signal on the flow cytometer compared to a similar experiment with untargeted liposomes. Endocytosis was inhibited in anti-GD2 surface binding experiments by performing treatments on ice. Preventing endocytosis was necessary to assess surface targeting without receptor internalization and potential degradation of liposomes. Additionally, rates and levels of endocytosis may vary between cancer types and cell lines, confounding results about effectivity of targeting.

We first analyzed LA-155N reactivity with anti-GD2 targeted vs non-targeted fluorescent liposomes at total lipid concentrations of 50-200 μ M, Figure 20.

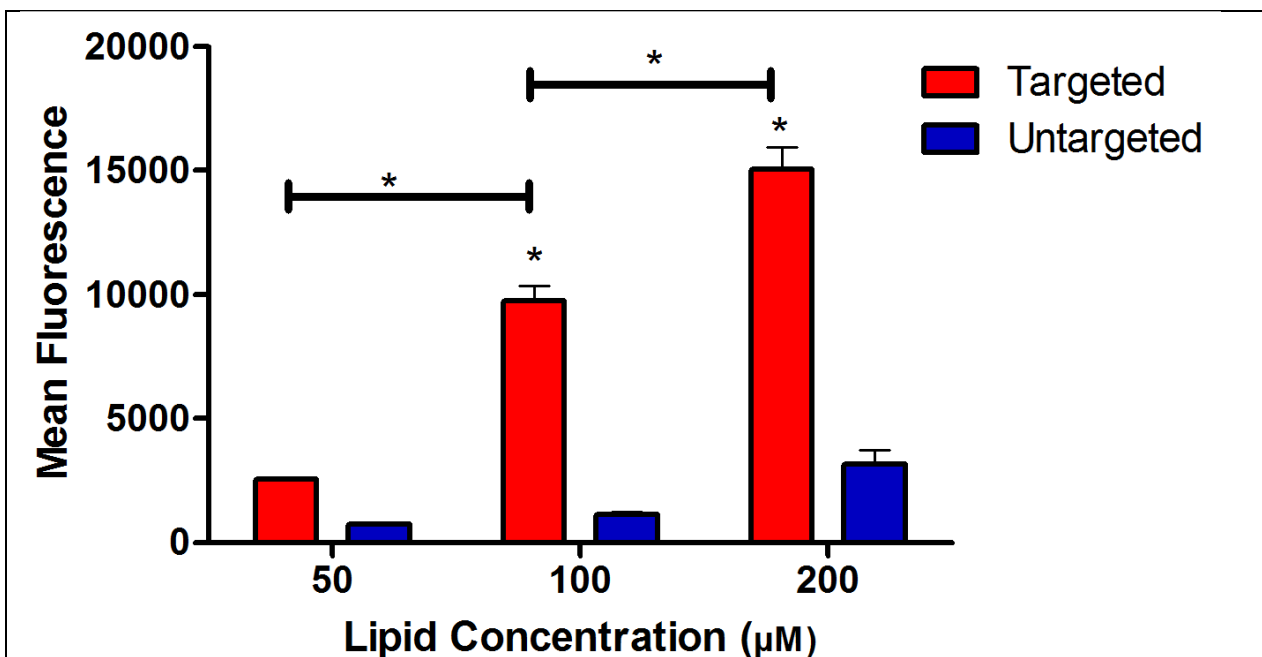


Figure 20. Anti-GD2 targeted immunoliposome targeting to LA-155N cells at different concentrations.

LA-155N cells were co-incubated with anti-GD2 targeted or untargeted liposomes produced with equivalent amounts of fluorescent lipids at 50, 100, or 200 µM lipid concentrations for 30 minutes on ice. We evaluated the surface attachment of anti-GD2 (red) and untargeted (blue) fluorescently labeled liposomes to the surface of cells by flow cytometry. * = $p < 0.05$

We found a significant increase in fluorescence of cells incubated with 100 and 200 µM anti-GD2 targeted compared to untargeted liposomes, suggesting that 100 µM is sufficient for future targeting experiments. Additionally, we found significant differences in cell targeting between each of the three anti-GD2 immunoliposome treatments. These data suggest that the cells were not completely saturated with anti-GD2 immunoliposomes at 200 µM.

Next, we evaluated the time course of the anti-GD2 liposome targeting experiment by performing incubation of LA-155N with 100 µM untargeted or anti-GD2 targeted immunoliposomes for 10, 20, or 30 minutes on ice, Figure 21.

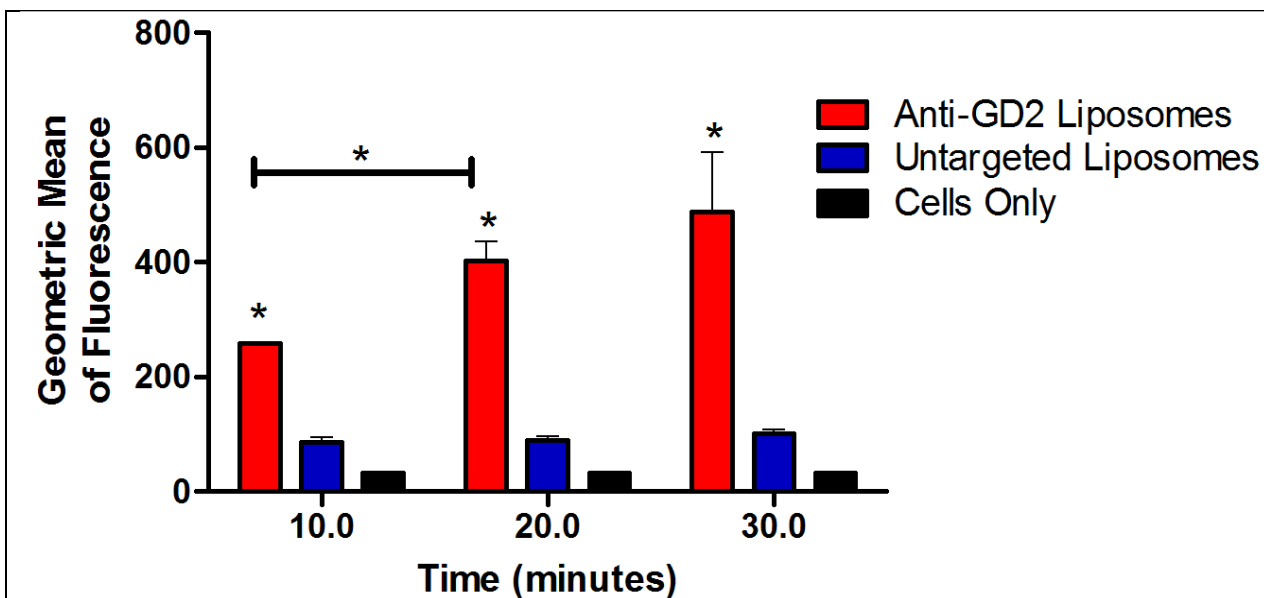


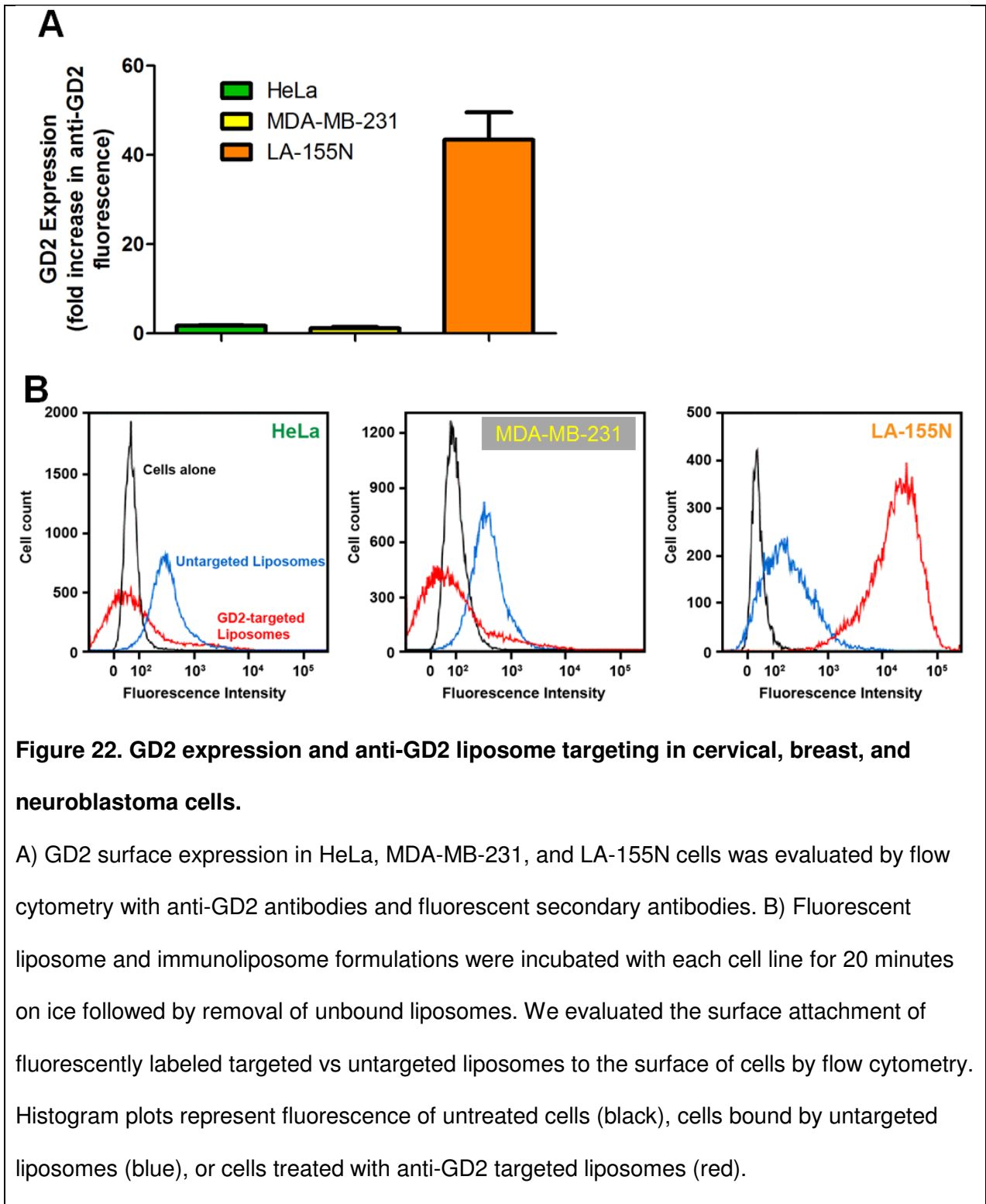
Figure 21. Anti-GD2 targeted immunoliposome targeting to LA-155N cells at different time points.

LA-155N cells were co-incubated with 10 μ M anti-GD2 targeted or untargeted liposomes produced with equivalent amounts of fluorescent lipids for 10, 20, or 30 minutes on ice. We evaluated attachment of fluorescently labeled anti-GD2 immunoliposomes (red) compared to untargeted liposomes (blue) to the surface of cells by flow cytometry. Untreated cells were analyzed for background fluorescence (black). * = $p < 0.05$

This experiment revealed a significant enhancement in cell surface labeling by targeted immunoliposomes compared to untargeted liposomes in all time points. Mean cell fluorescence by samples treated with anti-GD2 targeted liposomes also increased significantly between the 10 and 20 minute time points. These data suggest that detection of anti-GD2 immunoliposome targeting is likely best after 20 minutes of incubation on ice.

Targeting was also assessed in cervical carcinoma (HeLa) and breast cancer (MDA-MB-231) cells with notably low levels of GD2 surface expression. Anti-GD2 immunoliposome or

control liposome binding to these cells in addition to LA-155N cells was assessed by flow cytometry after 20 minutes of incubation with liposomes at 100 μ M, Figure 22.



Here, we found comparable levels of cell fluorescence for untargeted control liposomes and anti-GD2 targeted liposomes in the two cell lines with low GD2 expression. Conversely, effective anti-GD2 targeting was observed in LA-155N cells. Absent anti-GD2 targeting in the cell lines with low GD2 expression suggests that anti-GD2 immunoliposomes are specifically binding cells with high levels of surface GD2.

We separated the eight cell lines characterized for surface GD2 expression into two groups based on GD2 expression levels and evaluated anti-GD2 targeting using the flow cytometric technique described above. Figure 23 depicts cell fluorescence histograms after treatment with anti-GD2 targeted vs untargeted liposomes in high GD2 expressing neuroblastoma lines LA-155N, SKNAS, and IMR-32 as well as osteosarcoma 143B cells.

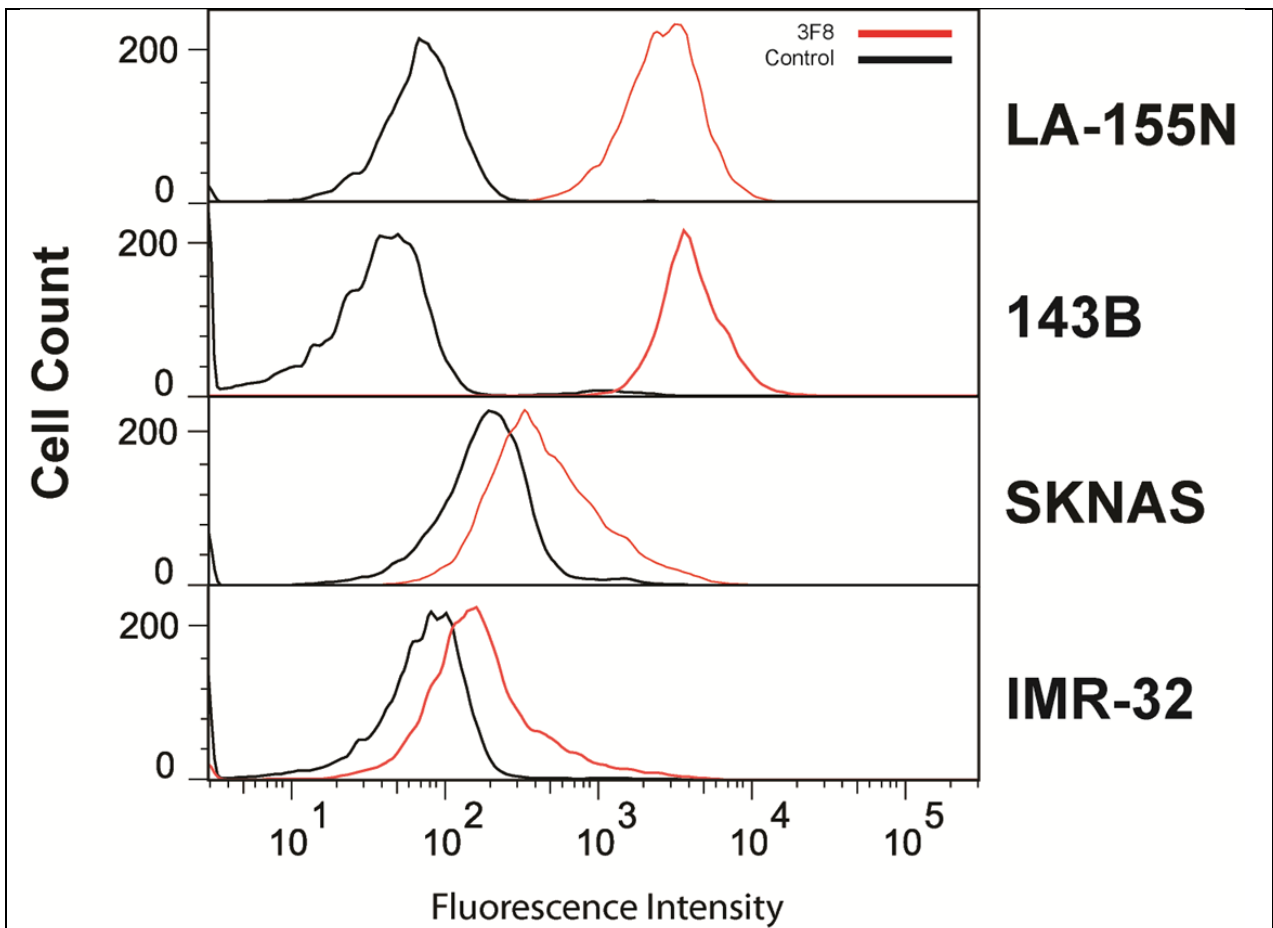


Figure 23. Comparison of targeted vs untargeted liposomal binding in cells with high GD2 expression.

Untargeted “Control” liposomes and anti-GD2 “3F8” immunoliposomes produced with equivalent amounts of fluorescent lipids were incubated with LA-155N, 143b, SKNAS and IMR-32 for 30 minutes on ice. Treated cells were analyzed by flow cytometry, and liposome surface labeling of cells was represented by fluorescence intensity plotted against cell count in each cell line. Cells treated with fluorescent untargeted “Control” liposomes are shown in black; cells treated with fluorescent anti-GD2 “3F8” immunoliposomes are represented by the red line.

Figure 24 portrays cell fluorescence after immunoliposome treatment in moderate GD2 expressing A375 melanoma and SHEP neuroblastoma cells as well as very low GD2

expressing adenocarcinoma HeLa and SY5Y neuroblastoma cells. These data imply heterogeneous immunoliposome targeting between the different neuroblastoma cell lines and confirm a lack of targeting in cell lines with very low GD2 expression.

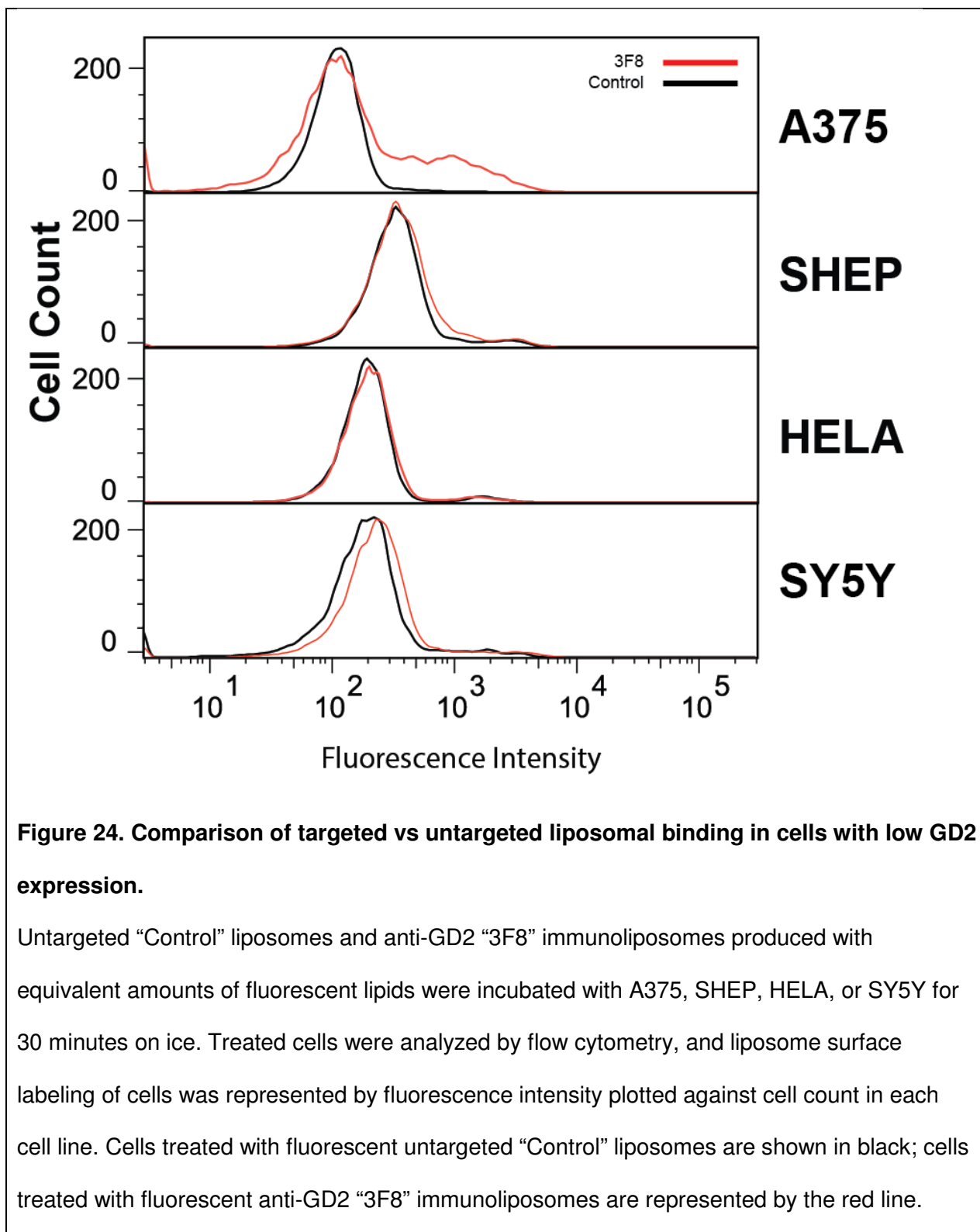


Figure 24. Comparison of targeted vs untargeted liposomal binding in cells with low GD2 expression.

Untargeted “Control” liposomes and anti-GD2 “3F8” immunoliposomes produced with equivalent amounts of fluorescent lipids were incubated with A375, SHEP, HELA, or SY5Y for 30 minutes on ice. Treated cells were analyzed by flow cytometry, and liposome surface labeling of cells was represented by fluorescence intensity plotted against cell count in each cell line. Cells treated with fluorescent untargeted “Control” liposomes are shown in black; cells treated with fluorescent anti-GD2 “3F8” immunoliposomes are represented by the red line.

Specific anti-GD2 targeting in the 8 cell lines characterized for GD2 expression was further investigated by the creation of additional antibody-decorated immunoliposomes to serve as negative controls. Immunoliposomes without specific GD2 binding antibodies were produced to verify that non-specific interactions of liposome-bound antibodies did not affect targeting to GD2 positive cells. Non-specific mouse IgG and monoclonal antibodies to the intracellular protein, STAM were conjugated to liposomes. These two formulations were hypothesized to behave similar to the untargeted liposomes. Targeting experiments with flow cytometry were repeated with the new controls, and thresholds were set based on the untargeted treatment group to determine relative fractions of cell populations labeled with fluorescent liposomes. LA-155N and 143B both displayed a dramatic increase in targeting with liposomal labeling the entire population of cells analyzed by flow cytometry (Figure 25, top two rows).

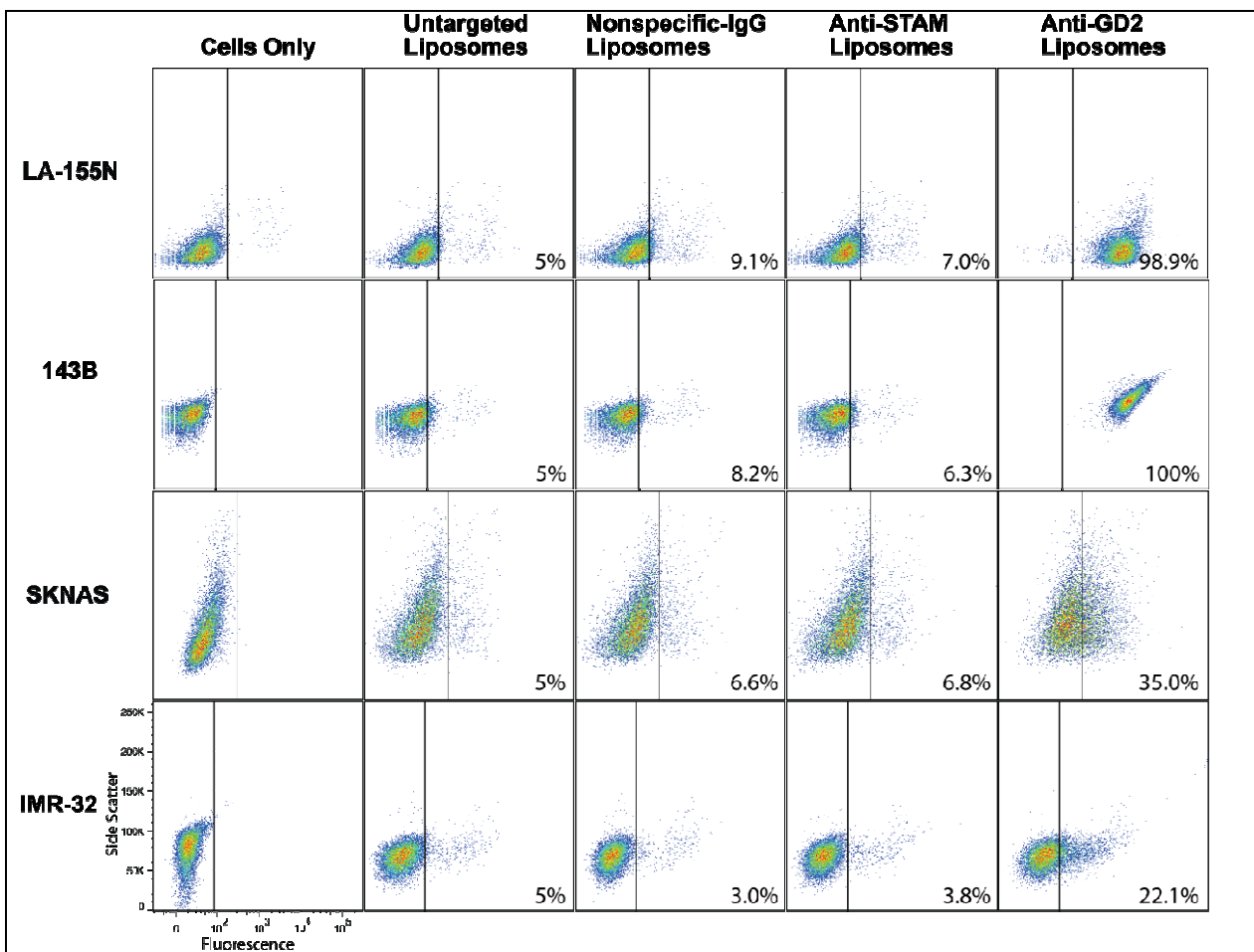


Figure 25. Characterization of targeted and mis-targeted immunoliposomes in cell lines with high GD2 expression.

LA-155N, 143b, SKNAS and IMR-32 cells were treated with various liposome formulations produced with equivalent amounts of fluorescent lipids and analyzed for surface labeling via flow cytometry. Liposome treatments included (columns from left to right): untreated cells, untargeted liposomes, anti-IgG immunoliposomes, anti-STAM immunoliposomes, or anti-GD2 immunoliposomes. Anti-IgG, anti-STAM, and untargeted liposomes represent negative controls. Thresholds were set in each cell line at 5% fluorescence intensity in the untargeted liposome treatment group. Percentiles (boxes, bottom right) represent the fraction of the cell population above the control threshold.

However, SKNAS cells that express high GD2 levels were only bound by 3F8 liposomes in 35% of analyzed cells, similar to that of cells with moderate GD2 expression (Figure 26, middle row). Cells with moderate GD2 expression IMR-32, A375, and SH-EP were partially targeted by immunoliposomes with 22.1%, 30.7% and 35.9% positively labeled compared to control liposomes, respectively (Figure 26, bottom, Figure 27, top two rows).

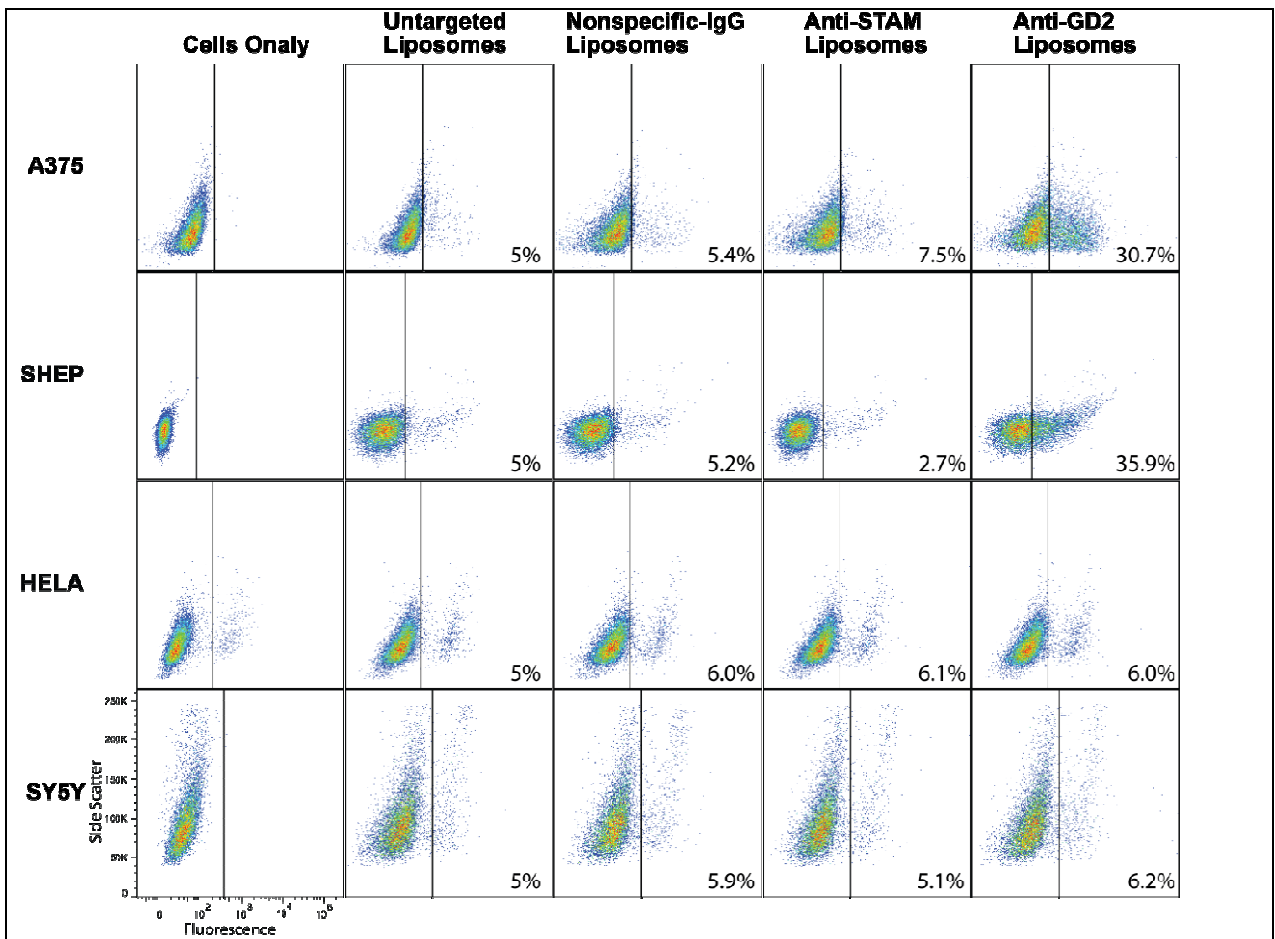


Figure 26. Characterization of targeted and mis-targeted immunoliposomes in cell lines with low GD2 expression.

A375, SHEP, HELA, and SY5Y cells were treated with various liposome formulations produced with equivalent amounts of fluorescent lipids and analyzed for surface labeling via flow cytometry. Liposome treatments included (columns from left to right): untreated cells, untargeted liposomes, anti-IgG immunoliposomes, anti-STAM immunoliposomes, or anti-GD2 immunoliposomes. Anti-IgG, anti-STAM, and untargeted liposomes represent negative controls. Thresholds were set in each cell line at 5% fluorescence intensity in the untargeted liposome treatment group. Percentiles (boxes, bottom right) represent the fraction of the cell population above the control threshold.

As expected, GD2-negative cell lines HeLa and SY5Y were bound by 3F8 immunoliposomes at levels comparable to non-specific anti-IgG liposomes (Figure 26, bottom two rows). Negative controls, immunoliposomes targeted to the unrelated STAM cytoplasmic protein, or labeled with nonspecific IgG antibodies, displayed insignificant cell binding in all cell lines (Figure 26-27, middle columns).

Flow cytometry targeting experiments with all four treatment groups were repeated three times each on different days, and average cell populations above the control threshold were quantified in Figure 27 and 28 for cells with high and low surface GD2 expression, respectively.

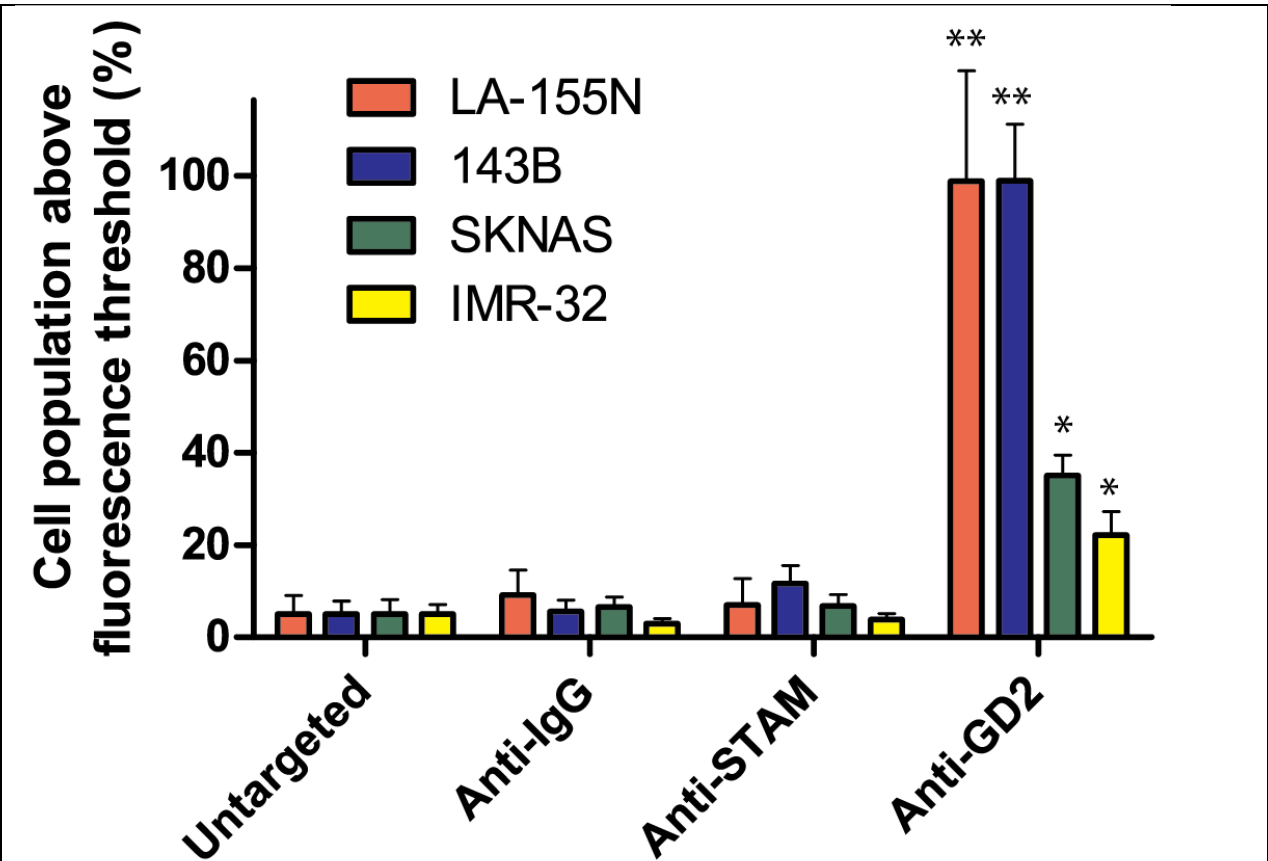
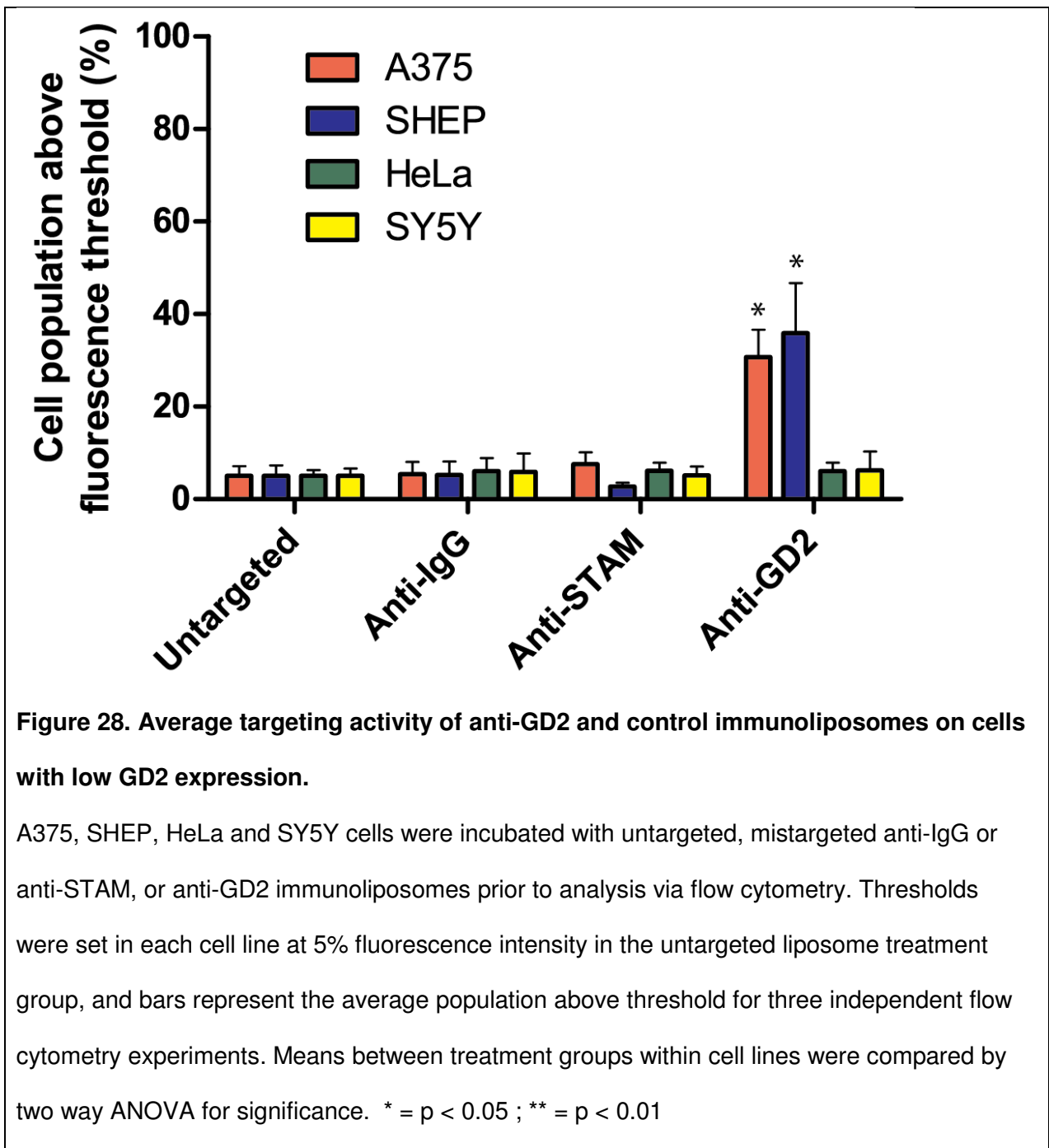


Figure 27. Average targeting activity of anti-GD2 and control immunoliposomes on cells with high GD2 expression.

LA-155N, 143b, SKNAS and IMR-32 cells were incubated with untargeted, mistargeted anti-IgG or anti-STAM, or anti-GD2 immunoliposomes prior to analysis via flow cytometry.

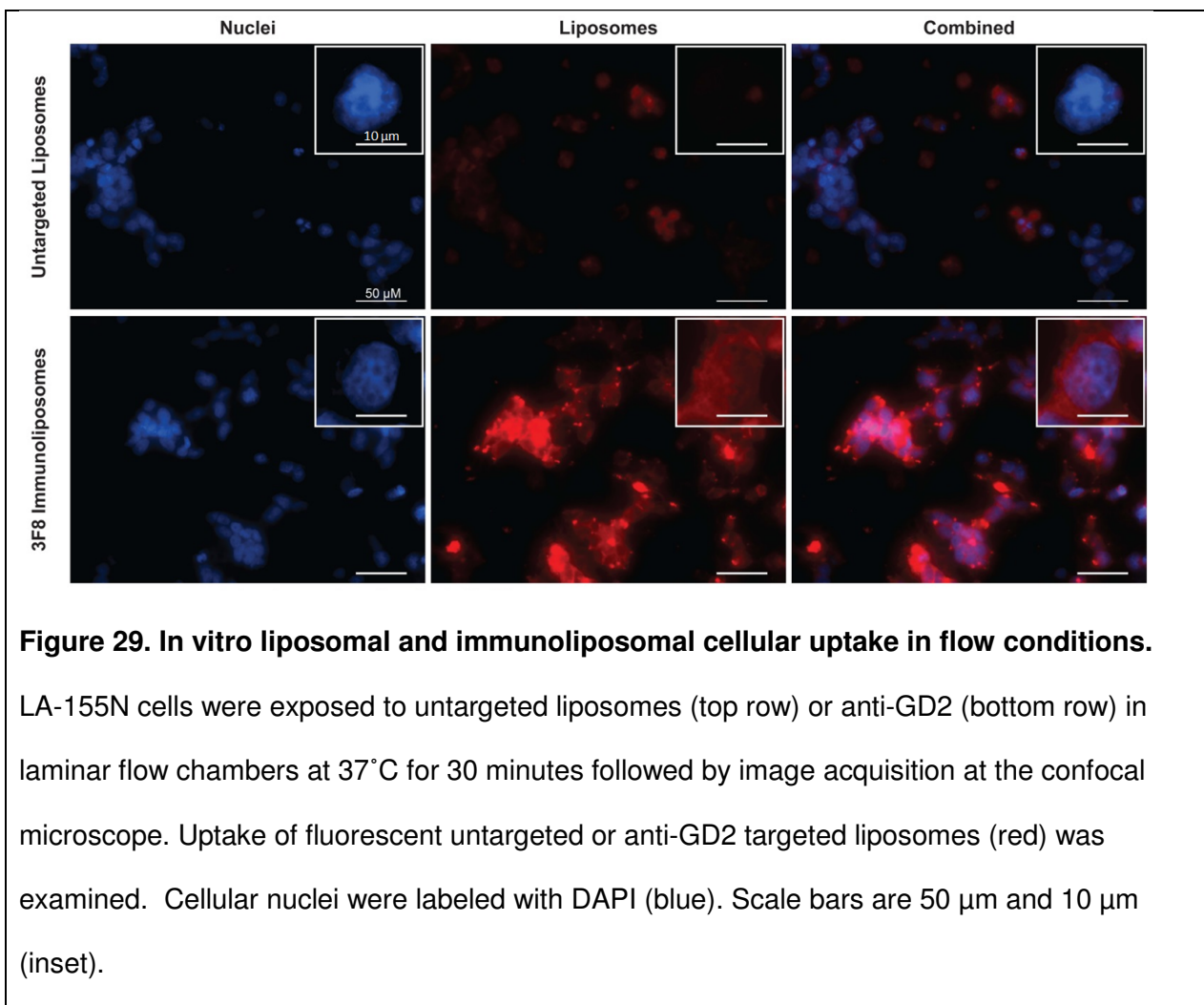
Thresholds were set in each cell line at 5% fluorescence intensity in the untargeted liposome treatment group, and bars represent the average population above threshold for three independent flow cytometry experiments. Means between treatment groups within cell lines were compared by two way ANOVA for significance. * = $p < 0.05$; ** = $p < 0.01$



We found significant surface targeting cells treated with anti-GD2 liposomes in all cell lines except low GD2 expressing SY5Y and HeLa cells. These data support earlier findings suggesting that anti-GD2 liposomes specifically bind GD2 expressing cell lines.

Surface targeting is followed by particle uptake in the time course of targeted drug delivery. We sought to understand the dominant endocytic mechanism of entry for immunoliposomes with target cells. Liposome internalization was investigated via fluorescence and confocal microscopy.

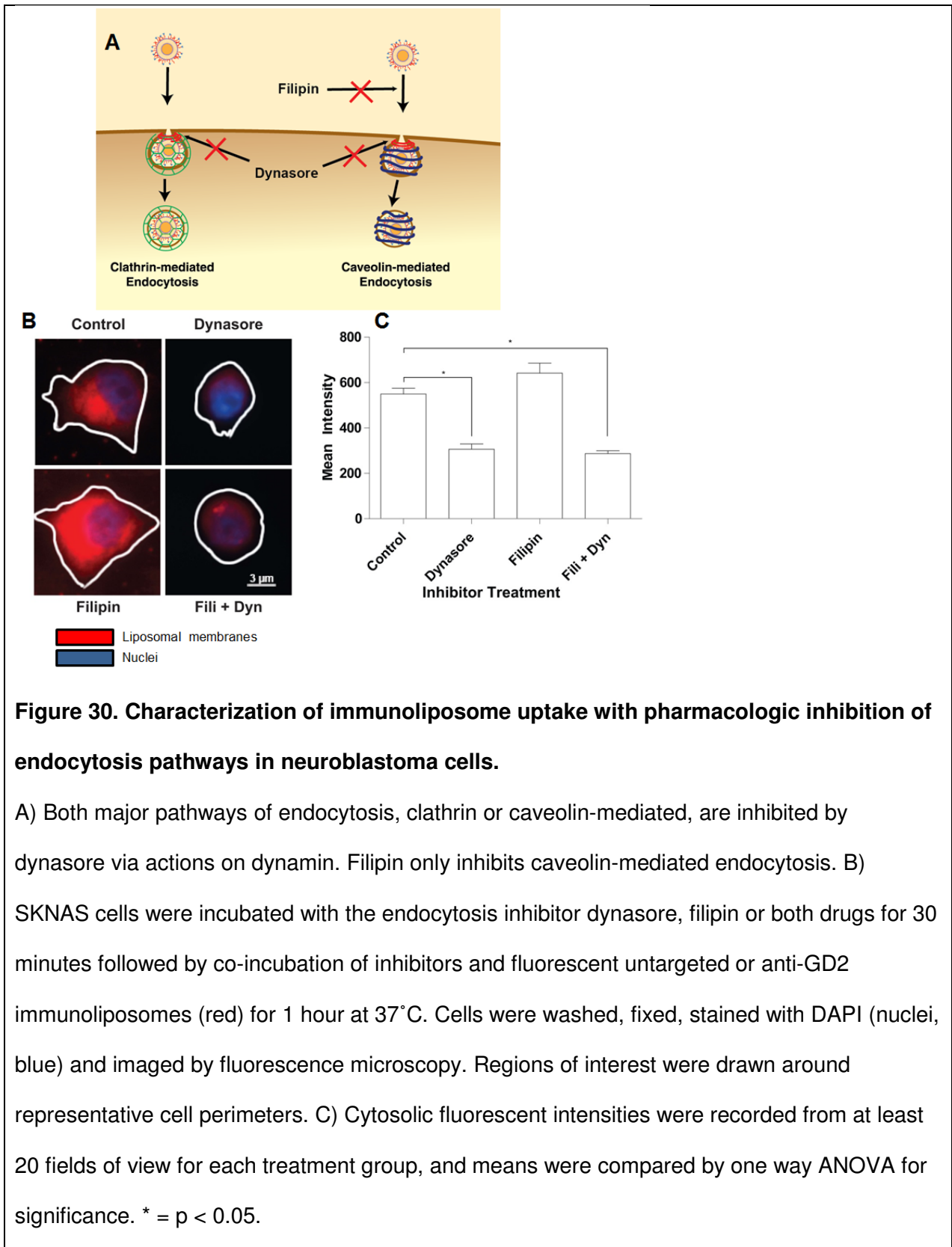
5.3 Anti-GD2 immunoliposome flow chamber cellular uptake. Uptake of fluorescent immunoliposomes into cells was observed using flow chamber slides and confocal microscopy. Flow chambers have a channel where media and liposome solutions can be administered with laminar flow over cultured cells, simulating the dynamic flow environment of the microvasculature. After treatment with fluorescent liposomes, cells are fixed within the chamber slide and analyzed at the microscope. We visualized the GD2 expressing cell line, LA-155N, with a DAPI nuclear stain after treatment with anti-GD2 immunoliposomes or untargeted liposomes. These experiments were conducted at the physiologic temperature of 37 °C to allow cellular uptake of particles over the course of 30 minutes under flow conditions, Figure 29.



These data suggest that anti-GD2 immunoliposomes are capable of being internalized by target cells while in a simulated circulatory environment.

While internalization was evident during confocal analysis due to visualization of fluorescent lipids within treated cells, the method of entry into the cell was not clear. There are several potential pathways for the internalization of liposomes and immunoliposomes and the primary pathway involved in anti-GD2 immunoliposome uptake was investigated using pharmacologic endocytosis inhibitors.

5.4 Inhibition of immunoliposome endocytosis. Endocytosis is the active cellular process cells utilize to take in extracellular material. Immunoliposomes are suggested in the literature to be taken up by receptor mediated endocytosis^{74, 116}. Although, particle endocytosis is known to depend on the cell type as well as particle features such as size, shape, charge and which receptor is being bound¹¹⁷. LA-155N was analyzed for anti-GD2 immunoliposome uptake by pre-treating cells with two different types of internalization inhibitors: dynasore and filipin, Figure 30, A.



Filipin is an antifungal chemical compound found to inhibit the caveolae pathway within mammalian cells¹¹⁷. Caveolae are small membrane buds (about 50 nm) that form flask-shaped pits and internalize extracellular molecules. Caveolin, the fundamental protein forming caveolae, is known to associate with cholesterol enriched membranes and glycolipids. GD2, being a subtype of glycolipid, could have been involved in this type of internalization. Dynasore inhibits the action of the cytosolic protein, dynamin. Dynamin is required for both caveolar and clathrin-mediated endocytosis during the pinching off of membrane buds¹¹⁸. Clathrin endocytosis is responsible for many types of receptor-mediated endocytosis, initiated by a ligand binding a surface protein or lipid. Clathrin-coated vesicles are usually about 100 nm in diameter, much closer to typical immunoliposome diameter. We hypothesized that clathrin-mediated endocytosis is the primary mechanism for internalization of anti-GD2 immunoliposomes due to the size of clathrin-coated pits and clathrin involvement in receptor-mediated endocytosis.

We investigated immunoliposome uptake mechanisms in SKNAS cells by pharmacologically inhibiting endocytosis pathways using dynasore, filipin, or a combination of the two inhibitors, Figure 30, B. Average liposomal fluorescence intensity within cells was quantified by drawing regions of interest around individual cells and calculating mean intensities across treatment groups, Figure 30, C. These data suggest that dynasore inhibition restricted receptor mediated endocytosis of immunoliposomes via clathrin-coated pits while filipin inhibition of the caveolar pathway had no effect on liposomal uptake in accordance with literature on uptake of other forms of immunoliposomes¹¹⁹. Thus, the primary mode of immunoliposome internalization in target cells is likely receptor-mediated clathrin-dependent endocytosis.

5.4 Conclusions for anti-GD2 immunoliposome targeting and uptake. Immunoliposome targeting relies on both the stability of the immunoliposome in the vicinity of the target cell as well as the fidelity of binding between the cellular target ligand and targeting moiety. In our studies, an effective 3F8-GD2 binding was required to observe liposome-associated fluorescence in cells. Increased fluorescence in anti-GD2 immunoliposome treated cells compared to control liposomes suggests that targeted immunoliposomes would be taken up more efficiently and deliver more drugs to GD2 positive cells during cancer therapy. Alternatively, increased fluorescence in cell lines with higher GD2 overexpression treated with the same amount of anti-GD2 immunoliposomes would suggest that patients with GD2 expressing tumors might have differential responses to anti-GD2 immunoliposomal therapy based on their levels of GD2 expression.

Quantitative assessment of targeting efficiency via flow cytometry revealed that GD2 expression was positively correlated with increased amounts of 3F8 mediated liposomal targeting in some, but not all cell lines. LA-155N and 143B both displayed a dramatic increase in targeting with liposomal labeling the entire population of cells analyzed by FACS. However, SKNAS cells that express high GD2 levels were only bound by 3F8 liposomes in 35% of analyzed cells, similar to that of moderate GD2 expressors. Moderate GD2 expressors IMR-32, A375, and SH-EP were partially targeted by immunoliposomes with 22.1%, 30.7% and 35.9% positively labeled compared to control liposomes, respectively.

We concluded that anti-GD2 mediated targeting occur heterogeneously between cancer types and within different neuroblastoma cell lines, supporting our hypothesis that targeting is not an all-or-none phenomenon, but rather a spectrum of targeting efficacy that appears to correlate with GD2 expression in some, but not all cell lines. For example, cell lines with high GD2 expression resulted in high anti-GD2 targeting in some cell lines (LA-155N and 143B) and

medium levels in others (SKNAS). This alludes to the idea that the drug may have variable success with respect to tumor GD2 expression and other unknown factors.

Section III: *In Vitro* Efficacy and *In Vivo* Pilot Study

Rationale: Translation of anti-GD2 immunoliposomes into clinical studies requires exhaustive characterization of *in vitro* and *in vivo* efficacy. In particular, inhibition of tumor growth and tumor regression must be demonstrated in comparison to standards of care. Treatment with free etoposide for high grade cancer represents the primary treatment for comparison with etoposide immunoliposomes.

Despite being established drug carriers, drug-loaded liposomes and immunoliposomes face many hurdles to exceeding the efficacy of free drugs. Liposomes must possess the necessary surface chemistry and charge to allow cellular uptake, and once internalized, liposomes must facilitate transfer of the drug into the cellular compartment where it acts. Etoposide must avoid degradation in the lysosome or expulsion from the cell before reaching its molecular target, topoisomerase II, which is localized within the nucleus of the cell.

In vitro cell proliferation inhibition following treatment with etoposide liposomes advocates this activity, but additional investigations would be required to determine the precise mechanisms of cell death following treatment. The liposomal components: DPPC, cholesterol, and PEG chains all have established non-toxic profiles *in vivo*, and current studies suggest that 3F8 anti-GD2 MAbs require complement and circulating leukocytes to induce toxicity in target cells. These data suggest that etoposide is responsible for ensuing effects on cell proliferation. *In vivo* studies incorporate organ system and tumor microenvironmental effects into the assessment of effective therapy. In particular, the dynamic nature of circulation has multiple effects on targeted liposomal drug delivery. Serum proteins potentially bind and inhibit targeting moieties, and the MPS actively removes foreign substances from systemic circulation. While much more powerful than *in vitro* studies, *in vivo* results also deviate from expected results in humans because animals' immune systems react to stimuli differently than a human's. Serum proteins may have dissimilar drug inactivation effects, and the sheer differences in blood

volume and organ size between small animals and humans effect clearance and antitumor effects of treatment.

Chapter 6: *In Vitro* Inhibition of Cancer Cell Proliferation

6.1 Inhibition of proliferation over time. Etoposide action on topoisomerase II in cancer cells results in arrest of cell growth and cell death in a dose-dependent manner. Proliferation assays using tetrazolium salts such as MTT or WST-1 are research standards of determining the level of growth arrest *in vitro*¹²⁰. MTT and WST-1 are tetrazolium salts that undergo reduction by mitochondrial oxidoreductase enzymes forming the purple insoluble chemical, formazan. Formazan can then be measured colorimetrically. Only living cells bear the active reducing enzymes, and the resulting levels of reduced salts can be correlated with cell proliferation. During initial testing with liposomes in proliferation studies, WST-1 was utilized because it has been reported to be more sensitive, and the assay has fewer steps, decreasing human error. Unfortunately, WST-1 results of immunoliposome treated cells were repeatedly unstable with unacceptably high standard deviations, and we suspected that one or more components of the immunoliposome complex may be interfering with the assay. Hence, we implemented the MTT test and found reproducible results.

We first evaluated the toxicity of non-drug vehicle substances prior to the use of etoposide. Phosphate buffered saline (PBS, < 10% v/v), dimethylsulfoxide (DMSO, < 1% v/v), and unloaded liposomes in PBS were incubated with SKNAS cells for 72 hours and analyzed for cell proliferation every 24 hours, Figure 31.

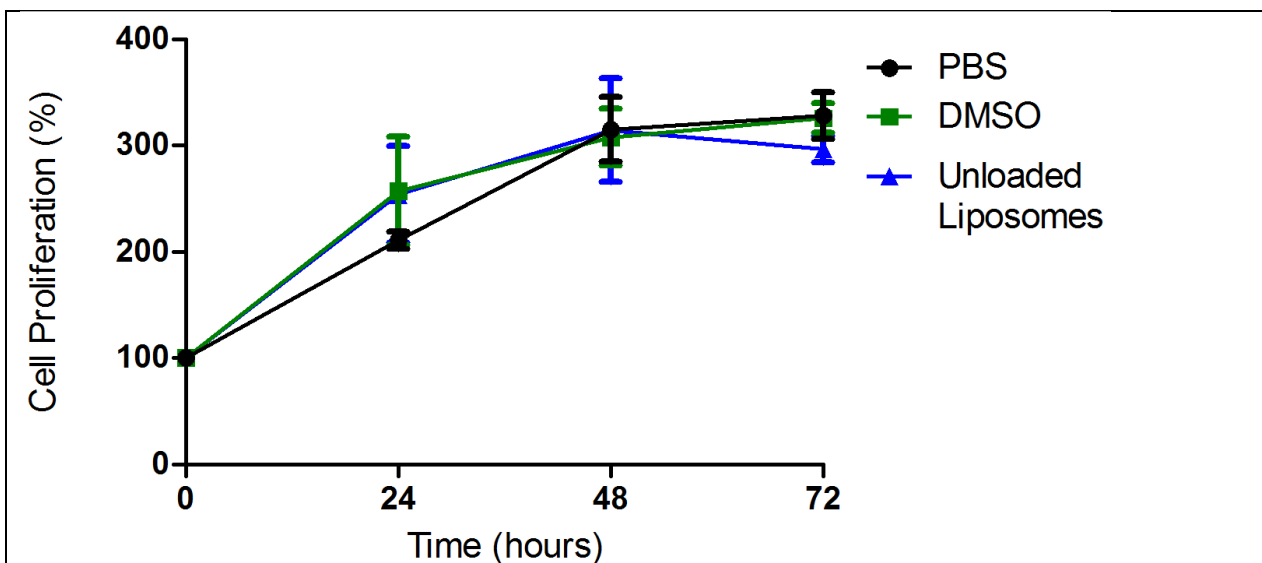


Figure 31. Cell proliferation effects on cells treated with empty liposomes and drug emulsifiers.

To assess the effects of non-drug substances administered during drug treatments, SKNAS cells were incubated with 10 % v/v phosphate buffered saline (PBS, black), drug emulsifying agent (1% v/v DMSO, green) or liposomes without drug (10 mM unloaded liposomes, blue) in cell media at concentrations similar to that of experiments with liposomal etoposide and free etoposide. Cell proliferation was assessed via MTT assay at 24 hour time points up to 72 hours. Values represent percent proliferation compared to untreated control cells.

We found no significant changes in proliferation between the three vehicle substances suggesting that the carrier substances would not interfere with subsequent studies on drug efficacy. Next, we evaluated etoposide-loaded immunoliposomes compared to drug alone or untargeted etoposide liposomes each at equal etoposide concentrations over the course of 72 hours, Figure 32.

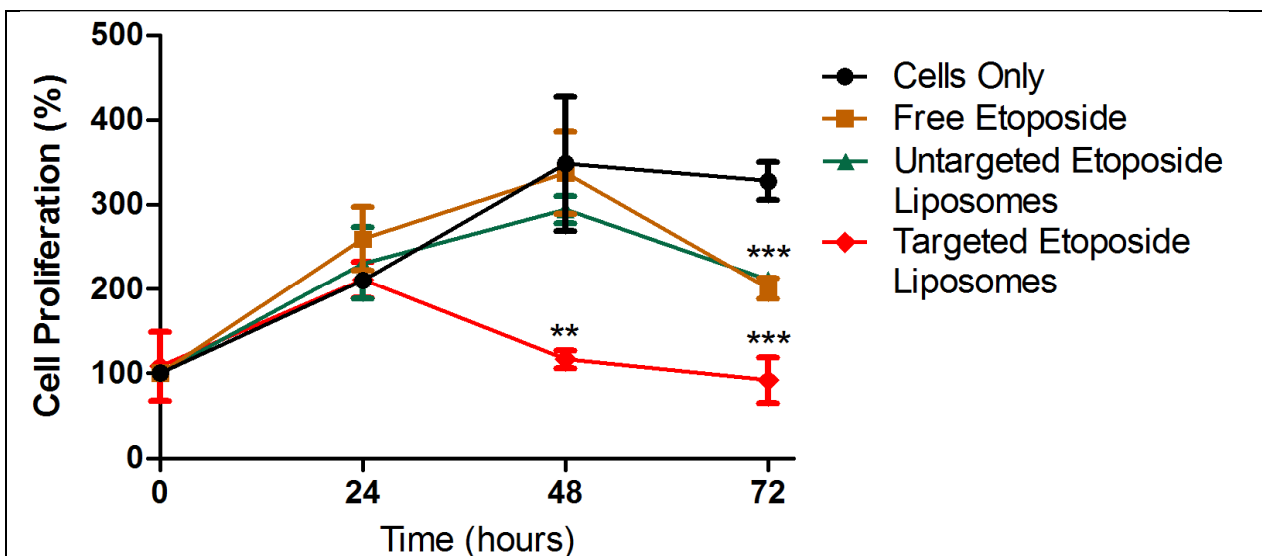


Figure 32. Cell proliferation effects on neuroblastoma cells exposed to liposomal and free etoposide.

SKNAS cells were incubated with free etoposide (brown), untargeted liposomal etoposide (green), or within anti-GD2 immunoliposomes all at etoposide concentrations of 10 $\mu\text{g}/\text{mL}$. Plates were analyzed for cell proliferation by MTT assay at 24 hour time points up to 72 hours. Cell proliferation was displayed as percent compared to untreated control cells (black). ** = $p < 0.01$ and *** = $p < 0.001$

Cell proliferation of cells treated with anti-GD2 targeted liposomes was observed at 100% compared to control cell proliferation exceeding 300%. This data suggests that the targeted liposomes enhance the delivery and anti-proliferative action of etoposide. Next, we sought to determine the response of cells to increasing dosages of the different delivery mechanisms of etoposide.

6.2 Anti-GD2 etoposide liposome dose escalation study. Encouraging results of anti-GD2 liposomal delivery of etoposide at low concentrations (10 $\mu\text{g}/\text{mL}$ etoposide) justified further experimentation with higher concentrations of particles and etoposide. One objective measure

of the efficacy for a drug or drug delivery system *in vitro* is called the IC_{50} . The IC_{50} indicates the amount or concentration of a substance needed to inhibit 50% of a biological function or activity. In the setting of etoposide treatment and tumor cell growth, the IC_{50} is the concentration of etoposide (free or within liposomes) required to inhibit proliferation to 50% over a given time period.

We evaluated the IC_{50} for etoposide and anti-GD2 immunoliposomal etoposide in neuroblastoma and osteosarcoma via MTT assay, Figure 33-34.

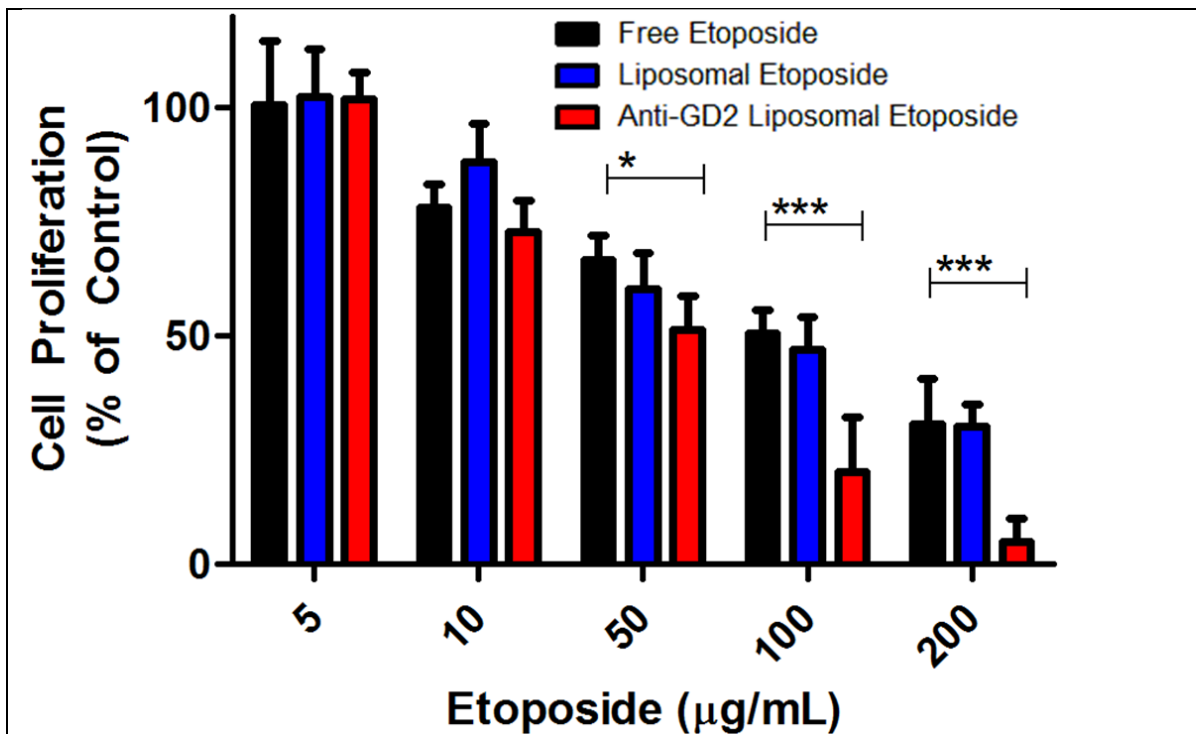
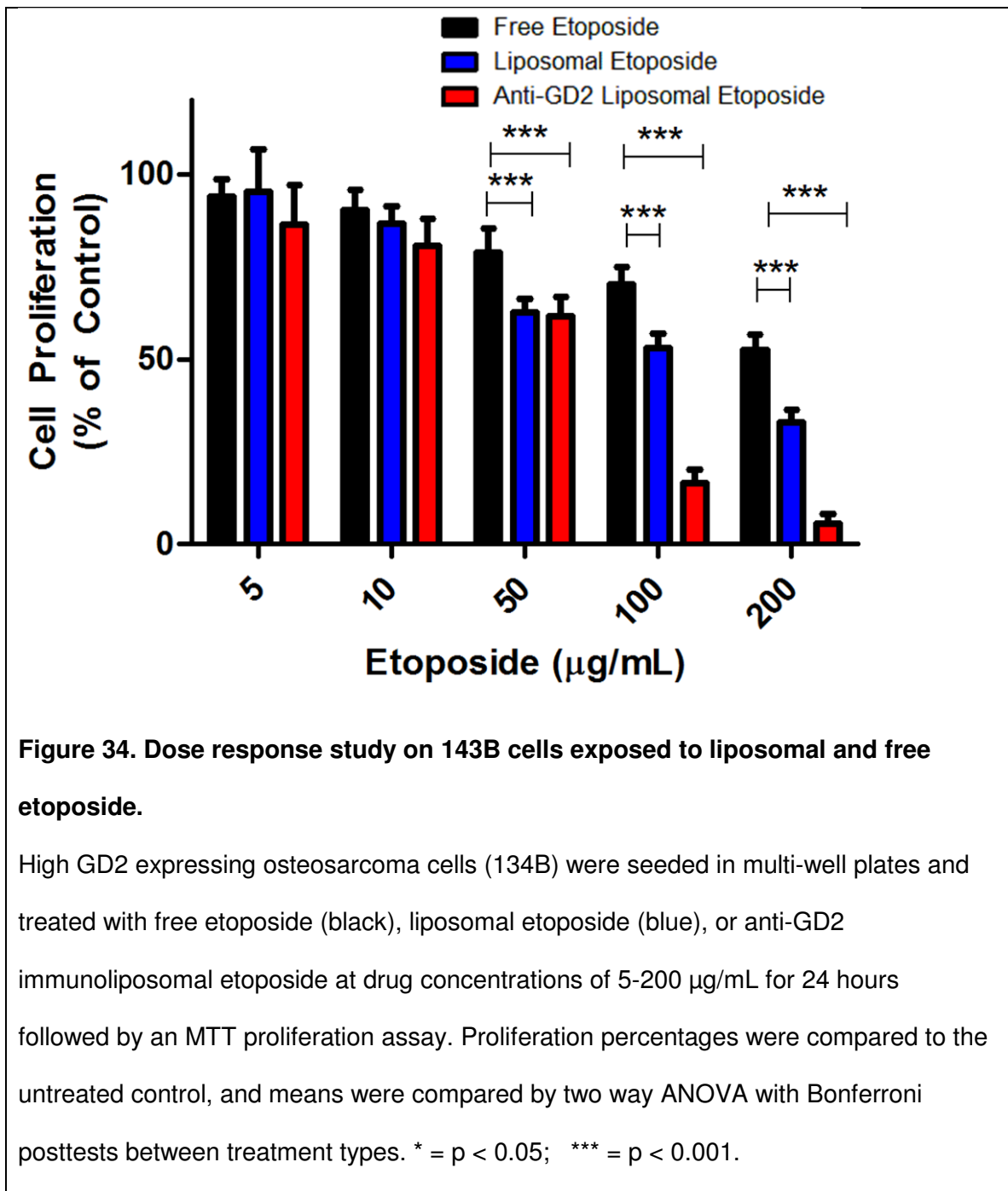


Figure 33. Dose response study on LA-155N cells exposed to liposomal and free etoposide.

High GD2 expressing neuroblastoma cells (LA-155N) were seeded in multi-well plates and treated with free etoposide (black), liposomal etoposide (blue), or anti-GD2 immunoliposomal etoposide at drug concentrations of 5-200 µg/mL for 24 hours followed by an MTT proliferation assay. Proliferation percentages were compared to the untreated control, and means were compared by two way ANOVA with Bonferroni posttests between treatment types. * = $p < 0.05$; *** = $p < 0.001$.



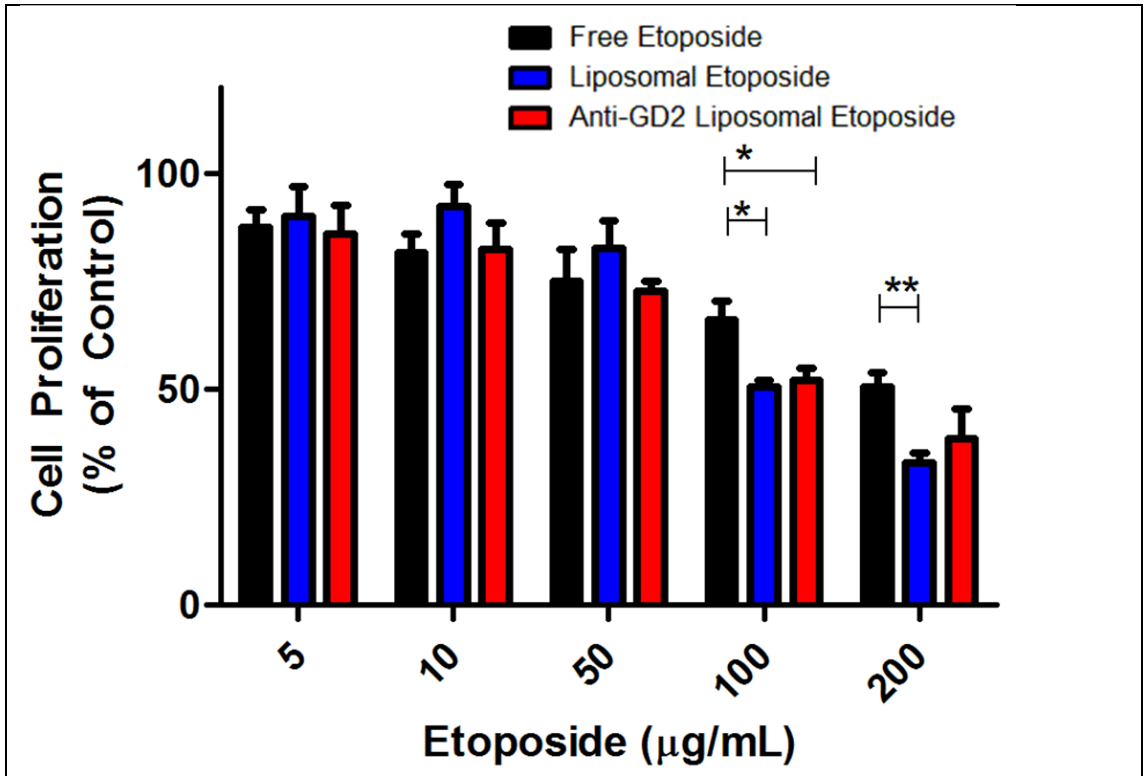


Figure 35. Dose response study on SY5Y cells exposed to liposomal and free etoposide.

Very low GD2 expressing neuroblastoma cells (SY5Y) were seeded in multi-well plates and treated with free etoposide (black), liposomal etoposide (blue), or anti-GD2 immunoliposomal etoposide at drug concentrations of 5-200 µg/mL for 24 hours followed by an MTT proliferation assay. Proliferation percentages were compared to the untreated control, and means were compared by two way ANOVA with Bonferroni posttests between treatment types. * = $p < 0.05$; ** = $p < 0.01$.

The osteosarcoma cell line, 143B, and one of the neuroblastoma cell lines, LA-155N were previously determined to exhibit high levels of GD2 at the cell surface. Conversely, the second neuroblastoma line, SY5Y exhibited little to no GD2 expression and served as a

negative control for targeting. Treatments varied in etoposide concentration from 5 to 200 $\mu\text{g}/\text{mL}$. We hypothesized that anti-GD2 liposomal etoposide would have the higher efficacy in GD2 expressing cells, represented by a lower IC_{50} , compared to free drug or untargeted etoposide liposomes.

We observed a significant enhancement of efficacy in GD2 targeted immunoliposomes compared to untargeted liposomes or drug alone at 50 - 200 $\mu\text{g}/\text{mL}$. The targeting advantage was only present in the two GD2 overexpressing cell lines. Interestingly, the GD2 negative cell line SY5Y had no significant improvement of IC_{50} in anti-GD2 immunoliposomes over untargeted liposomes, although liposomal etoposide encapsulation did increase toxicity at both 100 and 200 $\mu\text{g}/\text{mL}$ compared to free drug.

These data suggests that liposomal encapsulation of etoposide enhances efficacy at higher concentrations, and targeting to GD2 further enhances antitumor activity only in GD2 expressing cells. Further testing is warranted to determine if lower dosages are required at longer time points.

6.3 Anti-GD2 immunoliposome efficacy conclusions. Antitumor efficacy of the anti-GD2 etoposide immunoliposome complex was evaluated by repeated cell proliferation assays in cells treated with free drug, untargeted etoposide liposomes, or anti-GD2 etoposide liposomes. Changes in cell proliferation were compared to untreated cells, and controls were established to ensure that carrier substances such as DMSO or unloaded liposomes without etoposide did not significantly reduce proliferation. This means that changes in proliferation after treatment with free drug and encapsulated drug are very likely to be due to the action of the drug itself. We hypothesized that anti-GD2 liposomal etoposide would have a more dramatic reduction of viability on GD2 positive cell lines LA-155N and 143B compared to treatment with untargeted etoposide liposomes or free etoposide because we observed increased amounts of targeted liposomes being taken up by GD2 positive cells in previous experiments. Indeed, the IC_{50}

values of etoposide-loaded anti-GD2 immunoliposomes in GD2 positive cell lines LA-155N and 143B were 37.09 $\mu\text{g}/\text{mL}$ and 66.16 $\mu\text{g}/\text{mL}$ whereas the IC_{50} for the untargeted etoposide-loaded liposomes for LA-155N and 143B was 80.06 $\mu\text{g}/\text{mL}$ and 111.9 $\mu\text{g}/\text{mL}$ respectively. These data suggest that lower concentrations of anti-GD2 etoposide liposomes were required for a similar effect in cells treated with untargeted etoposide-loaded liposomes. From a clinical standpoint, this suggests that treatment with the anti-GD2 immunoliposomes would require a lower dosage than free drug or liposomal drug to have an equal effect on the tumor. Lower dosages should also result in fewer off-target effects and fewer patient toxicity events. These data warrant further investigation in an animal model where circulatory factors and biodistribution can be incorporated and assessed.

Chapter 7: Pilot *In Vivo* Study

7.1 In vivo pilot injections. Prior to a more involved pilot study, pilot injections of fluorescent immunoliposomes were performed in healthy mice to verify sufficient signal intensity for the IVIS imaging system. The IVIS animal imaging apparatus is capable of measuring infrared fluorescence as well as bioluminescence. Immunoliposomes were formulated with the infrared dye, DiR to facilitate *in vivo* imaging.

Liposomal injections representative of future therapeutic concentrations (100 μ L at a concentration of 10 mM lipids) were administered to the tail vein of brown mice. Mouse fur was chemically removed to prevent interference with the imaging camera, and fluorescence images were taken at 30 minutes and 3 hours with an infrared light filter, Figure 36.

40 minutes
after injection

3 hours after
injection

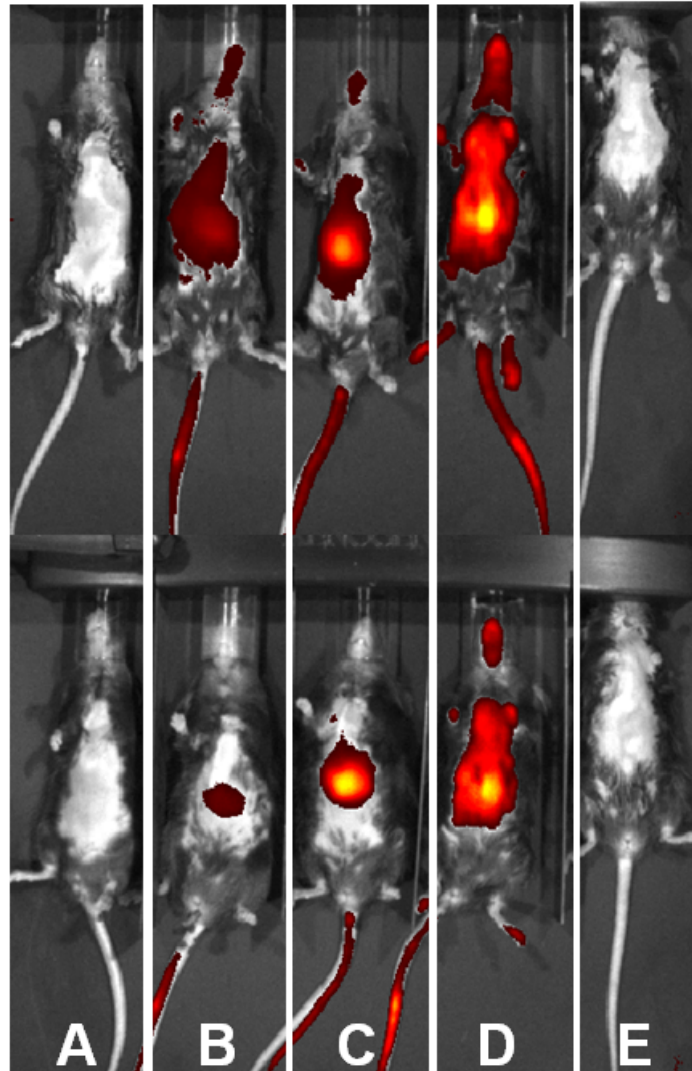


Figure 36. Preliminary in vivo imaging of mice injected with different formulations of fluorescent liposomes.

Liposomes were formed with near infrared fluorescent lipids at 0.2, 0.5, or 1.0 mole % of total lipids. C57BL/6 mice were given tail vein injections of either 0.2% (B), 0.5% (C), or 1.0% (D) fluorescent liposome formulations. Tail vein injections of saline (A) or etoposide (E) served as negative controls. Fluorescent images of the mice were acquired 40 minutes and 3 hours after injections.

Fluorescent signals were observed in all mice that received successful injections, and the fluorescence persisted for at least 3 hours, suggesting that the imaging system and liposome dye were compatible and appropriate for the upcoming pilot study on antitumor activity.

7.2 In vivo antitumor activity of anti-GD2 immunoliposomes. Orthotopic human xenografts composed of SY5Y or SKNAS were implanted into the adrenal glands of nude mice. The tumors were orthotopic because they often naturally occur in humans where they were implanted, and they were xenografts because human tumor cells were grown in mice. Nude mice were chosen for their ability to host the human neuroblastoma cell lines, SY5Y and SKNAS. Both cell lines were genetically modified to express luciferase for *in vivo* bioluminescence imaging.

Mice were randomly assigned to one of four treatment groups: Normal saline, free etoposide, untargeted liposomal etoposide, or anti-GD2 targeted liposomal etoposide. There were two groups of 6 and two groups of 7 for each tumor cell type. Mice received tail vein injections of 100 μ L with 20 mg/kg/day of etoposide for drug-containing treatment groups. Mice were injected with saline, etoposide, untargeted or anti-GD2 targeted immunoliposomes twice per week and imaged for liposome fluorescence after each injection cycle. Injections of luciferin were given abdominally prior to imaging to produce tumor luminescence. Example images are shown in Figure 37.

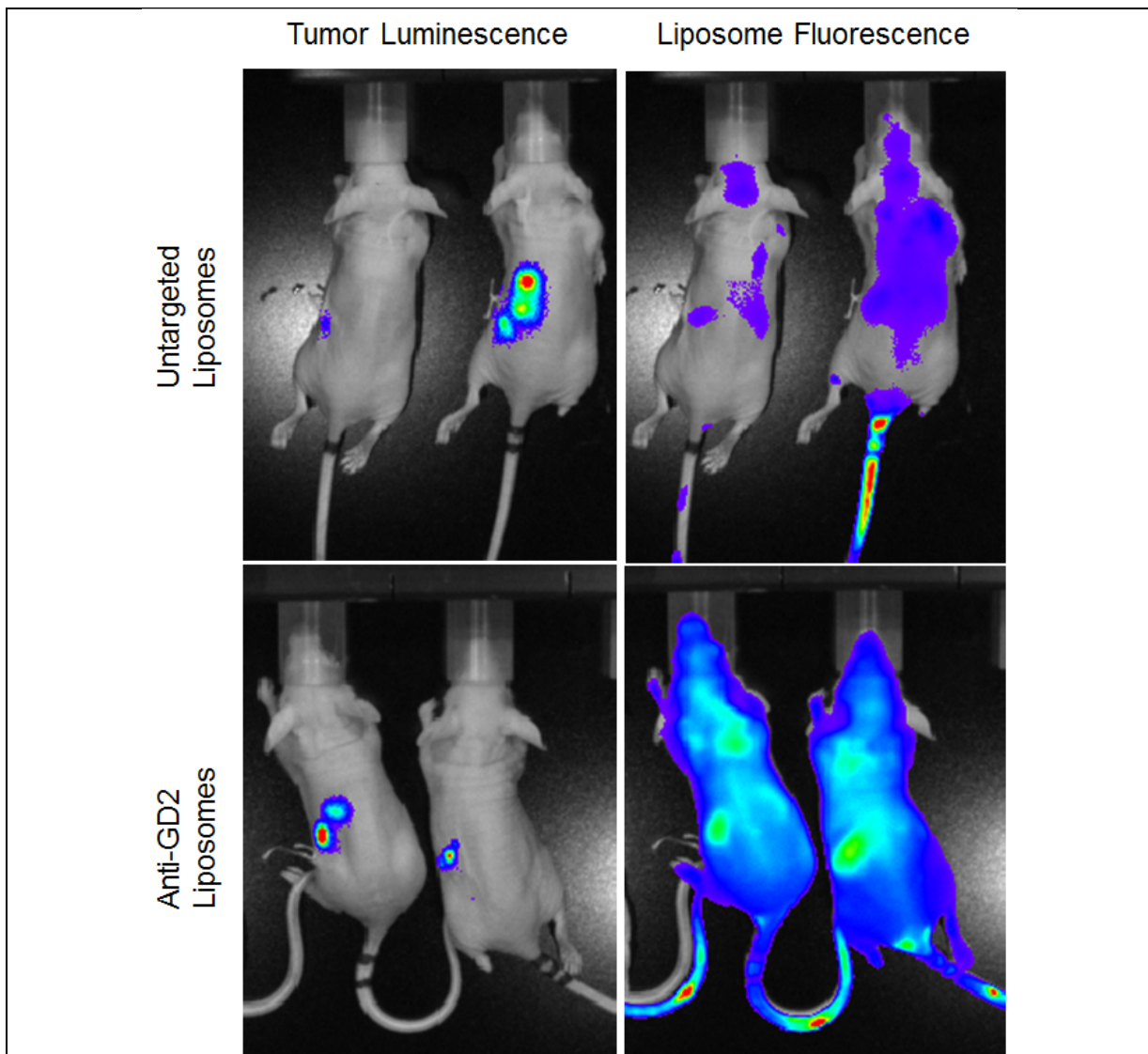


Figure 37. In vivo imaging of mice bearing luciferase-expressing SKNAS orthotopic xenografts after injection of GD2 targeted and untargeted immunoliposomes.

Human neuroblastoma SKNAS cells were injected into mouse adrenal glands on day 0. Mice received tail vein injections of nonspecific IgG-immunoliposomes or anti-GD2 immunoliposomes at 20 mg/kg/dose etoposide 30 minutes prior to imaging. Abdominal luciferin injections were given immediately prior to imaging for both luminescence and fluorescence.

In general, tumor targeting was not detected significantly more in anti-GD2 than in untargeted liposomes at this concentration. We also found that fluorescence due to liposomes persisted for days after injections, raising the possibility that fluorescent lipids were not immediately broken down and remained in tissue after liposomal degradation.

Following the third week of treatment, the mice were sacrificed, tumors were explanted and tumor weights were obtained, Figure 38.

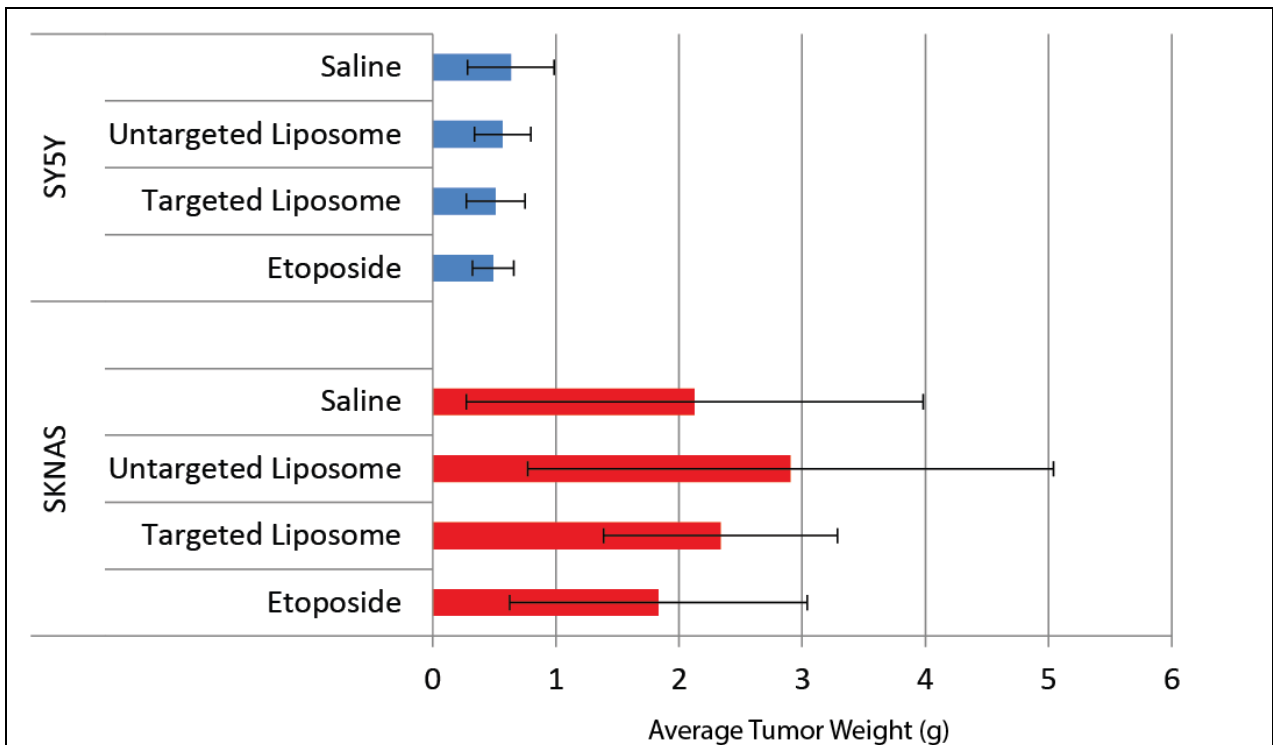


Figure 38. Explanted tumor weights from orthotopically implanted neuroblastoma xenografts in mice treated with etoposide.

Human neuroblastoma SY5Y (blue) or SKNAS (red) cells were injected into mouse adrenal glands on day 0. Treatment was begun on day 12. Mice received a total of four treatment cycles of 20 mg/kg/treatment of untargeted liposomal etoposide, targeted liposomal etoposide, free drug or saline. Mice were sacrificed on day 30 and tumors were explanted and weighed.

We did not detect a significant difference between any of the treatment groups, including the control and free drug treatment groups. These data suggest that some component of the initial study setup was not optimal. Further investigation of the cell types, SKNAS and SY5Y, suggest that they may not be ideal for this particular animal study.

7.3 In vivo pilot study conclusions. Neuroblastoma SY5Y and LA-155N orthotopic xenografts were implanted into mice in efforts to obtain preliminary *in vivo* data about the efficacy and biodistribution of anti-GD2 immunoliposomes. Tumors expressed luciferase which produces bioluminescence upon exposure to luciferin, and liposomes contained DiR near infrared dye for *in vivo* imaging. The study was preliminary because the relative variability between tumor sizes within control groups had not yet been established with the protocol we were using for tumor implantation. A power analysis to determine the necessary number of mice for an expected reduction in tumor size requires this estimate of tumor variability. A similar protocol evaluating the same surgical technique with a different neuroblastoma cell line found that with 10 mice per group, an average tumor weight reduction of 50% in treated mice compared to control mice was required to obtain statistically significant results with an alpha of 0.05 and power of 0.8. We hypothesized that anti-GD2 immunoliposomes carrying etoposide would cause a larger decrease in tumor weights than free drug due to increased accumulation of immunoliposomes and loaded drug at the tumor site. We also hypothesized that tumor weight variability would be similar to that of the previous surgical protocol because the procedure and mouse model were identical while tumor cells were of the same general cancer type (neuroblastoma).

We found that tumor size variation exceeded expected levels based on the implantation protocol in mice of all treatment groups. This suggests that larger treatment groups would be necessary to produce sufficient statistical power if the expected reduction in tumor size was 50%. Unfortunately, we did not observe a downward trend in tumor size in anti-GD2

immunoliposomes or drug alone, suggesting that higher treatment doses are required for the reduction in tumor size. An additional pilot study would be invaluable to determine the maximally tolerated dose to prevent excessive mouse overdose during treatment. Immunoliposome fluorescence was detected throughout the mice with particular intensity near the left flank where the tumors were implanted. The average fluorescent intensity near this region was higher in targeted immunoliposome-treated mice than in untargeted liposome-treated mice; however, it is difficult to ascertain if the fluorescence was increased at the actual tumor site, or the underlying mouse spleen. We concluded that the anti-GD2 immunoliposomes can be detected in mice via *in vivo* imaging, and larger follow-up studies are warranted to assess liposome-delivered etoposide effects on tumor growth.

Section IV: Discussion and Future Directions

Chapter 8: Discussion

Current approaches for GD2-directed therapy include immunotherapy with anti-GD2 antibodies, antibody-toxin conjugates, and genetically modified T-cells with the capacity to target GD2 positive tumor cells. Clinical trials with anti-GD2 antibodies for neuroblastoma over the past two decades have set the stage for further anti-GD2 therapeutic strategies. Anti-GD2 antibodies now have established safety and efficacy profiles, but limitations persist, particularly with acute pain toxicity and inability to treat bulky tumors⁵⁶. The potency of anti-GD2 therapeutics was accomplished by conjugating anti-GD2 antibodies to immunotoxins such as pseudomonas exotoxin A¹²¹. These studies reported immediate killing of GD2 positive cells in vitro, but concerns exist about immunogenicity of the treatment, and no GD2-targeted immunotoxins have reached human clinical trials¹²².

A third avenue of GD2 targeted therapy involves the genetic modification of T-cells to express a GD2 binding protein at their surface called a chimeric antigen receptor (CAR). T-cells expressing the CAR protein have been shown to release cytokines, proliferate and kill neuroblastoma cells¹²³. Moreover, preliminary phase I clinical trials have found tumor response in half the patients tested¹²⁴. This approach, while promising, carries a significant concern with respect to cost and preparation standards. The large-scale production of targeted, membrane-based drug-loaded immunoliposomes represents a potential therapeutic angle that could mitigate the problems encountered in other anti-GD2 targeted approaches.

This work provides data suggesting that anti-GD2 etoposide immunoliposomes can target GD2-expressing tumor cells and inhibit their proliferation. Overall results with respect to synthesis, characterization, and biological activity of the proposed immunoliposome model are encouraging, although additional testing remains prior to preclinical and clinical translation. Furthermore, results and problems encountered in this work will allow for the accelerated

production and characterization of future targeted nanoparticle projects by highlighting and avoiding potential pitfalls.

Applications for liposome-formulated drugs in medicine are expanding as the benefits of this system for controlled systemic delivery are appreciated. Liposomal delivery methods also show promise for other routes of entry such as transdermal, oral, and inhalation⁸⁰⁻⁸². The advent of targeting these formulations will result in more efficient use of pharmaceuticals and rescue some drugs that may have been unusable due to high side-effect profiles or low efficacy. Targeting of liposomal nanoparticles will also bring new challenges and potential problems as the dynamic human immune system responds to an influx of foreign substances with particular epitopes and immunoreactive molecules. Integration of targeting moieties must be carefully controlled.

Post-insertion of targeting moieties onto liposomes has proved to be very useful in the synthesis of targeted immunoliposomes for two key reasons. First, incorporation of PEG and crosslinkers to the limiting membrane reduces the loss of intraluminal space that would otherwise be occupied if PEG and maleimide were incorporated during initial ethanol injection. Second, conjugation of the targeting moiety is more controlled and less subject to hydrolysis of the maleimide crosslinker compared to synthesis methods without post-insertion where maleimide is exposed to all reagents of the ethanol injection process for longer periods of time. Drawbacks of the post-insertion method include the unknown quantity of unincorporated micelles after post-insertion. This also adds some level of uncertainty to the fraction of lipids carrying PEG chains; although exact levels of PEG-ylation do not appear critical because more than 2 mole % of total lipids within a given liposomal formulation appears to have similar effects on circulation time when administered systemically.

Maleimide conjugation during immunoliposome functionalization may occur at Fab binding fragment of the antibody, causing it to orient incorrectly with the Fc region facing

outward and potentially decreasing its ability to bind the target ligand. There are commercial kits available that use carbohydrate-rich regions of the Fc antibody region for conjugation. This conjugation strategy could result in higher binding activity of liposome-tethered MAbs, but also requires more specialized reagents and more complex crosslinking chemistry. Fortunately, effective targeting by our immunoliposomes in GD2 positive cells indicated that enough anti-GD2 antibodies were oriented correctly to enable detectable levels of ligand binding via flow cytometry.

Scaling production of targeted liposomes for mass production must be possible for more elaborate animal studies and translation into clinical trials. There are multiple difficulties in large-scale production of a multi-component system such as anti-GD2 immunoliposomes. Firstly, MAbs such as 3F8 currently are expensive and produced via a multistep purification process. Currently, treatment with one of the top nine biological in the US costs an average of \$200,000 per year¹²⁵. High material costs limit experimentation to small-batch synthesis experiments for most labs. Secondly, processes such as post-insertion for large-scale manufacture have not been sufficiently investigated to warrant large scale use of the technique. However, preliminary studies suggest it is a viable strategy for attaching targeting molecules to liposomes at large-scale¹²⁶.

Current drug therapy for cancers range from “classical” cytotoxic chemicals to more recent biological therapies including immunotherapy and monoclonal antibody based therapeutics. Emerging nanomedicines enhance traditional therapies while limiting weaknesses and off-target effects. A clinically available liposome formulation of doxorubicin provides an example of this enhancement by increasing circulation time and delaying the release compared to unencapsulated doxorubicin⁶⁹. Anti-GD2 immunoliposomes carrying etoposide stably released their drug over 6 hours with continued release up to 12 hours compared to unencapsulated drug that disseminates rapidly when administered systemically. This controlled

release decreases the dosing required to maintain a therapeutic level of a given drug over time, and smaller quantities of the drug would be necessary as the liposomes accumulate at the target site via passive and active targeting mechanisms. The drawback to a delayed release profile is that adverse effects of the drug may be prolonged after the drug is discontinued.

The same issues encountered with etoposide treatment clinically also cause difficulties when characterizing etoposide-loaded liposomes. In particular, poor solubility of etoposide in aqueous solutions complicates the quantification of etoposide release from nanoparticles into physiologic mediums. Problems to be expected in future applications involving etoposide encapsulation include the chemical decomposition of etoposide in a dissolved state as well as changes in etoposide stability with scaled up production.

Another consideration for the translation of anti-GD2 immunoliposomes into clinical use involves the storage of immunoliposomes prior to administration. Shelf life of clinically approved MAbs approaches 3 years if dried and frozen and less than 48 hours when in solution. For this reason, freeze-drying of the immunoliposomes must be analyzed and optimized. Freeze-drying, or lyophilisation, has been accomplished with immunoliposomes targeted to the breast cancer target, HER2, successfully, but no evidence is available supporting the successful lyophilization of anti-GD2 immunoliposomes carrying etoposide ¹²⁷. Our experience suggests that lyophilization could cause precipitation of etoposide due to its poor solubility and previous difficulties with liposomal encapsulation. Immunoliposomes may need addition of cryopreservative agents such as glycerol prior to lyophilization to avoid damage to liposomal membranes.

We described the surface GD2 expression and anti-GD2 targeting liposomal targeting to osteosarcoma, melanoma, cervical carcinoma, and four different neuroblastoma cancer lines. Surface expression was valuable for correlating to targeting efficacy. However, gene expression and variations in GD2 expression over time and during treatment remain to be

investigated. Aggressive cancer cells might resist treatment by downregulation of GD2 expression following repeated exposure to anti-GD2 therapeutics. Treatment resistance by GD2 downregulation may still incur some cytostatic or cytotoxic effects, as some evidence exists that GD2 downregulation is correlated with decreased tumor survival *in vitro*¹²⁸. Further studies of GD2 metabolism following anti-GD2 immunoliposome treatment are warranted to evaluate potential resistance mechanisms in GD2 positive malignancies.

Gangliosides such as GD2 are produced in the Golgi apparatus where they are regulated predominantly by the activity of the enzymes required for their synthesis, GD2 and GD3 synthase. The mechanisms by which tumor cells dramatically increase GD2 synthesis is not well understood, but may involve tumor cell adhesion and metastatic transition that increases GD2 synthesis or decreases its metabolism. Our studies suggest that clinical trials with anti-GD2 immunoliposomes would benefit from patient stratification by levels of GD2 surface expression. Study organizers may decide to exclude patients with GD2 positive tumors that overexpress the ganglioside at lower levels relative to other patients with GD2 positive disease. Stratification by GD2 expression is likely to increase the sensitivity of the study in regard to tumor response and remission rates. Ongoing clinical trials of 3F8 immunotherapy, to our knowledge, do not stratify patients by levels of GD2 expression. Currently, 3F8 treatment protocols are designed for patients with high-risk neuroblastoma, including patients with bulky disease, refractory or relapsed disease, and bone marrow disease. The only GD2 requirement that is noted in clinical trial documents is “positive immunostaining with m3F8”¹². Our studies with anti-GD2 immunoliposomes rely on 3F8 binding activity which implicates a strong possibility that future 3F8 clinical studies would also benefit from GD2 expression stratification. However, our study did not address efficacy of free 3F8 immunotherapy with respect to GD2 expression. Further studies are warranted to address these issues.

We found that GD2-targeted immunoliposome-mediated inhibition of proliferation can occur in multiple cancer cell lines *in vitro*. Efficacy *in vitro* provides evidence that functional nanocarriers are present and the drug payload retains bioactivity for the duration of our experiments. Recall that 3F8 exerts antitumor effects via antibody-directed cellular cytotoxicity. Therefore, more significant antitumor effects may be observed with anti-GD2 immunoliposomes in the presence of whole blood components such as complement proteins and circulating leukocytes. Isolated *in vitro* experiments lack the structural and biological complexity of animal bodies that can inhibit antitumor efficacy. Immunoliposomes are particularly sensitive to removal by the MPS *in vivo*. PEGylation of immunoliposomes delays MPS uptake, but the degree and duration of delay is less characterized than in untargeted liposomes. Additionally, the benefits of PEGylation vary with the type and density of targeting antibodies¹⁰⁵. PEGylation may reduce observed uptake *in vitro*, hence we may be underestimating the efficacy that would occur *in vivo* due to increased circulation time for targeted particle uptake.

We synthesized and evaluated etoposide loaded anti-GD2 immunoliposomes and examined their targeting and potential to affect tumor proliferation *in vitro*. In addition to the expansion of studies with these particles, other liposomal formulations utilizing these methods could benefit from this combination of drug loading and targeting strategies. We also evaluated GD2 surface expression in multiple cell lines and found it to vary dramatically across tumor types and within neuroblastoma cell lines. This is significant due to clinical implications for immunotherapy and targeted nanoparticle efficacy. Moreover, neuroblastoma patients may benefit from quantitative GD2 expression profiling as a predictive measure of anti-GD2 therapy. Finally, we showed that lower concentrations of targeted etoposide anti-GD2 liposomes were required for an equivalent effect of etoposide alone to inhibit proliferation of multiple cancer cell lines. These data suggest that smaller doses of GD2 targeted liposomal etoposide may be able to be given to patients. This has the important effect of potentially fewer and less severe off-

target effects, lower cost, and a larger therapeutic window if higher doses are required. The final effect of these advances compared to current treatments is a less toxic and more effective treatment strategy for tumors with high levels of ganglioside GD2 expression.

Chapter 9: Future Directions

9.1 Expansion of *in vivo* evaluation. Future anti-GD2 immunoliposome testing *in vivo* would be altered based on lessons learned in the pilot study in mice. Two major issues in the pilot study involve the cell lines chosen and the primary outcome of the tumors that arose from those cell lines. One of the two neuroblastoma cell lines used in the pilot, SY5Y, expresses very little GD2 and was actually used as a negative control in targeting experiments. The other cell line, SKNAS, was found to express GD2 at high levels, but exhibited unexceptional anti-GD2 liposomal targeting *in vitro*. The *in vitro* results were preliminary when the *in vivo* study was being designed, and SKNAS was a well-established cell line involved in multiple other projects beyond the immunoliposome study. Nonetheless, the neuroblastoma cell lines were not optimal cell lines for the observation of a maximum effect from the anti-GD2 immunoliposomes.

In retrospect, we might have observed more dramatic anti-tumor effects in mice treated with anti-GD2 targeted formulations if we chose a cell line with higher levels of surface GD2 expression. Future studies should focus on one or two cell lines with high GD2 expression and high GD2 targeting, such as LA-155N or 143B, where a larger antitumor effect would be expected. The previous pilot study also revealed a large variance in tumor sizes explanted from mice injected with the same number of cancer cells of the same cancer cell line. This could have been due to restricted volume of the adrenal medulla where cancer cells were seeded, or a large variance in the number of cells surviving the tumor seeding. Additional pilot studies could investigate the effect of seeding density and orthotopic site on variable tumor sizes; however, time and resource constraints would likely persuade us to repeat the study with larger treatment groups to account for the large tumor size variability.

In its entirety, the next animal study would consist of a larger, more representative pilot experiment to determine variability between mice with similar treatments. This would facilitate a

more accurate power analysis to determine the minimum number of mice needed in each treatment group. The second, larger part of the study would contain sufficient power so that the treatment of anti-GD2 etoposide-loaded liposomes, if more effective than etoposide alone or untargeted liposomes, would yield significant differences in tumor weights and drug accumulation.

9.2 Future applications of anti-GD2 immunoliposomes. Roles of the anti-GD2 immunoliposome platform are not limited to neuroblastoma therapy. Other drug delivery opportunities exist that could benefit from the targeting and drug delivery potential of anti-GD2 targeting. For example, anti-GD2 immunoliposomes produced with the DiR infrared dye or other contrast agents could be administered as targeted radiological agents to delineate GD2 positive cancer remnants after surgery or distant metastases. Liposomes have been successfully developed as enhanced carriers of the MRI contrast agent, gadolinium¹²⁹.

Alternatively, targeted liposomes could be combined with adjuvant immunotherapies such as IL-2 and GM-CSF (traditionally combined with 3F8 immunotherapy) to enhance antibody-mediated cellular cytotoxicity⁵⁹. These immunomodulators enhance the function of 3F8 compared to 3F8 administered alone and may induce a synergistic effect when combined with etoposide-loaded liposomes. The issue of antibody directed cytotoxicity that may occur with MAb targeted immunoliposomes is not well understood. Studies to assess this effect include dose response with complement and targeted liposomes *in vitro* for proliferation inhibition of tumor cells in addition to more comprehensive *in vivo* studies with immunocompetent mice capable of mounting an immune response.

Other targets that express high levels of GD2 could also be investigated as potential therapeutic opportunities for GD2 immunoliposomes containing chemotherapeutics. Recently, breast cancer stem cells were found to have higher levels of GD2 expression than other breast cancer cells in at least one breast cancer cell line¹²⁸. Cancer stem cells are a subpopulation of

tumor cells capable of establishing metastases and are resistant to conventional therapies¹³⁰¹³¹. Breast cancer cells expressing the GD2 ganglioside were found to share other proteomic markers of cancer stem cells, and genetic knockdown of GD2 synthesis in these cells halted tumor progression *in vivo*¹²⁸. Similar cells were identified in the bone marrow of breast cancer patients by an independent group¹³². Targeted killing of these tumor initiator cells could improve survival and cure rates in patients being treated for breast cancer.

9.3 The future of multifunctional nanoparticles. Targeted therapies and multifunctional nanomedicines continue to become increasingly complex, and new nanoparticles incorporate an increasing amount of cell-like features. Several vaccines have been formulated with liposome carriers such as the avian retrovirus (chickenpox) vaccine¹³³ and hepatitis A vaccine¹³⁴. Immunoliposomes can closely resemble an enveloped virus, and as such could be useful for vaccine encapsulation as well as gene therapy.

Cells are also capable of producing and expelling immunoliposome-like particles, called exosomes. Exosomes are lipid bilayer vesicles, about 70-100 nm in diameter produced by the vast majority of cell types. Cancer cell-produced exosomes are being studied for their ability to prepare sites for metastases¹³⁵, and experimentally modified dendritic cells are being stimulated to release exosomes carrying genetic and protein material to improve symptoms of multiple sclerosis¹³⁶. Exosomes produced by dendritic cells are also being investigated for immunotherapeutic vaccines targeted to melanoma and non-small cell lung cancer¹³⁷. Future applications of exosomes are diverse due to their high surface protein density and ability to carry both genetic and protein payloads. There may be efforts to create exosomes outside of cells using the necessary machinery, resulting in higher output and more simplistic exosome purification. One current issue with biologically derived exosomes is the relatively complex procedure to isolate and purify exosomes via serial ultracentrifugation and separation on density gradients¹³⁸.

Another strategy for liposome drug delivery is the application of fusogenic liposomal membranes¹³⁹. Some liposomes are being constructed with modified lipids that induce membrane fusion after encountering a lower pH¹³⁹. In this scenario, intact liposomes are endocytosed and fuse with the endocytic membrane as it acidifies¹⁴⁰. The liposome-endosome fusion results in release of the liposomal contents directly into the cytoplasm¹⁴¹. Cytoplasmic release of liposomal contents via pH responsive membranes or viral proteins delays drug degradation by lysosomes resulting in higher quantities of active drug reaching intracellular targets¹³⁹. Drawbacks of the strategy include uncontrolled fusion with non-pathological cells and decreased particle circulation time due to premature membrane fusion¹⁴⁰.

9.4 The future of targeted nanomedicine development. Potential applications involving nanotechnology in medicine have garnered significant media attention in recent years due to the theoretical features nanomaterials possess. Nanomedicines have failed to keep up with the media hype in part due to unrealistic expectations by the public, expensive and difficult path to clinical approval by the FDA, and difficulties controlling solubilized nanomaterials. True paradigm-shifting nanomedicines will result from the synergistic combination of all fields of science. In particular, advances in fields such as genetics, epigenetics, proteomics, medical physics, molecular biology, *in silico* simulation and computational biology, as well as micromanipulation and additive manufacturing will combine to form future nanomedicines. Gene therapy, artificial organs, cybernetic limbs, and implants that interface with the nervous system are no longer future directions, but current projects being refined for clinical approval. Progressive advances in these fields will eventually produce artificial cells and organelles, potentially creating new calls to readdress the classical definitions of life.

The first generation of targeted nanomedicines reaching clinical approval in the near future will likely be immunoliposomes due to an established toxicity profile of liposomes in combination with previously FDA approved MAbs as targeting moieties. Adoption of new

targeted therapies by physicians will depend on additional factors, including cost, differences in efficacy compared to traditional treatments, and reimbursement by insurance companies.

Considerable work remains to be done prior to first-line targeted nanoparticle formulations, but the foundation is set, and the technology has unprecedented potential impact for human health.

Chapter 10: Materials and Methods

10.1 Chemicals and lipids. Dipalmitoyl-*sn*-glycero-3-phosphocholine (DPPC), 1,2-dioleoyl-*sn*-glycero-3-phosphoethanolamine-N-(lissamine rhodamine B sulfonyl) (DOPE-Rhodamine), 1,2-distearoyl-*sn*-glycero-3-phosphoethanolamine-N-[methoxy(polyethylene glycol)-2000] (DSPE-mPEG2000) and 1,2-distearoyl-*sn*-glycero-3-phosphoethanolamine-N-[maleimide(polyethylene glycol)-2000] (DSPE-mPEG200-Maleimide) were purchased from Avanti Polar Lipids (Alabaster, Alabama). 3β -hydroxy-5-cholestene (cholesterol), >99% dimethyl sulphoxide (DMSO), thiazolyl blue tetrazolium bromide (MTT salt), L-gulamine, tris-HCl, 40% Glycerol, red ponceau, and Tris buffered saline (TBS) were obtained from Sigma Aldrich (St. Louis, Missouri). Traut's reagent, penicillin, streptomycin, bromophenol blue and all cell culture media were acquired from ThermoFisher Scientific (Waltham, Massachusetts). Etoposide (VP16, >99% grade purity) was obtained from Biotang (Waltham, Massachusetts). Tween 20 was acquired from Aurion (Rotterdam, The Netherlands). Horseradish peroxidase was purchased from Cell Signaling Technology (Beverly, Massachusetts). Alexa Flour 488 goat anti mouse IgG was purchased from Invitrogen (Carlsbad, California). Murine IgG3 monoclonal antibody 3F8 (3F8 anti-GD2) was a kind gift from Nai-Kong Cheung (Memorial Sloan Kettering Cancer Center, New York, NY). All other chemicals were of analytical grade and purchased from Sigma Aldrich.

10.2 Liposome preparation and physicochemical characterization. Liposomes were prepared using a modified ethanol direct injection technique previously reported.¹⁴² Briefly, DPPC and Cholesterol at a molar ratio of 60:40 were dissolved in 100% ethanol heated to 60°C under continuous stirring. 0.2 mole % of the fluorescent lipid, DOPE-Rhodamine was dissolved into ethanol and injected into a warm solution of PBS at a ratio of 1:9 by volume under continuous stirring (2000rpm). The ethanol was then removed by rotary evaporation (Buchi,

Switzerland). Where necessary, etoposide dissolved in DMSO (at 50mg/mL) was added to the ethanol phase prior to injection, thus obtaining a final concentration in the range from 1-4 mg/mL. Entrapment efficiency and drug loading were calculated by the following formulas:

$$\text{Entrapment Efficiency (\%)} = (\text{Quantity of drug encapsulated}) / (\text{Total quantity of drug added}) \times 100\%$$
$$\text{Drug Loading (\%)} = (\text{Quantity of drug encapsulated}) / (\text{Total quantity of lipids added}) \times 100\%$$

Average size, size distribution, and zeta potential were analyzed using Malvern Zetasizer Nano ZS (Malvern, Worcestershire, UK) as previously reported.¹⁴³ Briefly, liposomes were diluted (1:100 molar ratio) using isotonic PB buffer (pH 7.4), previously filtered (pore size 0.22 mm) through polypropylene membranes (Whatman Inc., Clifton, NJ, USA) to avoid multiscattering phenomena and loaded into size and Z-potential disposable cuvettes before analysis.

Photocorrelation spectroscopy was applied to evaluate average size and narrow size distribution. The instrument was set up using the following parameters: real refractive index 1.59, imaginary refractive index 0.0, medium refractive index 1.330, medium viscosity 1.0 mPa × s and medium dielectric constant 80.4. Z-potential was performed using the Doppler laser anemometry and hence the electrophoretic mobility. A Smoluchowsky constant F (Ka) of 1.5 was applied to measure electrophoretic mobility of samples.

10.3 Preparation of 3F8 anti-GD2 immunoliposomes. Micelles containing DSPE-mPEG2000 and DSPE-mPEG2000-maleimide at a 99:1 molar ratio were co-dissolved in an ethanol solution and added drop wise into a warm PBS solution containing 2 mM EDTA at a ratio of 1:1 v/v creating the final micellar solution. 50µL of micellar solution (10mM, pH 7.4) was added to the preformed liposome mixture with agitation and heating at 65°C thus allowing post insertion.

Meanwhile, 3F8 anti-GD2 monoclonal antibodies were sulfonated at a 1:10 molar ratio using Traut's reagent and purified using Zebaspin desalting columns (ThermoFisher Scientific, Waltham, Massachusetts). After the liposomal solution returned to room temperature, the purified sulfonated antibody was added to the liposomal solution and incubated at 4 °C overnight under constant stirring to obtain the final immunoliposomes.

10.4 Transmission electron microscopy (TEM). TEM analysis was performed using a JEM 1010 transmission electron microscope (JEOL, Inc., Peabody, Massachusetts) at a voltage of 80kV. Liposomes underwent negative staining and placed on formvar coated carbon grids followed by 1 minute staining with 1% v/v ammonium molybdate (pH 7.0). Immunogold staining of samples was performed by blocking liposomes for 30 minutes with 5% BSA in PBS solution (pH 7.4), followed by 30 minute incubation with secondary goat-anti-mouse 6nm gold antibodies (1:25 v/v dilution) followed by three washes in water to remove salts and unbound immunogold.

10.5 Fourier transformed infrared spectroscopy (FTIR). Bonds conjugated with DSPE-mPEG2000-Maleimide linker and the 3F8 antibody were qualitatively identified by using the FTIR apparatus. Concentrated samples (10 mM) were prepared by the application of 3 μ L followed by desiccation on the SMART ATR diamond surface on a Nicolet 6600 FTIR spectrophotometer. The DSPE-mPEG2000-Maelimide and 3F8 antibody were analyzed individually and then conjugated. Unconjugated linker was removed by Zebaspin desalting columns followed by Amicon centrifuge filters (Millipore, Billerica, MA) with a 30kDa molecular weight cutoff at 14,000 \times g for 10 minutes prior to analysis of the conjugated sample. The detector was used at room temperature at a 4 cm^{-1} resolution in absorbance mode averaging 16 runs. Peak analysis was carried out using Omnic Spectra software.

10.6 Cell Culture. Neuroblastoma cell lines NBL5, LA-155N, IMR-32, SH-EP, and SH-SY5Y were validated by STR analysis and cultured in DMEM/F12. Adenocarcinoma cell lines HeLa and MDA-MB-231 were cultured in DMEM and Leibovitz L15 respectively. Malignant melanoma cell lines SK-MEL-28 and A375 were cultured in DMEM. Osteosarcoma cell line 143B was also cultured in DMEM. All media was supplied with FBS (10% v/v), penicillin G-streptomycin mixture (1% v/v), and L-glutamine (1% v/v). Cell lines were cultured in incubators at 37°C and 5% CO₂.

10.7 Flow cytometry analysis of GD2 expression and liposome targeting. In order to assess the expression of GD2 on the surface of different cell lines, 3×10^5 cells per treatment group of each line were collected. Cells were lifted using a 2 mM treatment of EDTA to retain surface protein structure and counted using hemocytometry. They were then re-suspended in 3% v/v BSA in PBS solution (pH 7.4) and placed on ice for the remainder of the analysis. After 30 minutes of blocking in 3% v/v BSA, cells were treated with primary 3F8 antibodies and incubated for 1 hour. Cells were then washed in BSA solution and further incubated for 30 minutes with Alexa Fluor 488 goat anti mouse IgG. Control groups were treated with secondary antibody only. After final washing in PBS solution (pH 7.4), samples were analyzed by the Fortessa cell counter (Becton Dickinson, Bedford, MA) with excitation at 488 nm and an emission bandpass filter at 530 nm.

10.8 Liposome targeting to cancer cells. To assess 3F8 immunoliposome targeting to the cell lines mentioned, 3×10^5 cells of each line were collected and counted as herein reported. The collected cells were exposed to DOPE-Rhodamine liposomes with or without targeting agents for 30 minutes under continuous rotation (10 rpm) at 4°C. Each treatment group was

washed three times with PBS solution (pH 7.4) and analyzed on the FACS Fortessa cell counter (Becton Dickinson, Bedford, MA) with excitation at 488nm and an emission bandpass filter at 530nm.

10.9 Confocal imaging of liposome uptake. Optical analysis of liposome uptake was done on the Nikon A1 confocal laser scanning microscope (Nikon Corporation, Tokyo, Japan). Cells were grown on 4-well chamber slides at a seeding density of 7×10^4 cells per well and allowed to attach overnight. Cells were treated with 3F8 immunoliposomes or untargeted liposomes for 30 minutes in cell culture conditions. Prior to imaging, cells were fixed with 4% v/v paraformaldehyde and mounted with Prolong Gold with DAPI.

10.10 High pressure liquid chromatography quantification of drug loading. The amount of etoposide entrapped inside liposomes was performed using high performance liquid chromatography (H.P.L.C.) (Hitachi, Tokyo, Japan). Etoposide loaded liposomes were separated from unencapsulated etoposide by ultracentrifugation at 150,000 $\times g$ at 4 °C for 1 hour in a Fiberlite F50L-24 \times 1.5 rotor, followed by Amicon filtration with 30 kDa centrifuge filters at 14000 $\times g$ for 10 minutes. Filtered liposomes were then diluted in methanol followed by injection and flow through a Zobrax Eclipse Plus C18 column (4.6mm \times 150 mm, i.d. 5 μ m) (Agilent Technologies, Santa Clara, CA) at a flow rate of 0.65 mL/min. The mobile phase was composed of 50% v/v methanol and 50% v/v acetic acid. Absorbance was detected at 228 nm, and samples were run in triplicate. Results are the average of three different measurements \pm standard deviation.

10.11 Etoposide-induced proliferation inhibition. Neuroblastoma cells (cell line: LA-155N, SKNAS, or SY5Y) were seeded at a cell density of 7500 cells/well using 96 well cell culture

plates. Cells were allowed to attach overnight in the incubator after which the media was removed and replaced with treatment solutions. Cells were treated with 100 μ L PBS, etoposide alone (control), untargeted etoposide liposomes, or 3F8 targeted etoposide loaded liposomes. All etoposide concentrations were tested at 50 μ g/mL for 72 hour experiments. Cytotoxicity was inferred from the results of repeated MTT proliferation assays (Sigma Aldrich, St. Louis, MO). For 24 hour dose-response experiments, cells were treated with 100 μ L PBS, etoposide alone (control), untargeted etoposide liposomes, or 3F8 targeted etoposide loaded liposomes at etoposide concentrations increasing from 0-200 μ g/mL. Proliferation studies were performed via MTT assay (Sigma Aldrich, St. Louis, MO). MTT reduction was assessed by absorbance measurement at 570 nm with a reference wavelength of 690 nm according to the manufacturer's instructions. IC₅₀ calculations were performed via nonlinear regression via GraphPad Prism software v5.03.

10.12 Endocytosis inhibition study. To assess through which pathway immunoliposomes were internalized, SKNAS neuroblastoma cells were cultured on chamber slides as described previously. The cells were washed twice with PBS and the media was replaced with culture medium without serum to avoid serum inactivation of inhibitors. The cells were pretreated Dynasore (80 μ M), Filipin (10 μ M), or a combination of both drugs for 30 minutes. Rhodamine-labeled 3F8 immunoliposomes (0.1 mM) were then added for 1 hour at 37°C to allow for internalization. Cells were washed three times with PBS, fixed with 4% v/v paraformaldehyde and mounted with DAPI Prolong Gold antifade reagent (Molecular Probes, Grand Island, NY). Cells without inhibitors treated with and without immunoliposomes served as positive and negative controls, and cells were treated with fluorescent EGF to verify inhibition of clathrin-dependent endocytosis. Twenty fields of view were captured and analyzed for mean fluorescent intensity of Rhodamine within individual cells delineated by regions of interest on

Nikon Elements software version 3.22. Intensity means were compared by one way ANOVA, and p-values < 0.05 were considered significant.

10.13 Etoposide release study. Differences in drug release between liposomes and immunoliposomes were realized in a 72h release study. Particles were centrifuged in a 3.5mL Amicon Ultra-4 100 kDa filter at 4000xg for 30 minutes and resulting supernatant was diluted to reach 3.5mL volume. 1mL of colloidal particles was placed in Spectra/Por Float-A-Lyzer G2 cellulose ester membranes (MWCO 100kD, 1mL vol) for 72 hours with samples collected at different time points. The receptive phase consisted of a 50mL solution of PBS (pH 7.4) and Tween20 (1% v/v). Study was conducted at 37°C under continuous stirring (300rpm) and 1mL samples withdrawn were replaced with new PBS + Tween20 solutions. Samples were analyzed via HPLC as previously reported.

10.14 Mouse orthotopic xenografts. NCr athymic nude mice (4-6 weeks old) were anesthetized and the kidneys were accessed surgically according to the surgical protocol put forth by Shohet et al. Meanwhile, SKNAS or SY5Y cells transduced to express the luciferase reporter gene were trypsinized and prepared for injection into the superior pole of the kidney under the renal capsule (1 x 10⁶ SKNAS or SY5Y cells per mouse per injection). Tumors were allowed to grow for 10 days before initiation of treatment. Mice were randomly assigned to treatment groups for either vehicle only (saline with <1% DMSO), free etoposide, liposomal etoposide, or anti-GD2 liposomal etoposide. All etoposide-containing treatments were at 20 mg etoposide per kg of mouse per injection. Treatments were administered followed by bioluminescence and fluorescence imaging at the IVIS in vivo imaging system twice weekly for two weeks. On the third week, mice were sacrificed, and tumors were explanted and weighed.

BIBLIOGRAPHY

1. Society AC. Cancer Facts & Figures. Atlanta, GA: American Cancer Society, 2013.
2. Jemal A, Simard EP, Dorell C, Noone AM, Markowitz LE, Kohler B, et al. Annual Report to the Nation on the Status of Cancer, 1975-2009, featuring the burden and trends in human papillomavirus(HPV)-associated cancers and HPV vaccination coverage levels. *J Natl Cancer Inst* 2013; 105:175-201.
3. Hanahan D, Weinberg RA. Hallmarks of cancer: the next generation. *Cell* 2011; 144:646-74.
4. Anand P, Kunnumakkara AB, Sundaram C, Harikumar KB, Tharakan ST, Lai OS, et al. Cancer is a preventable disease that requires major lifestyle changes. *Pharm Res* 2008; 25:2097-116.
5. Ward EM, Thun MJ, Hannan LM, Jemal A. Interpreting cancer trends. *Ann N Y Acad Sci* 2006; 1076:29-53.
6. Kaatsch P. Epidemiology of childhood cancer. *Cancer Treat Rev* 2010; 36:277-85.
7. Ottaviani G, Jaffe N. The epidemiology of osteosarcoma. *Cancer Treat Res* 2009; 152:3-13.
8. Osuna D, de Alava E. Molecular pathology of sarcomas. *Rev Recent Clin Trials* 2009; 4:12-26.
9. Cheung NK, Dyer MA. Neuroblastoma: developmental biology, cancer genomics and immunotherapy. *Nat Rev Cancer* 2013; 13:397-411.
10. Maris JM, Hogarty MD, Bagatell R, Cohn SL. Neuroblastoma. *Lancet* 2007; 369:2106-20.
11. Modak S, Kushner BH, LaQuaglia MP, Kramer K, Cheung NK. Management and outcome of stage 3 neuroblastoma. *Eur J Cancer* 2009; 45:90-8.

12. Kushner BH, Kramer K, Modak S, Cheung NK. Successful multifold dose escalation of anti-GD2 monoclonal antibody 3F8 in patients with neuroblastoma: a phase I study. *J Clin Oncol* 2011; 29:1168-74.
13. Matthay KK, Villablanca JG, Seeger RC, Stram DO, Harris RE, Ramsay NK, et al. Treatment of high-risk neuroblastoma with intensive chemotherapy, radiotherapy, autologous bone marrow transplantation, and 13-cis-retinoic acid. Children's Cancer Group. *N Engl J Med* 1999; 341:1165-73.
14. Delaney G, Jacob S, Featherstone C, Barton M. The role of radiotherapy in cancer treatment: estimating optimal utilization from a review of evidence-based clinical guidelines. *Cancer* 2005; 104:1129-37.
15. Lau L, Tai D, Weitzman S, Grant R, Baruchel S, Malkin D. Factors influencing survival in children with recurrent neuroblastoma. *J Pediatr Hematol Oncol* 2004; 26:227-32.
16. Okada H, Mak TW. Pathways of apoptotic and non-apoptotic death in tumour cells. *Nat Rev Cancer* 2004; 4:592-603.
17. Joel SP, Shah R, Slevin ML. Etoposide dosage and pharmacodynamics. *Cancer Chemother Pharmacol* 1994; 34 Suppl:S69-75.
18. McLeod HL, Evans WE. Clinical pharmacokinetics and pharmacodynamics of epipodophyllotoxins. *Cancer Surv* 1993; 17:253-68.
19. Rodman JH, Murry DJ, Madden T, Santana VM. Altered etoposide pharmacokinetics and time to engraftment in pediatric patients undergoing autologous bone marrow transplantation. *J Clin Oncol* 1994; 12:2390-7.
20. Smith IE, Dowsett M. Aromatase inhibitors in breast cancer. *N Engl J Med* 2003; 348:2431-42.
21. Urruticoechea A, Alemany R, Balart J, Villanueva A, Vinals F, Capella G. Recent advances in cancer therapy: an overview. *Curr Pharm Des* 2010; 16:3-10.

22. Bailar JC, 3rd, Gornik HL. Cancer undefeated. *N Engl J Med* 1997; 336:1569-74.
23. Cohen MH, Shen YL, Keegan P, Pazdur R. FDA drug approval summary: bevacizumab (Avastin) as treatment of recurrent glioblastoma multiforme. *Oncologist* 2009; 14:1131-8.
24. Cohen MH, Gootenberg J, Keegan P, Pazdur R. FDA drug approval summary: bevacizumab (Avastin) plus Carboplatin and Paclitaxel as first-line treatment of advanced/metastatic recurrent nonsquamous non-small cell lung cancer. *Oncologist* 2007; 12:713-8.
25. Cohen MH, Gootenberg J, Keegan P, Pazdur R. FDA drug approval summary: bevacizumab plus FOLFOX4 as second-line treatment of colorectal cancer. *Oncologist* 2007; 12:356-61.
26. Pagnan G, Montaldo PG, Pastorino F, Raffaghello L, Kirchmeier M, Allen TM, et al. GD2-mediated melanoma cell targeting and cytotoxicity of liposome-entrapped fenretinide. *Int J Cancer* 1999; 81:268-74.
27. Wiegandt H. The chemical constitution of gangliosides of the vertebrate nervous system. *Behav Brain Res* 1995; 66:85-97.
28. Ryan JM, Rice GE, Mitchell MD. The role of gangliosides in brain development and the potential benefits of perinatal supplementation. *Nutr Res* 2013; 33:877-87.
29. Posse de Chaves E, Sipione S. Sphingolipids and gangliosides of the nervous system in membrane function and dysfunction. *FEBS Lett* 2010; 584:1748-59.
30. Yu RK, Nakatani Y, Yanagisawa M. The role of glycosphingolipid metabolism in the developing brain. *J Lipid Res* 2009; 50 Suppl:S440-5.
31. Schnaar RL. Brain gangliosides in axon-myelin stability and axon regeneration. *FEBS Lett* 2010; 584:1741-7.

32. Cheresh DA, Harper JR, Schulz G, Reisfeld RA. Localization of the gangliosides GD2 and GD3 in adhesion plaques and on the surface of human melanoma cells. *Proc Natl Acad Sci U S A* 1984; 81:5767-71.
33. Cheresh DA, Pierschbacher MD, Herzig MA, Mujoo K. Disialogangliosides GD2 and GD3 are involved in the attachment of human melanoma and neuroblastoma cells to extracellular matrix proteins. *J Cell Biol* 1986; 102:688-96.
34. Sheikh KA, Deerinck TJ, Ellisman MH, Griffin JW. The distribution of ganglioside-like moieties in peripheral nerves. *Brain* 1999; 122 (Pt 3):449-60.
35. Chang HR, Cordon-Cardo C, Houghton AN, Cheung NK, Brennan MF. Expression of disialogangliosides GD2 and GD3 on human soft tissue sarcomas. *Cancer* 1992; 70:633-8.
36. Ahmed M, Cheung NK. Engineering anti-GD2 monoclonal antibodies for cancer immunotherapy. *FEBS Lett* 2014; 588:288-97.
37. Schumacher-Kuckelkorn R, Hero B, Ernestus K, Berthold F. Lacking immunocytological GD2 expression in neuroblastoma: report of 3 cases. *Pediatr Blood Cancer* 2005; 45:195-201.
38. Kramer K, Gerald WL, Kushner BH, Larson SM, Hameed M, Cheung NK. Disialoganglioside G(D2) loss following monoclonal antibody therapy is rare in neuroblastoma. *Clin Cancer Res* 1998; 4:2135-9.
39. Decker WK, Safdar A. Bioimmunoadjuvants for the treatment of neoplastic and infectious disease: Coley's legacy revisited. *Cytokine Growth Factor Rev* 2009; 20:271-81.
40. Nauts HC, Fowler GA, Bogatko FH. A review of the influence of bacterial infection and of bacterial products (Coley's toxins) on malignant tumors in man; a critical analysis of 30 inoperable cases treated by Coley's mixed toxins, in which diagnosis was confirmed by microscopic examination selected for special study. *Acta Med Scand Suppl* 1953; 276:1-103.
41. Strebhardt K, Ullrich A. Paul Ehrlich's magic bullet concept: 100 years of progress. *Nat Rev Cancer* 2008; 8:473-80.

42. Waldmann TA. Immunotherapy: past, present and future. *Nat Med* 2003; 9:269-77.
43. Elert E. Calling cells to arms. *Nature* 2013; 504:S2-3.
44. Platten M, Ochs K, Lemke D, Opitz C, Wick W. Microenvironmental clues for glioma immunotherapy. *Curr Neurol Neurosci Rep* 2014; 14:440.
45. Kantoff PW, Higano CS, Shore ND, Berger ER, Small EJ, Penson DF, et al. Sipuleucel-T immunotherapy for castration-resistant prostate cancer. *N Engl J Med* 2010; 363:411-22.
46. Small EJ, Schellhammer PF, Higano CS, Redfern CH, Nemunaitis JJ, Valone FH, et al. Placebo-controlled phase III trial of immunologic therapy with sipuleucel-T (APC8015) in patients with metastatic, asymptomatic hormone refractory prostate cancer. *J Clin Oncol* 2006; 24:3089-94.
47. Grimm EA, Mazumder A, Zhang HZ, Rosenberg SA. Lymphokine-activated killer cell phenomenon. Lysis of natural killer-resistant fresh solid tumor cells by interleukin 2-activated autologous human peripheral blood lymphocytes. *J Exp Med* 1982; 155:1823-41.
48. Restifo NP, Dudley ME, Rosenberg SA. Adoptive immunotherapy for cancer: harnessing the T cell response. *Nat Rev Immunol* 2012; 12:269-81.
49. Adams GP, Weiner LM. Monoclonal antibody therapy of cancer. *Nat Biotechnol* 2005; 23:1147-57.
50. Schwaber J, Cohen EP. Human x mouse somatic cell hybrid clone secreting immunoglobulins of both parental types. *Nature* 1973; 244:444-7.
51. Kohler G, Milstein C. Continuous cultures of fused cells secreting antibody of predefined specificity. *Nature* 1975; 256:495-7.
52. Milstein C. The hybridoma revolution: an offshoot of basic research. *Bioessays* 1999; 21:966-73.
53. Cheung NK, Saarinen UM, Neely JE, Landmeier B, Donovan D, Coccia PF. Monoclonal antibodies to a glycolipid antigen on human neuroblastoma cells. *Cancer Res* 1985; 45:2642-9.

54. Cheung IY, Lo Piccolo MS, Collins N, Kushner BH, Cheung NK. Quantitation of GD2 synthase mRNA by real-time reverse transcription-polymerase chain reaction: utility in bone marrow purging of neuroblastoma by anti-GD2 antibody 3F8. *Cancer* 2002; 94:3042-8.
55. Modak S, Cheung NK. Disialoganglioside directed immunotherapy of neuroblastoma. *Cancer Invest* 2007; 25:67-77.
56. Cheung NK, Lazarus H, Miraldi FD, Abramowsky CR, Kallick S, Saarinen UM, et al. Ganglioside GD2 specific monoclonal antibody 3F8: a phase I study in patients with neuroblastoma and malignant melanoma. *J Clin Oncol* 1987; 5:1430-40.
57. Cheung NK, Cheung IY, Kushner BH, Ostrovnaya I, Chamberlain E, Kramer K, et al. Murine anti-GD2 monoclonal antibody 3F8 combined with granulocyte-macrophage colony-stimulating factor and 13-cis-retinoic acid in high-risk patients with stage 4 neuroblastoma in first remission. *J Clin Oncol* 2012; 30:3264-70.
58. Kushner BH, Cheung IY, Kramer K, Modak S, Cheung NK. High-dose cyclophosphamide inhibition of humoral immune response to murine monoclonal antibody 3F8 in neuroblastoma patients: broad implications for immunotherapy. *Pediatr Blood Cancer* 2007; 48:430-4.
59. Kushner BH, Kramer K, Cheung NK. Phase II trial of the anti-G(D2) monoclonal antibody 3F8 and granulocyte-macrophage colony-stimulating factor for neuroblastoma. *J Clin Oncol* 2001; 19:4189-94.
60. Ahmed M, Goldgur Y, Hu J, Guo HF, Cheung NK. In silico driven redesign of a clinically relevant antibody for the treatment of GD2 positive tumors. *PLoS One* 2013; 8:e63359.
61. Navid F, Santana VM, Barfield RC. Anti-GD2 antibody therapy for GD2-expressing tumors. *Curr Cancer Drug Targets* 2010; 10:200-9.
62. Parsons K, Bernhardt B, Strickland B. Targeted immunotherapy for high-risk neuroblastoma--the role of monoclonal antibodies. *Ann Pharmacother* 2013; 47:210-8.

63. Yang RK, Sondel PM. Anti-GD2 Strategy in the Treatment of Neuroblastoma. *Drugs Future* 2010; 35:665.
64. Jiang L, Sun W, Gao Y, Zhao J. Geometric thermal phase diagrams for studying the thermal dynamic stability of hollow gold nanoballs at different temperatures. *Phys Chem Chem Phys* 2014; 16:6623-9.
65. Kessentini S, Barchiesi D. Quantitative comparison of optimized nanorods, nanoshells and hollow nanospheres for photothermal therapy. *Biomed Opt Express* 2012; 3:590-604.
66. Liong M, Lu J, Kovichich M, Xia T, Ruehm SG, Nel AE, et al. Multifunctional inorganic nanoparticles for imaging, targeting, and drug delivery. *ACS Nano* 2008; 2:889-96.
67. Slowing, II, Trewyn BG, Lin VS. Mesoporous silica nanoparticles for intracellular delivery of membrane-impermeable proteins. *J Am Chem Soc* 2007; 129:8845-9.
68. Al-Jamal WT, Kostarelos K. Liposomes: from a clinically established drug delivery system to a nanoparticle platform for theranostic nanomedicine. *Acc Chem Res* 2011; 44:1094-104.
69. Gabizon AA, Barenholz Y, Bialer M. Prolongation of the circulation time of doxorubicin encapsulated in liposomes containing a polyethylene glycol-derivatized phospholipid: pharmacokinetic studies in rodents and dogs. *Pharm Res* 1993; 10:703-8.
70. Barenholz Y. Doxil(R)--the first FDA-approved nano-drug: lessons learned. *J Control Release* 2012; 160:117-34.
71. Andreopoulou E, Gaiotti D, Kim E, Downey A, Mirchandani D, Hamilton A, et al. Pegylated liposomal doxorubicin HCL (PLD; Caelyx/Doxil): experience with long-term maintenance in responding patients with recurrent epithelial ovarian cancer. *Ann Oncol* 2007; 18:716-21.
72. Torchilin VP. Recent advances with liposomes as pharmaceutical carriers. *Nat Rev Drug Discov* 2005; 4:145-60.

73. Bendas G. Immunoliposomes: a promising approach to targeting cancer therapy. *BioDrugs* 2001; 15:215-24.
74. Kularatne SA, Low PS. Targeting of nanoparticles: folate receptor. *Methods Mol Biol* 2010; 624:249-65.
75. Godin B, Tasciotti E, Liu X, Serda RE, Ferrari M. Multistage nanovectors: from concept to novel imaging contrast agents and therapeutics. *Acc Chem Res* 2011; 44:979-89.
76. Loi M, Marchio S, Becherini P, Di Paolo D, Soster M, Curnis F, et al. Combined targeting of perivascular and endothelial tumor cells enhances anti-tumor efficacy of liposomal chemotherapy in neuroblastoma. *J Control Release* 2010; 145:66-73.
77. Pastorino F, Brignole C, Loi M, Di Paolo D, Di Fiore A, Perri P, et al. Nanocarrier-mediated targeting of tumor and tumor vascular cells improves uptake and penetration of drugs into neuroblastoma. *Front Oncol* 2013; 3:190.
78. Brignole C, Pastorino F, Marimpietri D, Pagnan G, Pistorio A, Allen TM, et al. Immune cell-mediated antitumor activities of GD2-targeted liposomal c-myc antisense oligonucleotides containing CpG motifs. *J Natl Cancer Inst* 2004; 96:1171-80.
79. Deshpande PP, Biswas S, Torchilin VP. Current trends in the use of liposomes for tumor targeting. *Nanomedicine (Lond)* 2013; 8:1509-28.
80. Sistla A, Smith DJ, Kobrinsky NL, Kumar K. Pharmacokinetics and tissue distribution of liposomal etoposide in rats. *Drug Deliv* 2009; 16:423-9.
81. Zhang T, Chen J, Zhang Y, Shen Q, Pan W. Characterization and evaluation of nanostructured lipid carrier as a vehicle for oral delivery of etoposide. *Eur J Pharm Sci* 2011; 43:174-9.
82. Jinturkar KA, Anish C, Kumar MK, Bagchi T, Panda AK, Misra AR. Liposomal formulations of Etoposide and Docetaxel for p53 mediated enhanced cytotoxicity in lung cancer cell lines. *Biomaterials* 2012; 33:2492-507.

83. Horne RW, Bangham AD, Whittaker VP. Negatively Stained Lipoprotein Membranes. *Nature* 1963; 200:1340.
84. Mashaghi S, Jadidi T, Koenderink G, Mashaghi A. Lipid nanotechnology. *Int J Mol Sci* 2013; 14:4242-82.
85. Scrimin P, Tecilla P. Model membranes: developments in functional micelles and vesicles. *Curr Opin Chem Biol* 1999; 3:730-5.
86. Nicholls P, West J, Bangham AD. Chlorophyll b containing liposomes: effect of thermal transitions on catalytic and spectral properties. *Biochim Biophys Acta* 1974; 363:190-201.
87. Cullis PR, Hope MJ, Tilcock CP. Lipid polymorphism and the roles of lipids in membranes. *Chem Phys Lipids* 1986; 40:127-44.
88. Almgren M. Mixed micelles and other structures in the solubilization of bilayer lipid membranes by surfactants. *Biochim Biophys Acta* 2000; 1508:146-63.
89. De La Vega JC, Elischer P, Schneider T, Hafeli UO. Uniform polymer microspheres: monodispersity criteria, methods of formation and applications. *Nanomedicine (Lond)* 2013; 8:265-85.
90. Szoka F, Jr., Papahadjopoulos D. Comparative properties and methods of preparation of lipid vesicles (liposomes). *Annu Rev Biophys Bioeng* 1980; 9:467-508.
91. Zhu TF, Budin I, Szostak JW. Preparation of fatty acid or phospholipid vesicles by thin-film rehydration. *Methods Enzymol* 2013; 533:267-74.
92. Litzinger DC, Buiting AM, van Rooijen N, Huang L. Effect of liposome size on the circulation time and intraorgan distribution of amphipathic poly(ethylene glycol)-containing liposomes. *Biochim Biophys Acta* 1994; 1190:99-107.
93. Mui B, Chow L, Hope MJ. Extrusion technique to generate liposomes of defined size. *Methods Enzymol* 2003; 367:3-14.

94. Jaafar-Maalej C, Diab R, Andrieu V, Elaissari A, Fessi H. Ethanol injection method for hydrophilic and lipophilic drug-loaded liposome preparation. *J Liposome Res* 2010; 20:228-43.
95. Stano P, Bufali S, Pisano C, Bucci F, Barbarino M, Santaniello M, et al. Novel camptothecin analogue (gimatecan)-containing liposomes prepared by the ethanol injection method. *J Liposome Res* 2004; 14:87-109.
96. Gentine P, Bourel-Bonnet L, Frisch B. Modified and derived ethanol injection toward liposomes: development of the process. *J Liposome Res* 2013; 23:11-9.
97. Sengupta S, Tyagi P, Chandra S, Kochupillai V, Gupta SK. Encapsulation in cationic liposomes enhances antitumour efficacy and reduces the toxicity of etoposide, a topoisomerase II inhibitor. *Pharmacology* 2001; 62:163-71.
98. Greish K. Enhanced permeability and retention (EPR) effect for anticancer nanomedicine drug targeting. *Methods Mol Biol* 2010; 624:25-37.
99. Fang J, Sawa T, Maeda H. Factors and mechanism of "EPR" effect and the enhanced antitumor effects of macromolecular drugs including SMANCS. *Adv Exp Med Biol* 2003; 519:29-49.
100. Greish K. Enhanced permeability and retention of macromolecular drugs in solid tumors: a royal gate for targeted anticancer nanomedicines. *J Drug Target* 2007; 15:457-64.
101. Gabizon AA. Pegylated liposomal doxorubicin: metamorphosis of an old drug into a new form of chemotherapy. *Cancer Invest* 2001; 19:424-36.
102. Simoes S, Filipe A, Faneca H, Mano M, Penacho N, Duzgunes N, et al. Cationic liposomes for gene delivery. *Expert Opin Drug Deliv* 2005; 2:237-54.
103. Kim JC, Bae SK, Kim JD. Temperature-sensitivity of liposomal lipid bilayers mixed with poly(N-isopropylacrylamide-co-acrylic acid). *J Biochem* 1997; 121:15-9.
104. Shen J, Burgess DJ. Dissolution Testing Strategies for Nanoparticulate Drug Delivery Systems: Recent Developments and Challenges. *Drug Deliv Transl Res* 2013; 3:409-15.

105. Noble GT, Stefanick JF, Ashley JD, Kiziltepe T, Bilgicer B. Ligand-targeted liposome design: challenges and fundamental considerations. *Trends Biotechnol* 2014; 32:32-45.
106. Ghaghada KB, Saul J, Natarajan JV, Bellamkonda RV, Annapragada AV. Folate targeting of drug carriers: a mathematical model. *J Control Release* 2005; 104:113-28.
107. Chen CW, Lu DW, Yeh MK, Shiao CY, Chiang CH. Novel RGD-lipid conjugate-modified liposomes for enhancing siRNA delivery in human retinal pigment epithelial cells. *Int J Nanomedicine* 2011; 6:2567-80.
108. Kastantin M, Ananthanarayanan B, Karmali P, Ruoslahti E, Tirrell M. Effect of the lipid chain melting transition on the stability of DSPE-PEG(2000) micelles. *Langmuir* 2009; 25:7279-86.
109. Nagai Y. Functional roles of gangliosides in bio-signaling. *Behav Brain Res* 1995; 66:99-104.
110. Kailayangiri S, Altvater B, Meltzer J, Pscherer S, Luecke A, Dierkes C, et al. The ganglioside antigen G(D2) is surface-expressed in Ewing sarcoma and allows for MHC-independent immune targeting. *Br J Cancer* 2012; 106:1123-33.
111. Yu AL, Gilman AL, Ozkaynak MF, London WB, Kreissman SG, Chen HX, et al. Anti-GD2 antibody with GM-CSF, interleukin-2, and isotretinoin for neuroblastoma. *N Engl J Med* 2010; 363:1324-34.
112. Czaplicki D, Horwacik I, Kowalczyk A, Wieczorek A, Bolek-Marzec K, Balwierz W, et al. New method for quantitative analysis of GD2 ganglioside in plasma of neuroblastoma patients. *Acta Biochim Pol* 2009; 56:423-31.
113. Schulz G, Cheresch DA, Varki NM, Yu A, Staffileno LK, Reisfeld RA. Detection of ganglioside GD2 in tumor tissues and sera of neuroblastoma patients. *Cancer Res* 1984; 44:5914-20.

114. Yu RK, Tsai YT, Ariga T. Functional roles of gangliosides in neurodevelopment: an overview of recent advances. *Neurochem Res* 2012; 37:1230-44.
115. Tong W, Gagnon M, Sprules T, Gilbert M, Chowdhury S, Meerovitch K, et al. Small-molecule ligands of GD2 ganglioside, designed from NMR studies, exhibit induced-fit binding and bioactivity. *Chem Biol* 2010; 17:183-94.
116. Koning GA, Kamps JA, Scherphof GL. Efficient intracellular delivery of 5-fluorodeoxyuridine into colon cancer cells by targeted immunoliposomes. *Cancer Detect Prev* 2002; 26:299-307.
117. Zhu J, Liao L, Zhu L, Zhang P, Guo K, Kong J, et al. Size-dependent cellular uptake efficiency, mechanism, and cytotoxicity of silica nanoparticles toward HeLa cells. *Talanta* 2013; 107:408-15.
118. Macia E, Ehrlich M, Massol R, Boucrot E, Brunner C, Kirchhausen T. Dynasore, a cell-permeable inhibitor of dynamin. *Dev Cell* 2006; 10:839-50.
119. Tivnan A, Orr WS, Gubala V, Nooney R, Williams DE, McDonagh C, et al. Inhibition of neuroblastoma tumor growth by targeted delivery of microRNA-34a using anti-disialoganglioside GD2 coated nanoparticles. *PLoS One* 2012; 7:e38129.
120. Sieuwerts AM, Klijn JG, Peters HA, Foekens JA. The MTT tetrazolium salt assay scrutinized: how to use this assay reliably to measure metabolic activity of cell cultures in vitro for the assessment of growth characteristics, IC50-values and cell survival. *Eur J Clin Chem Clin Biochem* 1995; 33:813-23.
121. Mujoo K, Reisfeld RA, Cheung L, Rosenblum MG. A potent and specific immunotoxin for tumor cells expressing disialoganglioside GD2. *Cancer Immunol Immunother* 1991; 34:198-204.
122. Thomas PB, Delatte SJ, Sutphin A, Frankel AE, Tagge EP. Effective targeted cytotoxicity of neuroblastoma cells. *J Pediatr Surg* 2002; 37:539-44.

123. Lo AS, Ma Q, Liu DL, Junghans RP. Anti-GD3 chimeric sFv-CD28/T-cell receptor zeta designer T cells for treatment of metastatic melanoma and other neuroectodermal tumors. *Clin Cancer Res* 2010; 16:2769-80.
124. Louis CU, Savoldo B, Dotti G, Pule M, Yvon E, Myers GD, et al. Antitumor activity and long-term fate of chimeric antigen receptor-positive T cells in patients with neuroblastoma. *Blood* 2011; 118:6050-6.
125. Shaughnessy AF. Monoclonal antibodies: magic bullets with a hefty price tag. *BMJ* 2012; 345:e8346.
126. Moreira JN, Ishida T, Gaspar R, Allen TM. Use of the post-insertion technique to insert peptide ligands into pre-formed stealth liposomes with retention of binding activity and cytotoxicity. *Pharm Res* 2002; 19:265-9.
127. Gao J, Sun J, Li H, Liu W, Zhang Y, Li B, et al. Lyophilized HER2-specific PEGylated immunoliposomes for active siRNA gene silencing. *Biomaterials* 2010; 31:2655-64.
128. Battula VL, Shi Y, Evans KW, Wang RY, Spaeth EL, Jacamo RO, et al. Ganglioside GD2 identifies breast cancer stem cells and promotes tumorigenesis. *J Clin Invest* 2012; 122:2066-78.
129. Ghaghada K, Hawley C, Kawaji K, Annapragada A, Mukundan S, Jr. T1 relaxivity of core-encapsulated gadolinium liposomal contrast agents--effect of liposome size and internal gadolinium concentration. *Acad Radiol* 2008; 15:1259-63.
130. Rosen JM, Jordan CT. The increasing complexity of the cancer stem cell paradigm. *Science* 2009; 324:1670-3.
131. Schatton T, Frank NY, Frank MH. Identification and targeting of cancer stem cells. *Bioessays* 2009; 31:1038-49.

132. De Giorgi U, Cohen EN, Gao H, Mego M, Lee BN, Lodhi A, et al. Mesenchymal stem cells expressing GD2 and CD271 correlate with breast cancer-initiating cells in bone marrow. *Cancer Biol Ther* 2011; 11:812-5.
133. Gregoriadis G, McCormack B, Obrenovic M, Saffie R, Zadi B, Perrie Y. Vaccine entrapment in liposomes. *Methods* 1999; 19:156-62.
134. Poovorawan Y, Theamboonlers A, Chumdermpadetsuk S, Gluck R, Cryz SJ, Jr. Safety, immunogenicity, and kinetics of the immune response to a single dose of virosome-formulated hepatitis A vaccine in Thais. *Vaccine* 1995; 13:891-3.
135. Zhang HG, Grizzle WE. Exosomes: a novel pathway of local and distant intercellular communication that facilitates the growth and metastasis of neoplastic lesions. *Am J Pathol* 2014; 184:28-41.
136. Pusic AD, Pusic KM, Kraig RP. What are exosomes and how can they be used in multiple sclerosis therapy? *Expert Rev Neurother* 2014.
137. Viaud S, They C, Ploix S, Tursz T, Lapiere V, Lantz O, et al. Dendritic cell-derived exosomes for cancer immunotherapy: what's next? *Cancer Res* 2010; 70:1281-5.
138. Lakhal S, Wood MJ. Exosome nanotechnology: an emerging paradigm shift in drug delivery: exploitation of exosome nanovesicles for systemic in vivo delivery of RNAi heralds new horizons for drug delivery across biological barriers. *Bioessays* 2011; 33:737-41.
139. Kunisawa J, Masuda T, Katayama K, Yoshikawa T, Tsutsumi Y, Akashi M, et al. Fusogenic liposome delivers encapsulated nanoparticles for cytosolic controlled gene release. *J Control Release* 2005; 105:344-53.
140. Karanth H, Murthy RS. pH-sensitive liposomes--principle and application in cancer therapy. *J Pharm Pharmacol* 2007; 59:469-83.

141. Kakudo T, Chaki S, Futaki S, Nakase I, Akaji K, Kawakami T, et al. Transferrin-modified liposomes equipped with a pH-sensitive fusogenic peptide: an artificial viral-like delivery system. *Biochemistry* 2004; 43:5618-28.
142. Chang WK, Tai YJ, Chiang CH, Hu CS, Hong PD, Yeh MK. The comparison of protein-entrapped liposomes and lipoparticles: preparation, characterization, and efficacy of cellular uptake. *Int J Nanomedicine* 2011; 6:2403-17.
143. Licciardi M, Paolino D, Celia C, Giammona G, Cavallaro G, Fresta M. Folate-targeted supramolecular vesicular aggregates based on polyaspartyl-hydrazide copolymers for the selective delivery of antitumoral drugs. *Biomaterials* 2010; 31:7340-54.

Brandon Scott Brown was born in Houston, Texas on January 30, 1984, the son of Walter Scott Brown and Christina Marie Brown. After completing his work at Pearland High School, Pearland, Texas in 2002, he entered The University of Texas at Austin. He received a degree of Bachelor of Science with a major in neurobiology from UT in August, 2006. For the next year he worked at UT as a research technician and moved to Breckenridge, Colorado where he worked for Vail Resorts. In June of 2007 he entered The University of Texas Medical School MD/PhD Program.

Permanent address:
3411 Crossbranch Court
Pearland, Texas 77581